THE EFFECT OF LOADING SPECTRA PARAMETERS ON FATIGUE LIFE

by

Paul Francis Kilty B.Sc.(Eng), A.C.G.I.

A thesis submitted for the degree of
Doctor of Philosophy of the
University of London
1969

ABSTRACT

Random loading can be characterised to some extent by the Irregularity Factor - that is the ratio of the number of mean-crossings to the number of max.+min. of the signal. It is well known that the distribution of maxima is a function of only this parameter and the standard deviation of the random signal. However other probability density distributions of interest to the fatigue engineer (particularly the distribution of ranges) are not known. This is probably due to the lack of versatile systems for recording and analysing random loading histories.

This thesis contains a description of the design and development of such a system. Magnetic tape is used as the recording medium and during replay the system produces punched paper tape for subsequent analysis by computer. The paper tape contains sufficient information about the signal to construct all of the histograms of interest in fatigue.

The system is used to make a series of recordings of typical random signals with various values of Irregularity Factor. These recordings are of filtered 'white' noise and car suspension loads. From the data, various distributions are constructed to indicate the effect of the Irregularity Factor. In particular the distributions of ranges are presented, based both on this recorded data and on other data contained in the literature.

Since the Irregularity Factor describes the distribution of peaks, and is seen to be a major parameter in the experimental family of range distribution curves, it would seem to indicate that it may be a controlling factor

in the lives obtained under true random loading conditions. Accordingly, an examination is made of random loading fatigue tests published in the literature to see if there are any consistent trends with the Irregularity Factor.

ACKNOWLEDGEMENTS

The author wishes to express his thanks to Professor J.H. Argyris; to Dr. K. Thomas who supervised this work; and to Mr. B.J. Belcher for the benefit of some helpful discussions.

This work was carried out whilst the author was employed by British Aircraft Corporation (Preston Division) as a 'Special Trainee' located full-time at Imperial College. Special acknowledgement is due to B.A.C. for this generous financial support, which was also extended to the supplying of an item of electronic instrumentation.

Finally the author wishes to express his gratitude to his wife for her help in the production of this Thesis.

I N D E X

1 INTRODUCTION

Several developments in the field of fatigue have indicated the necessity of a versatile system for recording and analysing continuous random signals. In a series of fatigue tests, Kowaleski (ref. 4) examined the effect of the traditional counting methods (for the contruction of histograms) in comparison with true random loading. In this work comparatively narrow band random noise was used, and Kowaleski introduced a parameter to describe the spectrum width. This parameter is simply the ratio between the number of maxima and minima and the number of mean crossings of the signal. The parameter is now called the Irregularity Factor.

The shortcomings in programme testing have stimulated the development of random loading fatigue research. The Irregularity Factor is a convenient and useful parameter to describe random signals. The work of Rice (ref. 1) shows that the probability density distribution of maxima is a function only of the r.m.s. value of the signal and the Irregularity Factor. Thus it is suggested by Swanson (ref. 11) that random fatigue tests using a twin lever machine could be performed. The lever combinations are simply set to simulate random loading with the same value of irregularity factor as is measured or predicted for the structure. The parameter is readily calculated from the power spectrum of the loading.

With the present investment in programmed fatigue testing equipment, and the use in industry of the linear cumulative damage theory, it is important to be aware of the effect of the spectrum width on the particular counting method used. One point worth study is the assumption that

the variation of mean stress (around the overall mean) can be neglected. Or, expressing this in terms of the traditional counting methods, will the range-mean count give similar estimated lives, or programme test lives, to the range count? Clearly the greater the spectrum width the greater is the effect of variation in mean stress.

It is also assumed in programmed tests (or life estimations) that very small stress amplitudes have a negligible effect. This omission of small stress amplitudes is performed after the range histogram has been constructed. Clearly the effect of leaving out these ranges before constructing the histogram is that a greater number of larger ranges will be detected. In the first case the following reduction takes place:

in the second:

The manner in which the various counting methods break down the data depends on the Irregularity Factor.

There is a further problem concerned with the range count. As is well known the theoretical determination of the distribution of ranges for a Gaussian signal is very difficult, except of course for very narrow bandwidth noise, when there is a Rayleigh distribution. Indeed the empirical distribution of ranges is unknown. It is possible

for example, that the distribution of ranges, like that of peaks, may depend only on the standard deviation of the signal and the Irregularity Factor. In order to find the empirical distribution of ranges a recording system with high resolution is required. A recording system with poor resolution will not find the true distribution due to the effect described above; i.e. the omission of small ranges leads to a completely different distribution of the remaining ranges.

There are, however, practical limits to the effective resolution of any recording system. For example when recording stress histories the familiar chain of strain gauge, strain-gauge bridge amplifying unit and measuring device leads to overall experimental accuracies of some 2 to 3%, and noise levels of about 0.2 to 0.3%. As far as the range distribution is concerned, a system with very high resolution breaks down the ranges still further because of the noise. A practical compromise is probably a resolution around ½% full scale. The range distribution can then be found making the assumption that there are proportionately very few ranges below this level. Indeed for a Rayleigh distribution of ranges (very narrow bandwidth signal) the proportion of ranges below this level is only 3 in 10,000 (assuming a standard deviation of 10% full scale). For wider bandwidth signals there will clearly be more, but even if there is an order of magnitude more, the range distribution will not be significantly affected.

The development of a recording system which would provide an automatic means of recording and analysing random strain histories is a necessity for studies of this kind. The first section of this thesis describes the design and development of such a system. A major criterion

in the design of the system is cost. Most high resolution systems, particularly digital ones, are very expensive. The design concepts are therefore evolved with cost in mind, consistent, of course, with the required overall accuracy of the system.

The recording system is then used in two series of tests. In the first series two examples of filtered 'white' noise are recorded with different band-pass filter settings for the two cases. In the second series the system is used for the measurement of car suspension loads to provide an example with a wider spectrum. From the recordings the following studies are made.

(i) The signals are examined to see if they are, in fact Gaussian. A comparison is made between actual and theoretical distributions of maxima for the measured values of the irregularity factor. For the filtered random noise recordings, where the spectral density distributions are known, the expected theoretical values of irregularity factor are compared with those obtained experimentally.

(ii) The various counting methods are compared, in particular the effect on the range distribution of omitting small ranges. All these comparisons are made using probability density distributions. These distributions illustrate the differences between the counting methods far more clearly than cumulative plots of the data. Indeed cumulative plots can be misleading in that respect. As an illustration of these comparisons a number of fatigue damage functions are contructed. These functions are used to compare all the above counting

methods assuming linear cumulative damage. This provides a quantitative indication of the effects of both the irregularity factor and the various counting methods on estimated fatigue lives.

(iii) An empirical distribution of ranges is established using, in addition to the data recorded here, data published by Naumann and Leybold (refs. 9 and 10).

Finally a survey is made of random fatigue testing to see if there are any clear trends in the effect of irregularity factor.

Before describing the digital recording system, however, a brief outline of random noise theory (principally the work of Rice, ref. 1) is presented. Particular attention is paid to the role of the irregularity factor in the theory.

2 THE IRREGULARITY FACTOR

2.1 Introduction

The parameter introduced by Kowaleski (ref. 4) to describe the spectrum width is simply the ratio between the number of maxima and minima and the number of mean crossings. It is a convenient parameter to describe random signals not only because its meaning is immediately obvious and it is easily measured, but because it also has particular relevance to random noise theory. It is now known as the Irregularity Factor.

In the classic random noise theory of Rice (ref. 1) the parameter is shown to be a simple function of three of the moments of the energy spectrum of the signal. From the equation derived by Rice for the distribution of maxima, Cartwright and Longuet-Higgins (ref. 2) have shown that the distribution of maxima depends only on the root-mean-square of the signal and a parameter which represents the frequency spectrum of the signal. This latter parameter is very simply related to the Kowaleski Irregularity Factor. Either parameter also relates the r.m.s. peaks to the r.m.s. of the continuous signal. There follows a brief outline of the theory derived by Rice and extended by Cartwright and Longuet-Higgins.

The Fourier series representation of random noise is an infinite number of sine-waves;

$$f(t) = \sum_{n=1}^{\infty} c_n \cos(\sigma_n t + \varepsilon_n)$$

where the frequencies σ_n are distributed throughout 0 to ∞ and the phases ε_n are distributed throughout 0 to 2π, and

the amplitudes c_n are such that

$$\sum_{\sigma_n=\sigma}^{\sigma+d\sigma} \tfrac{1}{2} c_n^2 = E(\sigma) \cdot d\sigma$$

where $E(\sigma)$ is the energy spectrum of $f(t)$. The summations then become Fourier integrals.

To obtain the expected number of maxima and mean-crossings per second, and also the distribution of maxima, use is made of the Central Limit Theorem. This theorem states that the joint probability density distribution of a number of random variables approaches a normal law when the distributions of the variables satisfy certain conditions (see refs. 1 or 5). Thus the multi-variate normal distribution can be used to find the distribution of maxima, etc. Again using Rice's notation the multi-variate normal distribution is

$$p(x_1, x_2, \ldots x_k) = 2\pi^{-k/2} \left| M \right|^{-\frac{1}{2}} \exp(-\tfrac{1}{2} x' M^{-1} x)$$

where

$$x = \{x_1, x_2, \ldots x_k\}$$

and

$$M = \begin{bmatrix} \mu_{11} \cdots \mu_{1K} \\ \mu_{K1} \cdots \mu_{KK} \end{bmatrix}$$

and

$$\mu_{ij} = \overline{x_i \, x_j}$$

Thus any particular distribution is found by calculating the relevant members μ_{ij} of M.

In the cases considered here the members μ_{ij} of M are simply the various moments of the energy spectrum $E(\sigma)$ of $f(t)$. The n^{th} moment is

$$m_n = \int_0^\infty E(\sigma) \cdot \sigma^n \cdot d\sigma$$

where the total energy per unit length of f(t) is

$$m_o = \int_c^\infty E(\sigma) \cdot d\sigma$$

2.2 Number of zeros per second

Rice evaluates the expected number of zeros per second by considering the probability that y will pass through zero with positive slope in the interval t_1, $t_1 + dt$ which is

$$P(\eta\, dt < \xi < 0) = dt \int_o^\infty \eta \cdot p(0, \eta ; t_1)\, d\eta$$

where

$$\xi = F(a_1, a_2 \ldots\ldots a_N ; t) \qquad \left[\text{i.e. } \xi = y \text{ at } t_1\right]$$

and

$$\eta = \left[\frac{\partial F}{\partial t}\right]_{t=t_1}$$

The probability density function for the two random variables ξ and η reduces to (using the Central Limit Theorem)

$$p(\xi, \eta ; t_1) = \frac{(-m_o\, m_2)^{-\frac{1}{2}}}{2\pi} \exp\left[\frac{-\xi^2}{2m_o} + \frac{\eta^2}{2m_2}\right]$$

The probability of having a zero in t_1, $t_1 + dt$ with positive slope is thus

$$dt \int_o^\infty \eta \cdot \frac{(-m_o m_2)^{-\frac{1}{2}}}{2\pi} \exp\left(\frac{\eta^2}{2m_2}\right) d\eta = \frac{dt}{2\pi}\left[\frac{-m_2}{m_o}\right]^{\frac{1}{2}}$$

Thus the expected number of zeros per second with positive slope is

$$N_{+o} = \frac{1}{2\pi}\left[-\frac{m_2}{m_o}\right]^{\frac{1}{2}}$$

2.3 Distribution of maxima.

The probability that y has a maximum in the rectangle (t_1, $t_1 + dt$; y_1, $y_1 + dy$) is

$$P(\zeta\, dt < \eta < 0 \text{ AND } y_1 \leqslant \xi \leqslant y_1 + dy) = -dt.dy. \int_{-\infty}^{0} p(y_1, 0, \zeta)\, d\zeta$$

where

$$\zeta = \left[\frac{\partial^2 F}{\partial t^2}\right]_{t=t_1}$$

The probability density function for the three random variables ξ, η and ζ required here is

$$p(\xi, 0, \zeta) = -2\pi^{-3/2} |M|^{-\frac{1}{2}} \exp\left[-\frac{1}{2|M|}\xi^2 + M_{33}\zeta^2 + 2M_{13}.\xi.\zeta\right]$$

where

$$M = \begin{bmatrix} m_0 & 0 & m_2 \\ 0 & -m_2 & 0 \\ m_2 & 0 & m_4 \end{bmatrix}$$

and M_{rs} is the cofactor of μ_{rs} in M.

The probability of a maxima in the rectangle is then obtained by integration with respect to ζ;

$$\frac{-dt\, dy}{M_{33}\sqrt{8\pi^3}}\left[|M|^{\frac{1}{2}} \exp\left(-\frac{M_{13}\xi^2}{2|M|}\right) + M_{13}\xi\left(\frac{\pi}{2M_{33}}\right)^{\frac{1}{2}} \cdot \left(1 + \operatorname{erf} \frac{M_{13}\xi}{(2|M|M_{33})^{\frac{1}{2}}}\right) \times \right.$$

$$\left. \times \exp\left(-\frac{\xi^2}{2m_0}\right) \right] \quad \ldots\ldots(1)$$

2.4 Number of maxima per second

Rice obtains the expected number of maxima per second by integrating the above with respect to t from t_1 to t_2 and with respect to y from $-\infty$ to $+\infty$. The expected number is

$$N_1 = \frac{t_2 - t_1}{2\pi} \cdot \left[\frac{m_4}{-m_2}\right]^{\frac{1}{2}} \quad \ldots\ldots(2)$$

and the expected number per second is

$$N_1 = \frac{1}{2\pi}\left[\frac{m_4}{-m_2}\right]^{\frac{1}{2}}$$

2.5 The Irregularity Factor

The Irregularity Factor is then

$$n = N_+ / N_1 = \frac{m_2}{(m_0\, m_4)^{\frac{1}{2}}}$$

2.6 Distribution of maxima in terms of Irregularity Factor

Cartwright and Longuet-Higgins (ref. 2) obtain the probability density distribution of maxima by dividing the equation for the probability of a maxima in the rectangle $(y_1, y_1 + dy ; t_1, t_1 + dt)$, given by equation (1), by the total number of maxima in the interval $(t_1, t_1 + dt)$, which is (from equation (2))

$$\frac{dt}{2\pi}\left[\frac{m_4}{-m_2}\right]^{\frac{1}{2}}$$

Cartwright and Longuet-Higgins then substitute for M and its cofactors in terms of the moments m_n of the energy spectrum, and then express the moments m_n in terms of a spectrum width parameter ε, given by

$$\varepsilon^2 = (m_0\, m_4 - m_2^2) / m_0\, m_4$$

to obtain the distribution equation in terms of ε. Clearly ε is related to the irregularity factor (n) by

$$\varepsilon^2 = 1 - n^2$$

The probability density distribution of maxima can now be expressed in terms of the irregularity factor by

$$p(x) = \underbrace{\sqrt{\frac{1-n^2}{2\pi}}\exp\left(-\frac{x^2}{1-n^2}\right)}_{\text{Gauss term}} + \underbrace{\frac{n}{2}x\left[1 + \operatorname{erf}\left(x\sqrt{\frac{n^2}{2(1-n^2)}}\right)\right]}_{\text{Rayleigh term}}$$

where

$$x = \xi / m_0^{\frac{1}{2}}$$

The distribution equation has two components, a Gauss term and a Rayleigh term. For the case of n = 0 the distribution is pure Gaussian and for n = 1 pure Rayleigh. The distributions are plotted in Fig. 2.1 for values of n from 0 to 1 showing the transition from the Gaussian distribution to the Rayleigh distribution.

Thus the distribution of maxima is a function only of the r.m.s. ($m_o^{\frac{1}{2}}$) and the irregularity factor (n).

2.7 Relation between r.m.s. maxima and r.m.s. function

After recordings using the Digital Recording System have been made, the data which is extracted to construct histograms consists of only maxima and minima. From this must be calculated the r.m.s. value of the continuous function originally recorded.

Cartwright and Longuet-Higgins (ref. 2) also show that the second moment (ν_2) of the variate ξ (the maxima) is

$$\nu_2 = (2 - \varepsilon^2) \, m_o$$

where $$\varepsilon^2 = (m_o \, m_4 - m_2^2) / m_o \, m_4$$

i.e. $$\varepsilon^2 = 1 - n^2$$

therefore $$m_o^{\frac{1}{2}} = \nu_2^{\frac{1}{2}} / (1 + n^2)^{\frac{1}{2}}$$

For example with a sine-wave (n = 1) the ratio between the r.m.s. peaks (in this case also the amplitude) and the r.m.s. of the continuous wave is 2 as expected.

2.8 Filtered Random Noise

To obtain examples of narrow spectrum noise for the sequence of recordings filtered random noise was used.

For filtered white noise (i.e. noise assumed to have constant energy distribution throughout the bandwidth) the irregularity factor is

$$n = \frac{m_2}{(m_0 m_4)^{\frac{1}{2}}} = \frac{\int_{f_1}^{f_2} \omega_0 \, f^2 df}{\left[\int_{f_1}^{f_2} \omega_0 \, df \int_{f_1}^{f_2} \omega_0 \, f^4 df\right]^{\frac{1}{2}}} \quad \ldots.(3)$$

where ω_0 is the constant energy density and f_1 and f_2 are the lower and upper limits of the band-pass filter - the latter assumed to be a perfect filter.

$$\therefore \quad n = \frac{\sqrt{5}}{3} \left[\frac{1 - \phi^3}{(1 - \phi)(1 - \phi^5)}\right]^{\frac{1}{2}} \quad \ldots.(4)$$

where

$$\phi = f_1 / f_2$$

This function is shown in Fig. 2.2

In practice because of the relatively poor characteristics of the band-pass filter equation (4) was used only as a guide in selecting pass-bands. The theoretical estimates of irregularity factor (required for comparison with the measured factors) were obtained from equation (3). The necessary integrations were performed using the filter response curves obtained from an independent calibration.

FIG. 2.1 PROBABILITY DENSITY DISTRIBUTION OF MAXIMA FOR VALUES OF I.F FROM 0 TO 1

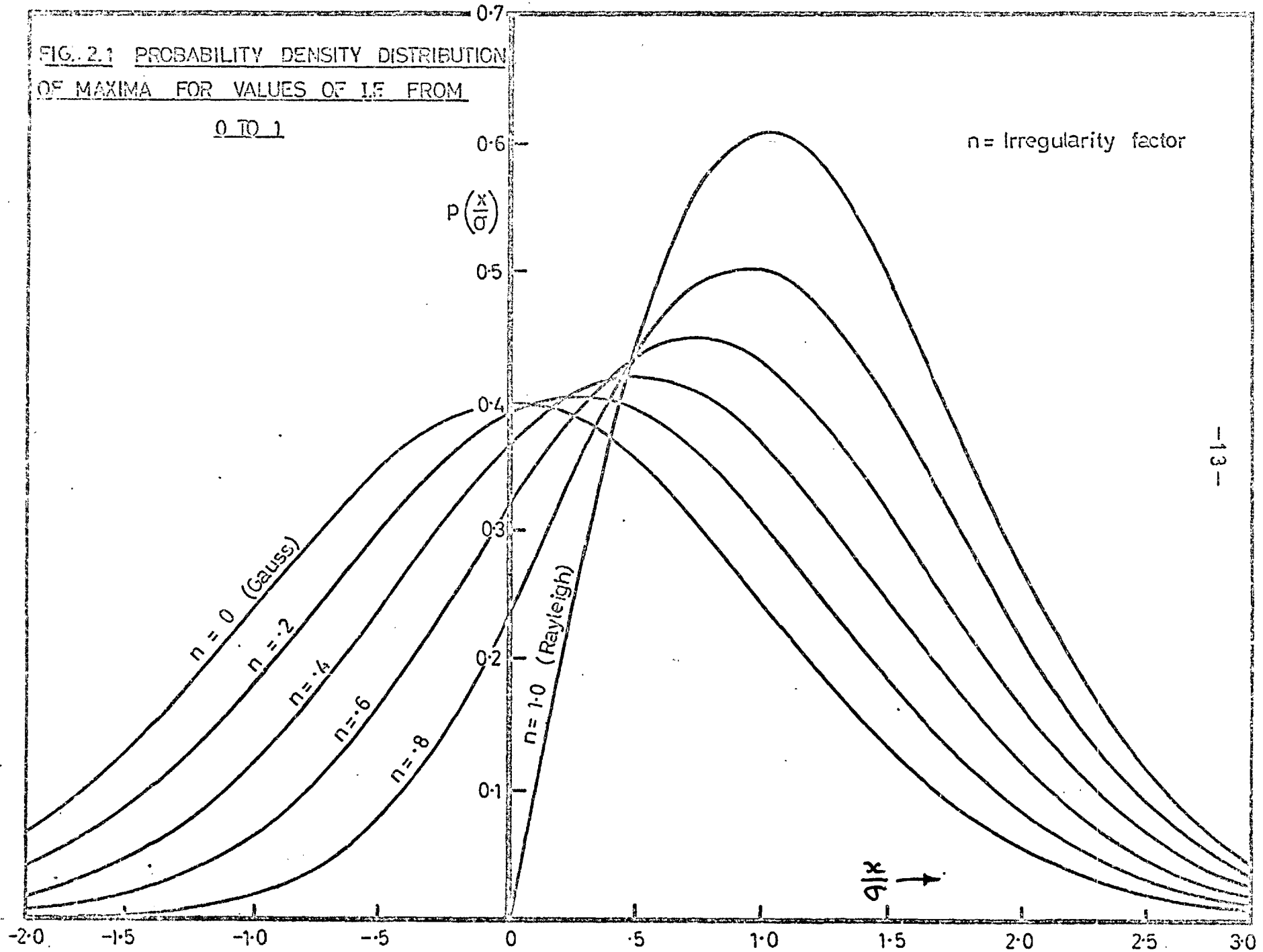

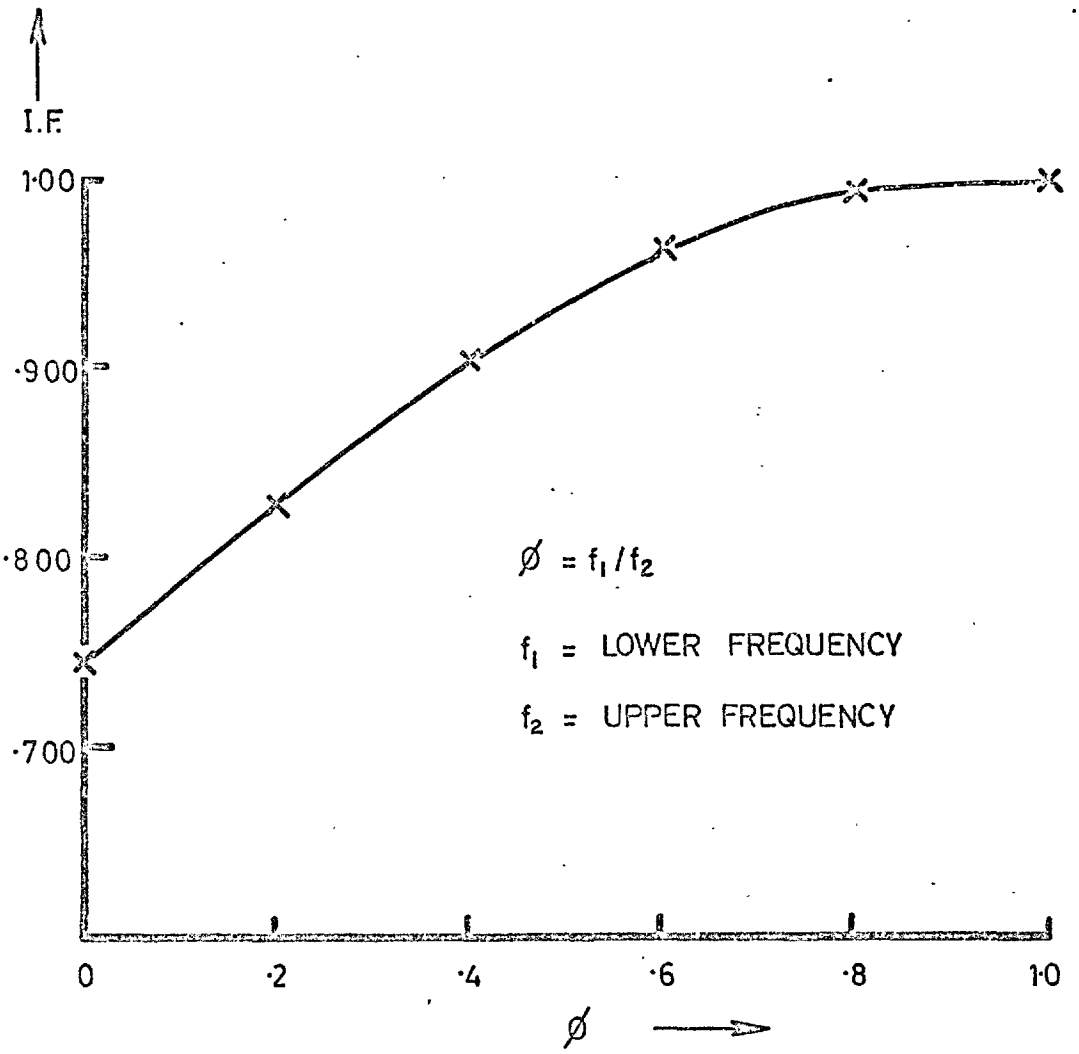

FIG. 2.2 IRREGULARITY FACTOR FOR BAND PASS FILTER.

3 DIGITAL RECORDING SYSTEM

3.1 Introduction

From an analogue signal various histograms are required relating to the maximum and minimum values of the signal. Thus a recording system providing automatic data-processing capabilities is necessary. Also the design of the recording system should not preclude its use as a general purpose recorder.

Using a digital computer for the generation of histograms the interface between recording system and computer must be established. Because of the continuous and sequential nature of the information it is feasible to use either on-line replay, or off-line with magnetic tape or paper tape. At the time of the development of the recording system the University was about to change to the Atlas computer and in these early days did not recommend any other than off-line usage with paper tape.

In order to reduce the volume of input to the computer only successive maximum and minimum values of the analogue signal are required on the paper tape. To process information up to a nominal 20c/sec. generated through a filter with slope of 20dB/oct. a maximum information rate of about 60c/sec. must be acceptable for three figure accuracy. Thus if a four character word represents each maximum or minimum this corresponds to a character rate of 480 char/sec. A Creed paper tape punch of 33 char/sec punching rate was available in the department at the time. Clearly the replay of the information for punching must take place at one sixteenth of the recording speed. The recording is to be done on magnetic tape and to obtain the information from the magnetic tape at

one sixteenth of the recording speed a flux-sensitive replay system is used.

Two methods of recording are considered; analogue (f.m.) and digital. The former means that digitization occurs on replay, and in the case of the latter, before recording. However f.m. recording is ruled out because of the ½% full scale resolution requirement. With digital recording of instantaneous values of the signal the volume of information is very large, necessitating fast (and expensive) digital systems. Conversely if we record only maximum and minimum values the volume of information is substantially reduced. However such a recording system would not be very useful for general purposes.

Incremental digital recording (that is the recording of increments in the signal) substantially reduces the volume of information about the signal. However it has the inherent characteristic of accumulative errors. Because of the limitations of magnetic tape (in respect of quality and wear) low pulse densities, together with careful tape handling and high standards of deck cleanliness, would be necessary.

Successful use in computers of magnetic tape with densities up to 800 p.p.i.*, together with manufacturers' claims (of one or less drop-outs over 1800ft. for eight tracks at 200 p.p.i.) encouraged the view that performance at 200 p.p.i. or less would be acceptable. Also the bit rate for incremental recording can be reduced by buffering the information. To record 16 full scale cycles per second using increments of 1/500 full scale means accepting a bit rate of 16 kc/sec. Through buffering up to seven pulses and recording a three bit word parallel tracks, the word rate to tape would be 2.3 kc/sec - quite acceptable at 15 i.p.s.**

* p.p.i. - pulses per inch.

** i.p.s. - inches per second.

In this application where maximum and minimum values are ultimately required, buffering has a negligible effect on accuracy as the signal changes less rapidly in the neighbourhood of maximum and minimum values. As far as general purpose recording is concerned it is equivalent to sampling the signal at a rate acceptable to the magnetic tape medium.

A further advantage of incremental recording is that slower digital systems may be used - thus each digital electronic unit will be cheaper. Wow and flutter characteristics of the tape deck are not critical as the digital information itself contains clock pulses.

Such a digital recording system requires a multi-channel tape recorder with acceptable skew characteristics. However at the time of development a recorder with the required tape speed ranges together with flux-sensitive replay facilities had just become commercially available at a reasonable price.

The system developed here is an incremental recording system with a clock frequency of 16kc/sec and input signal range of 0-1 volts. The incremental step is 1/500 full scale (i.e. 2 m V). The digital unit value used throughout is 1 mV so that the system counts in steps of two digits. The information corresponding to a step of 2 mV is called one bit. The system buffer accepts up to seven bits in every eight clock cycles. The tape speed for recording is 15 i.p.s., corresponding to a pulse density of 133 p.p.i.

There follows a description of the Digital Recording System. Details of the circuits of logic units, amplifiers and other units can be found in Appendix 1.

3.2 Principles of Operation of D.R.S.

3.2.1 Recording

The central unit of the system is an analogue to digital converter. A three figure BCD counter controls a set of current switches such that the current into the virtual earth (e, Fig. 3.1) is proportional to the number in the counter. The feedback in the system maintains the relation

$$v_{in} = i.R$$

that is

$$v_e = 0$$

in the following manner.

An out of balance in the above relation causes the virtual earth potential to change by the same amount. This out of balance is amplified and opens the gate (Fig. 3.1) allowing pulses from the oscillator into the counter. The counter polarity control is directed by the polarity of the out of balance. The gate remains open until the input voltage is balanced. Thus the number in the counter is always proportional to the input voltage.

The pulses passing through the gate are stored and output in batches onto magnetic tape. A 'batch' is the resultant count of pulses received during each cycle of eight oscillator pulses, and can be a count of up to plus or minus seven. The eighth clock pulse is directed from the gate to allow time for the store unit's output and reset operations. The maximum amount of seven means that only three magnetic tape tracks, for binary -coded recording (excluding polarity tracks), are required.

3.2.2 Replay

The batches of pulses are replayed from magnetic tape into a serializer and then input into the counter

with the polarity information. The system therefore integrates the information on tape into digital values which continuously represents the original data, and which can be sampled when required. Maxima and minima are detected by changes in batch -polarity, and the number then in the counter is stored in a memory unit for subsequent decoding and punching onto paper tape.

To cater for the low speed of paper tape punches the tape recorder is replayed at a fraction of the recording speed. The system was originally designed for a Creed punch (33 ch/sec) but was subsequently used with a Westrex (120 ch/sec)

A 'staircase' model of the original analogue signal can be constructed with the system in Fig. 3.2 which uses an operational amplifier.

3.3 Details of D.R.S.

3.3.1 Input Amplifiers, Gate and Polarity Control

The input amplifiers operate the gate and polarity control from the out-of-balance signal on the virtual earth. The amplifiers are d.c. differential; for the gate both output stages drive an OR unit and for the polarity control they drive either side of a bistable unit. There is more gain in the polarity control circuit so that polarity is registered ahead of the operation of the gate (Fig. 3.3).

The detection thresholds of the gate circuit are $\pm$ 2.5 mV. Thus there is a 'dead-space-region' to reduce the incidence of triggering of the system by noise.

3.3.2 Store Unit

The store unit receives the main counter input pulses and polarity information and is controlled by record-command signals from the record control unit. The count of pulses received between record-command signals is output in binary code (with polarity) to the magnetic tape recorder input modules. After each record-command signal the store unit resets itself to zero. When the count is zero a pulse is output on the "+" track so that the "+" and "-" tracks together constitute a clock record.

The unit consists of a four stage binary counter and the coding networks for output. The counter's first three stages store the batch count, the fourth stage is the batch polarity register (Fig. 3.4).

3.3.3 Binary Coded Decimal Counter

Four binary units connected in series form a sixteen bit counter, whose counting sequence is scale corrected to form a decimal counter. The scale correction technique used maintains a constant place 'weight' for each binary place of 1, 2, 4 and 2 respectively. The BCD counter is shown in Fig. 3.5 together with its counting sequence. The scale corrections are instantaneous transfers from 0001 to 0111 when adding and 1011 to 1110 when subtracting (least significant bit on the left).

Each binary unit controls a current switch whose output into the virtual earth is proportional to the place weight.

Three of these BCD counters connected in series form a three digit counter. By removing the binary unit for the

last significant place the resolution of the counter is changed to 2 in 1000. This involves a modification to the scale correction circuitry for this stage (Fig. 3.6).

3.3.4 Control Unit (Record)

The function of the control unit is to provide a clock of 16 kc/sec, to direct seven out of eight clock pulses to the gate, and to provide the record-command signal for the store unit. It consists of a square-wave oscillator and a three stage binary counter (Fig. 3.7).

The square wave oscillator is formed by interconnecting two logic units with a resistor-capacitor network. The square wave is not symmetric (i.e. does not reverse at half-period) to limit the scatter of the main-counter input pulses (see below).

3.3.5 Gate and Polarity Control Timing Circuits

In Fig. 3.3 the logic unit 1 releases its inhibit on the gate randomly so that the length of the trigger pulse varies. A very short pulse may marginally trigger the main counter but not the store unit, or vice verse. To prevent this the gate is followed by a Schmidt trigger which drives a monostable. From the second (positive going) edge of the monostable output is derived a trigger pulse sufficient to drive both counter and store unit simultaneously and without ambiguity.

Optimum timing of the trigger pulses relative to the record and reset operations of the store unit is achieved through reducing the scatter on the triggering by reducing the period (t_o) when the clock is at zero (maintaining a constant clock frequency) Fig. 3.8. To prevent more than one trigger pulse per clock pulse a second monostable inhibits further triggering.

Whilst the pulses go through the counter, transient spikes appear on the virtual earth. For example in the count 499 to 500 the counter takes the steps 499, 490, 400, 500. The unbalance is usually of the same polarity as the step taking place, as in the example. However during scale correction transient reversals of polarity can occur whilst a pulse is in transit through the counter. The response of the polarity control is therefore damped by introducing a delay in polarity switching. Changes in polarity occur only if still required after the delay (during which the gate is kept closed, Fig. 3.9).

3.3.6 Serializer

The principles of operation of the serializer are to set a three stage binary counter to the bit pattern of the batch and to subsequently recycle this counter to zero - the clock pulses effecting this being the serial pulses required.

The bit pattern from tape is received into buffer bistables which set the three stage counter. The setting of a polarity buffer initiates the cycling of the replay control unit. During the second half cycle of the control unit pulses are gated into the three stage counter (and of course into the main counter) until the three stage counter reaches zero. The main counter polarity control is directed from the polarity input buffers. The three binary digit buffers are reset and locked for the second half cycle of the control unit (Fig. 3.10).

3.3.7 Control Unit (Replay)

The function of the control unit is to provide a

clock of 8 kc/sec which controls the replay sequence through a four stage binary counter, cycling over sixteen clock pulses. This cycle takes place whenever a polarity input bistable is set, but after the delay period necessitated by tape skew.

The control unit times the commands to the memory unit and encoder in the data output channel, and directs the second half-cycle of pulses into the serializer. During the second half-cycle the three bit input buffers are reset and locked. At the end of the cycle the polarity buffers are reset. (Fig. 3.11).

3.3.8 Data Output

The data output channel is triggered by changes in batch polarity. The number then in the counter is stored in a memory unit and coded to the input requirements of a commercial encoder. This encoder is triggered by a 1 ms. pulse derived from the second half-cycle of the control unit. Further triggering of the output channel is inhibited until the 'punch-complete' signal is received from the encoder, when the memory unit is also reset. (Fig. 3.12).

The input code of the encoder is ten parallel lines per digit, a signal voltage being on the line corresponding to the required digit. This is achieved with the decoding network in Fig. 3.13, the code of the memory unit being that of the counter; binary coded decimal.

The encoder punch command signals are synchronized from the punch unit which cycles at a constant rate corresponding to 120 char./sec (for the Westrex). The paper tape records consist of three decimal characters and one terminating character. The average maximum triggering rate of the output channel is therefore about 23 records per second.

The reconstructed analogue signal is used for monitoring the replay operation. The circuit which generates the analogue signal, and its performance, are given in detail in Fig. 3.14.

The data output channel is also triggered by the manual sampling facility on the system console.

3.4 Input and Output

3.4.1 Recording Mode

Five tracks of binary information are to be recorded with the facility for replay at 1/16 of the recording speed, using a flux sensitive replay system. Three modes of recording are considered, which involve leaving the tape periodically fully saturated (either positively or negatively) or without any magnetization (zero flux). The first mode is non-return-to-zero (NRZ) where the tape is always fully saturated in one or other direction. A recorded pulse is stored as an instantaneous change of the saturation polarity (Fig. 3.15a). The second is return-to-saturation (RS) where the tape is saturated at one polarity except where a pulse is recorded, when there is a temporary reversal of polarity (Fig. 3.15b). The third is return-to-zero (RZ) where the tape is unmagnetized except where a pulse is stored, when there is a temporary saturation of the tape in one direction (Fig. 3.15c).

Although a flux-sensitive system can read flux while the tape is stationary it cannot satisfactorily read signals of long wavelength. NRZ saturation recording or RS recording leaves a flux distribution per cycle corresponding to two bar magnets laid end to end in opposite directions.

As the wavelength increases the field strengths at the centres of the effective magnets decrease because their poles move further apart, leading to the replay signal in Figs. 3.15d and 3.15e.

Thus neither NRZ or RS recording can be used here as the gaps between pulses are indeterminate. The RZ mode in Fig. 3.15f is used leaving the tape saturated for fixed lengths or otherwise unmagnetized.

3.4.2 Recoder Limitations

The system records signal increments and is therefore an accumulative error system. Loss of information must therefore be highly improbable for acceptable performance. To minimise drop-outs from tape the maximum pulse density tolerable is 200 p.p.i. consistent with computer practice - although systems incorporating re-reading, noise detection, parity and such-like allow higher densities. Secondly without sophisticated 'de-skewing' hardware the recording system is skew-limited (see section on I/O circuits).

The recording clock frequency of 16 kc/s.(note; the tape recording frequency of 2 kc/s. leads to a minimum tape speed of 15 i.p.s.) results in a packing density of 133 p.p.i.

The incidence of drop-outs at this packing density was examined using counting instruments monitoring the data channels for both output and input when respectively recording and replaying random noise. In twenty sample recordings lasting one minute each no drop-outs were registered.

3.4.3 Input/Output Circuits

The I/O circuits are designed according to the tape skew and speed characteristics. The manufacturers specification for tape skew is less than .002 ins. across four tracks which includes the static skew, due to misalignment of the record and replay heads. This misalignment was virtually removed by the manufacturers who specially machined the relevant surfaces. Tests were carried out at the record and replay speeds measuring the effect of skew as the scatter in pulses on replay after being recorded simultaneously on the five tracks used.

A square wave pulse of duration equal to the interval between the first and last pulse was displayed on an oscilloscope. The persistence and brightness of the oscilloscope were adjusted so that the distribution of the pulse duration could be ascertained. Deviates of similar brightness enclosing most of the distribution were 0.2 and 0.6 msec. Assuming a Rayleigh distribution, a very safe estimate of the standard deviation is 0.4 msec. (corresponding to 10% and 90% confidence limits of 0.18 and 0.86 msec. respectively. The maximum scatter the input circuits can accept is 2.5 msec., corresponding to a probability of exceeding of 1 in 3.3×10^{-9}, or an expectation of one in about 40 hours of recording time. This figure is, of course, very sensitive to the estimate of the standard deviation, but this estimate was made extremely conservatively.

To minimise the effect of skew the polarity tracks are positioned on either side of the three digit tracks so that a batch of pulses can occupy a maximum of four adjacent tracks.

Both the mains frequency stability and the wow and flutter characteristics of the tape deck affect the tape speed.

The recorder was powered by a static inverter. Continuous monitoring of the frequency of the inverter (which alters as the batteries drain) enables it to be maintained to well within 2 c/s. The wow and flutter specification for the recording and replay speeds used are 0.25% r.m.s. and 0.5% r.m.s. respectively, making an aggregate effect of $\pm$0.75%r.m.s.

In Fig. 3.16 is shown the timing of the replay sequence. It is evident from the figure that the nominal 8 ms. replay sequence cannot be reduced to below 4.5 ms. For example a permitted variation of $\pm$10c/s in mains frequency could lead in the worst case to an interval of 5.3 ms. between batches. Superimposed on this could be 0.8 ms. of wow and flutter, i.e. thirteen standard deviations (or for a Gaussian distribution a probability of exceeding of 1 in 10^{38}). Clearly there is more than adequate margin for both static and dynamic variation in tape speed.

3.5 Performance of D.R.S.

The basis characteristics of the recording system are an accuracy of $\pm$2.5 mv. in a signal range of 0 to 1 v., and a maximum average following rate of 28 volts/sec. in 2 mv. steps. The input signal may be either d. c. coupled or a. c. coupled to a d. c. bias of half-full scale.

Some characteristics of the system have a reduced effect on its performance when considered only as a recorder of maxima and minima. The effect of recording in batches every eighth clock pulse is negligible in the region of maxima and minima, when the signal is changing least rapidly. In addition the system is more accurate at maxima (+ 2.5, - 0mv) and minima (+ 0, - 2.5 mv.). By adding or subtracting 1.25 mv. when processing the results the accuracy becomes $\pm$ 1.25 mv.

The performance of the system with respect to its accumulative error characteristic is next considered. Unlike analogue recording data introduced or lost through noise on h.t. lines, drop-outs on tape, etc. will affect the remainder of the record. The tape recorder performed excellently in drop-out tests. (See Appendix 1.) Adequate care was always taken in tape handling and deck cleanliness. Noise suppressors are incorporated into the mains supply.

The performance was measured as the drift of d.c. bias during three series each of twelve recordings. The recorded bias should be accurate to within $\pm$ 2 mv.) Two series were recordings of sine-waves and lasted 80 and 200 secs per recording respectively. In the third series filtered random noise was recorded for 80 secs per recording. The whole duration of all recordings was about 70 minutes. The d.c. values for each series lay within the tolerance of the system.

Finally the effect of the rate of following is shown in Fig. 3.17. This graph gives the maximum sine-wave amplitude against frequency for three cases:

1. Complete following of the sine-wave to within the maximum accuracy of the system (i.e. maximum gradient less than 28 v/sec.)
2. Following of the sine-wave such that only the maximum and minimum values are recorded accurately. The solution to this problem was found numerically (using the fact that it lies between the complete following case and the frequency for which the system can generate a saw-tooth waveform of the same amplitude (Fig. 3.18).
3. From actual measurements the following of the

sine-wave to give a peak out-of-balance of ± 20 mv. on the virtual earth. (This is a very artificial criterion and is used only because of the difficulties involved in measuring cases 1 and 2 accurately).

Case 3. demonstrates that the system is at least 12½% slower than Case 1. suggests. This is due to the delay in the polarity circuit, particularly during scale correction when transients occuring at the virtual earth cause the polarity circuit to block the gate for 150 μs. Whether or not the inhibit occurs during scale correction depends on the overall out-of-balance of the virtual earth. For low unbalances, most transients cause such an inhibit. For high unbalances most of the transients will not cause the virtual earth unbalance to change sign. Thus for the ±20 mv. unbalance (Case 3) the following rate is cut to less than 24.5 volts/sec. (for which complete following coincides with case 3). However for the larger unbalances occuring in Case 2 the effective clock frequency will approach 28 volts/sec. so that Case 2 is more representative of the system's actual performance.

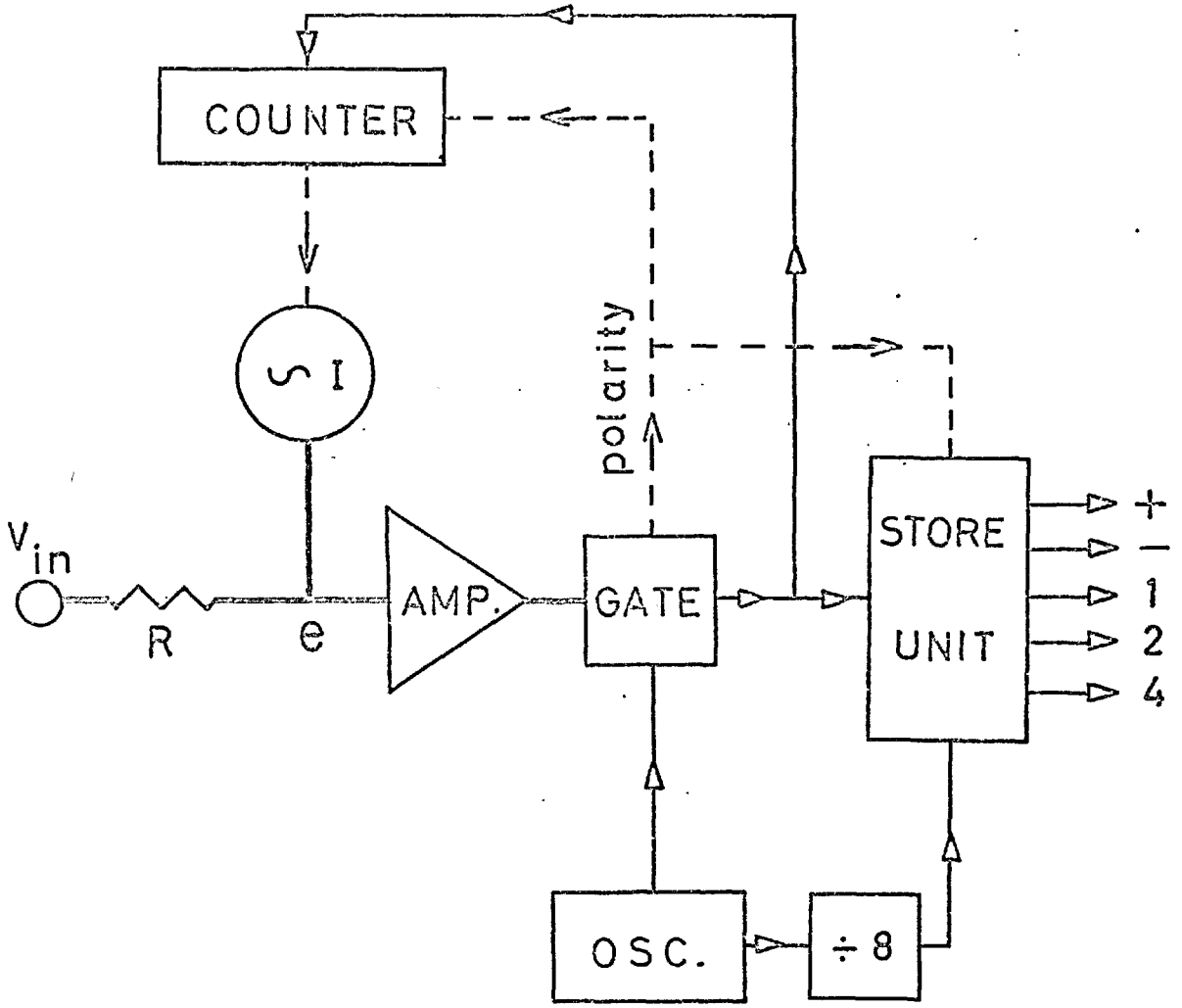

FIG. 3.1 RECORD SYSTEM

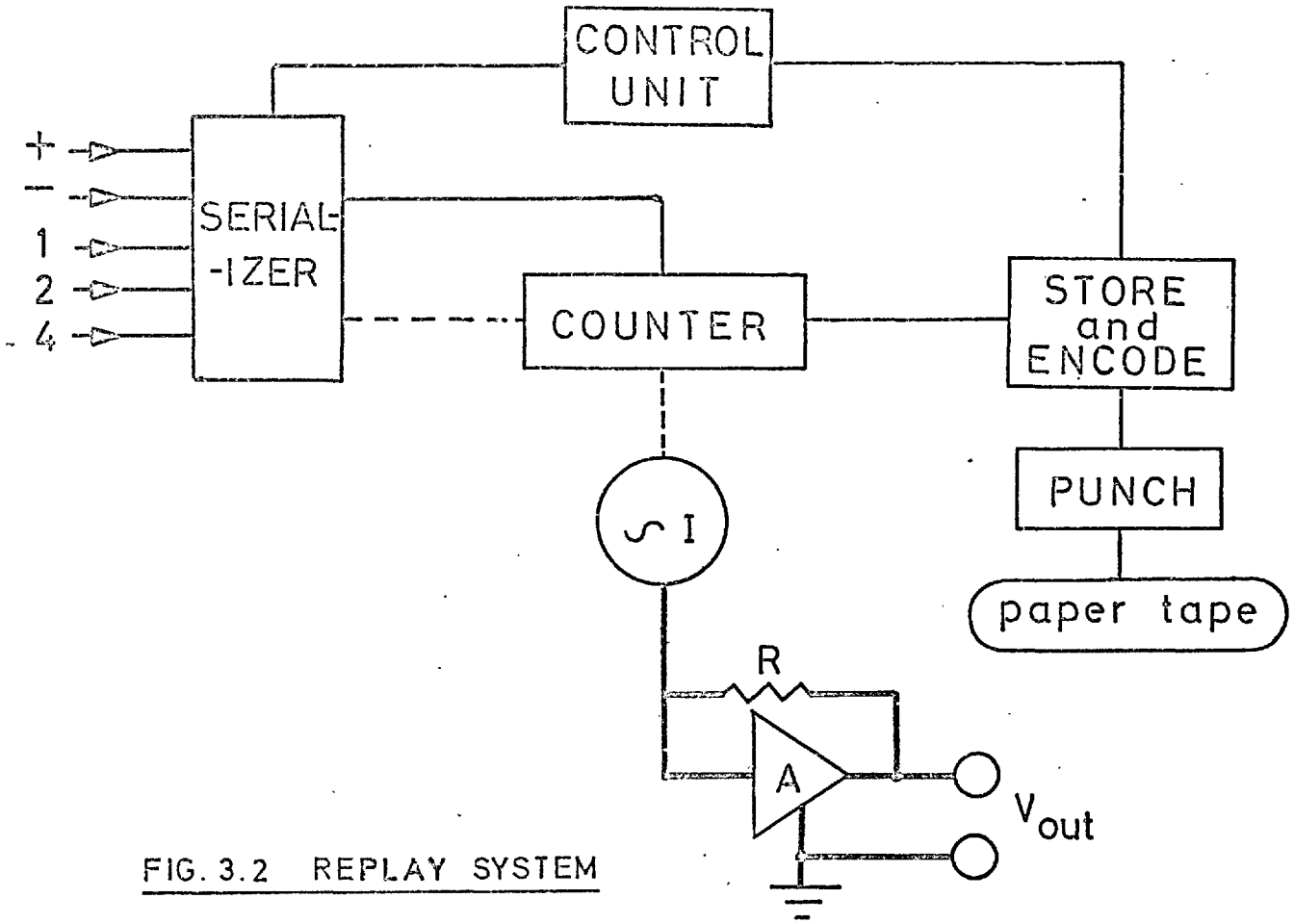

FIG. 3.2 REPLAY SYSTEM

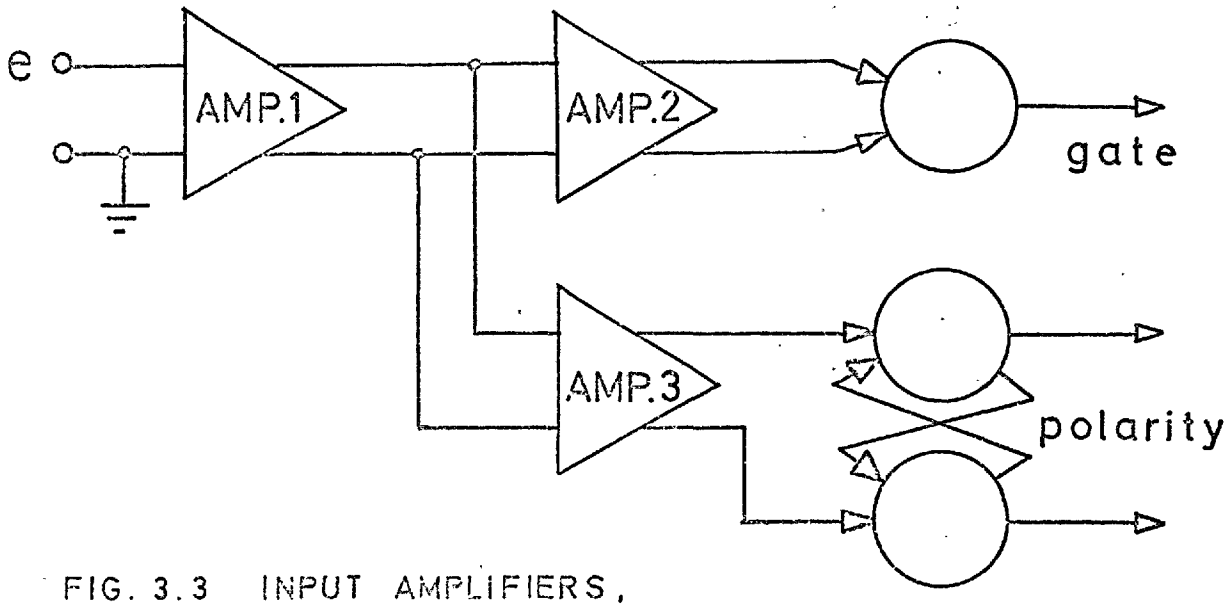

FIG. 3.3 INPUT AMPLIFIERS, GATE AND POLARITY CONTROL

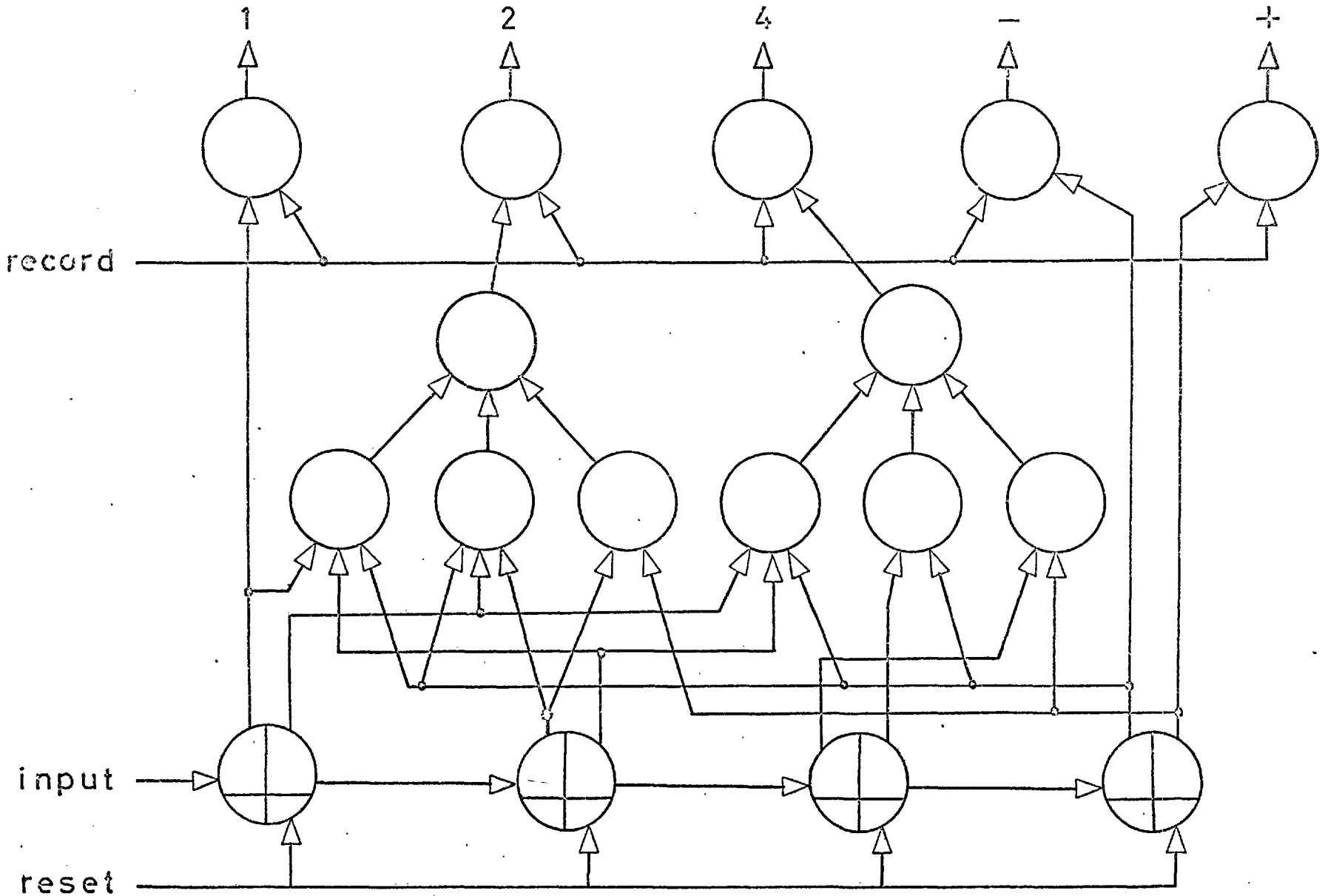

FIG. 3.4 STORE UNIT

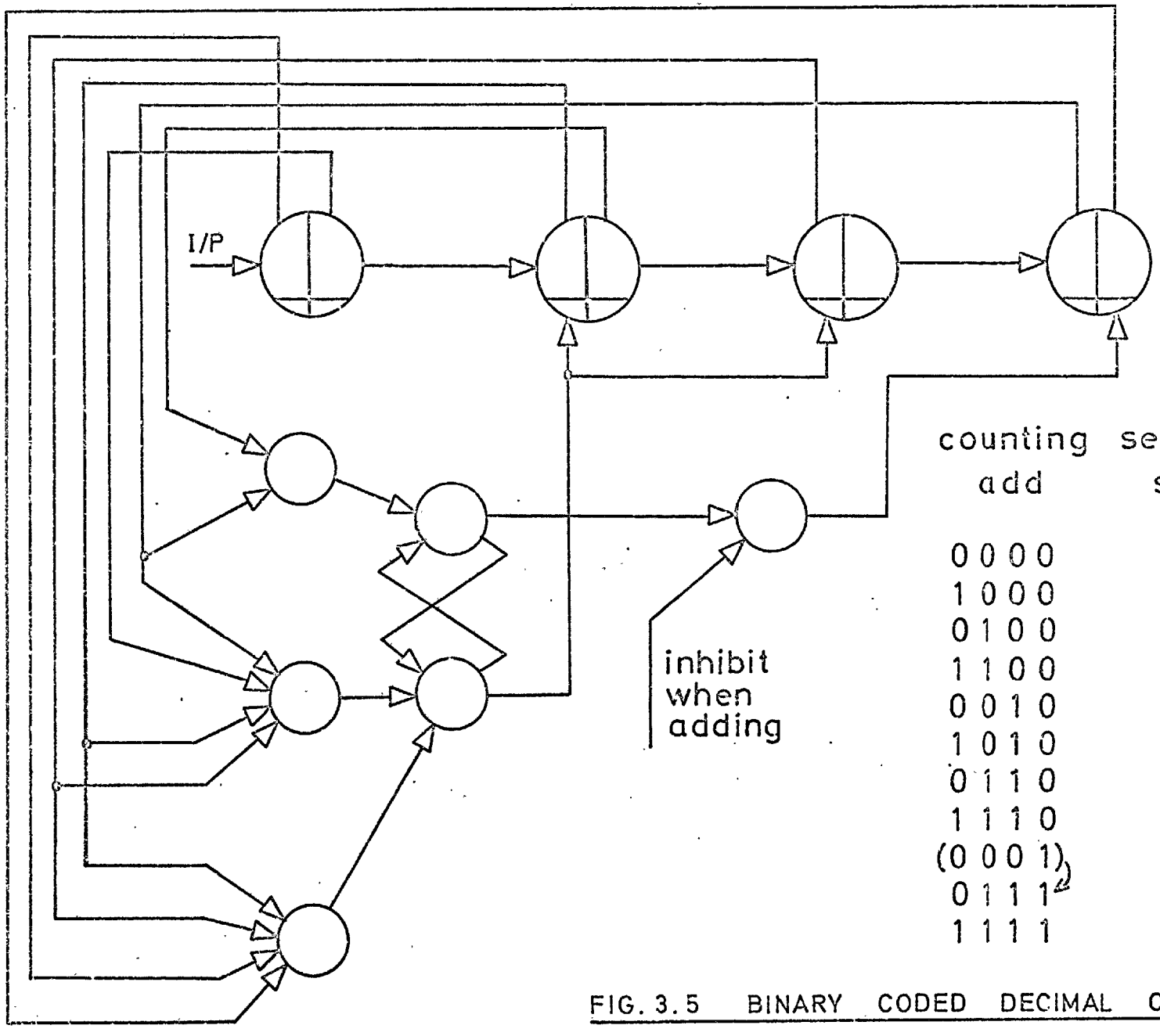

counting sequences	
add	subtract
0 0 0 0	0 0 0 0
1 0 0 0	1 0 0 0
0 1 0 0	0 1 0 0
1 1 0 0	1 1 0 0
0 0 1 0	0 0 1 0
1 0 1 0	1 0 1 0
0 1 1 0	0 1 1 0
1 1 1 0	1 1 1 0
(0 0 0 1)	(1 0 1 1)
0 1 1 1	0 1 1 1
1 1 1 1	1 1 1 1

FIG. 3.5 BINARY CODED DECIMAL COUNTER

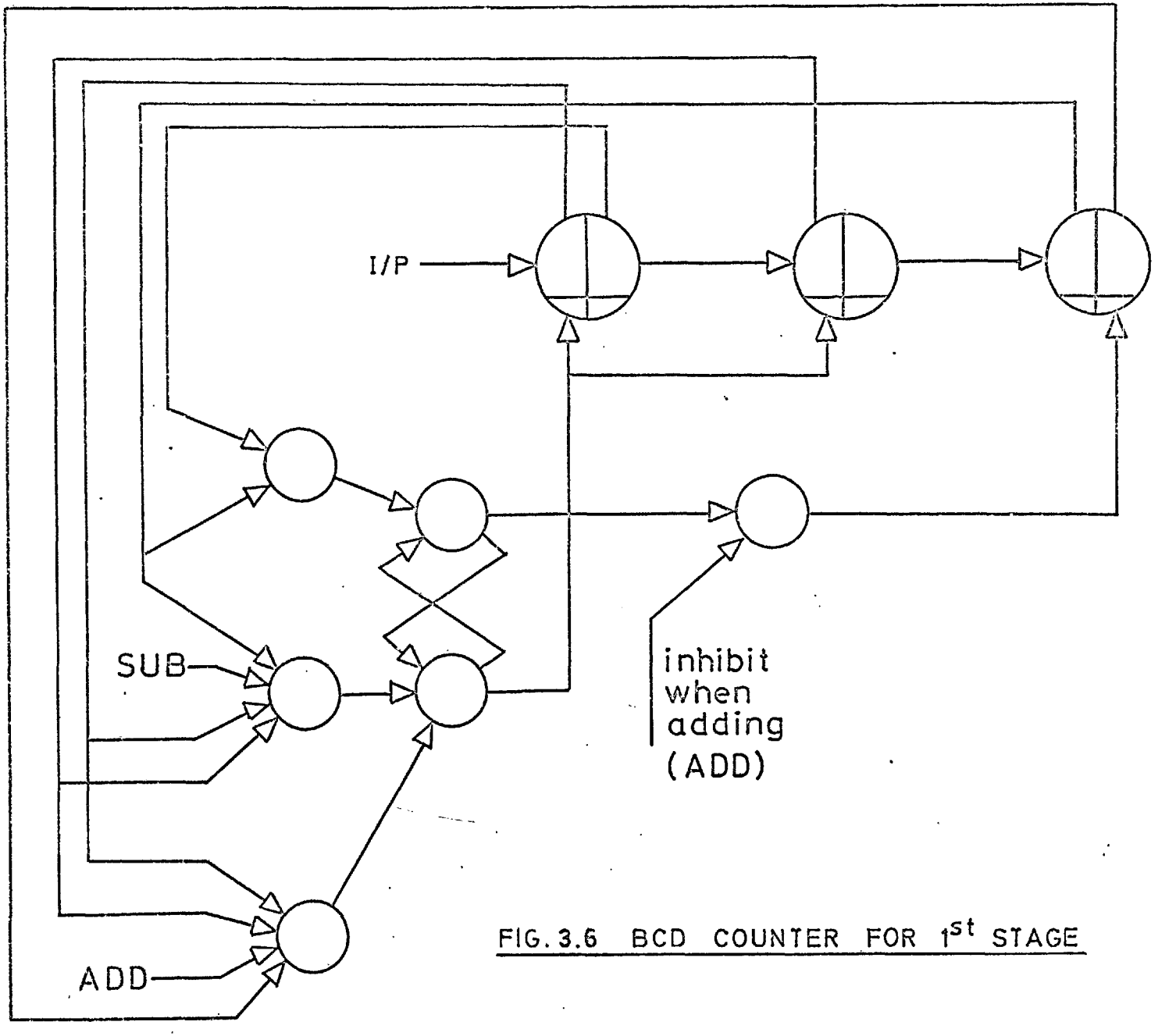

FIG. 3.6 BCD COUNTER FOR 1st STAGE

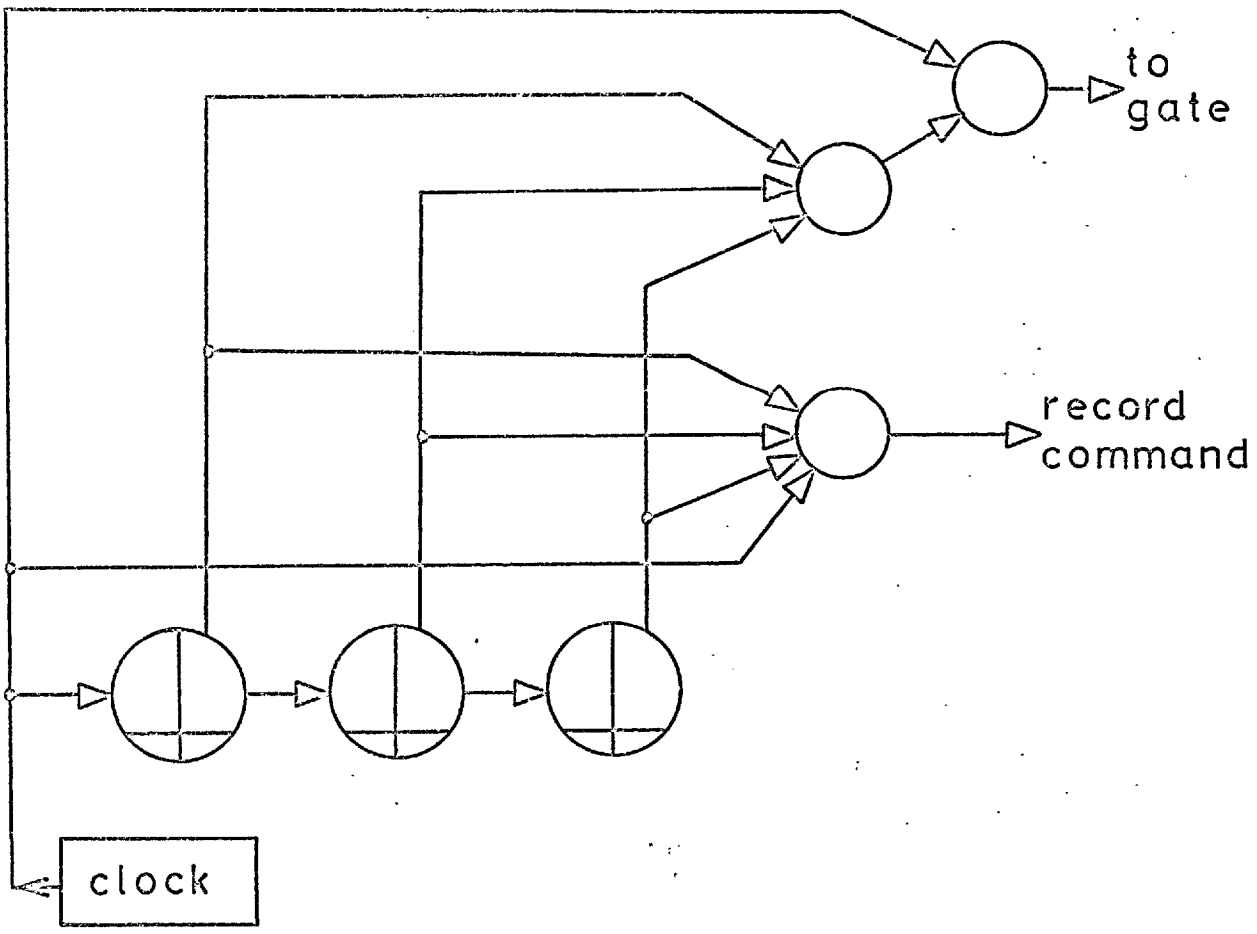

FIG. 3.7 CONTROL UNIT (RECORD)

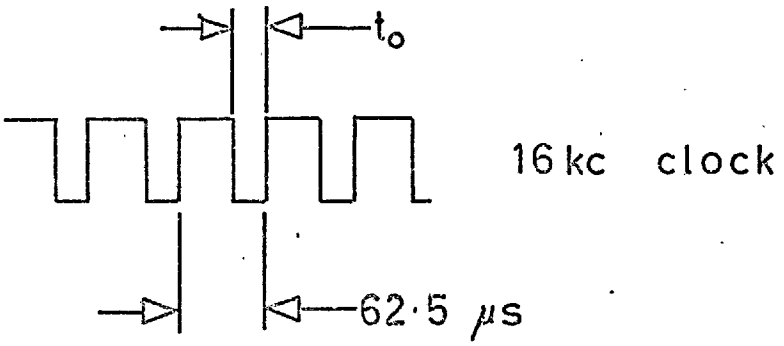

FIG. 3.8 CLOCK WAVEFORM

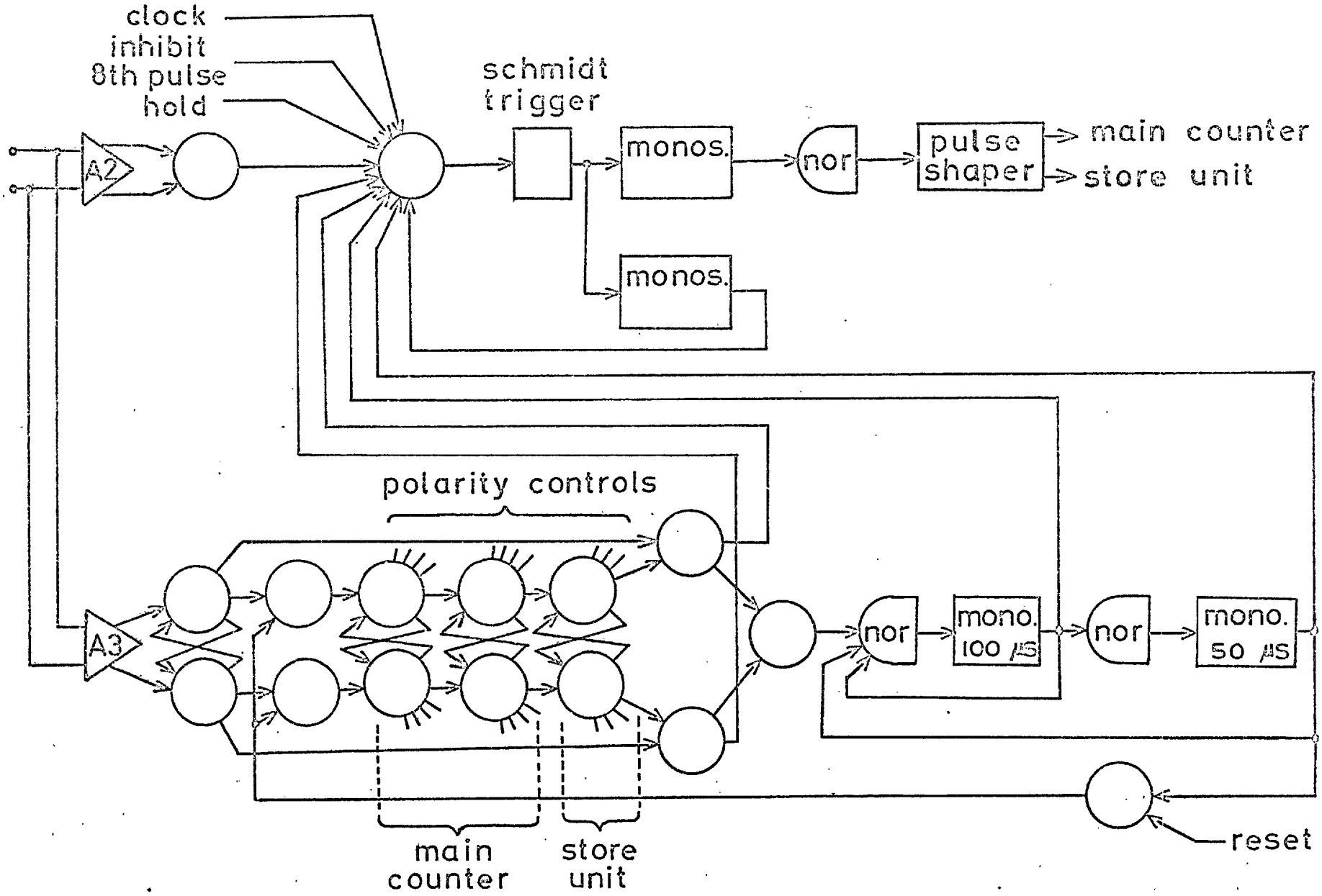

FIG. 3.9 GATE & POLARITY CONTROL TIMING CIRCUITS

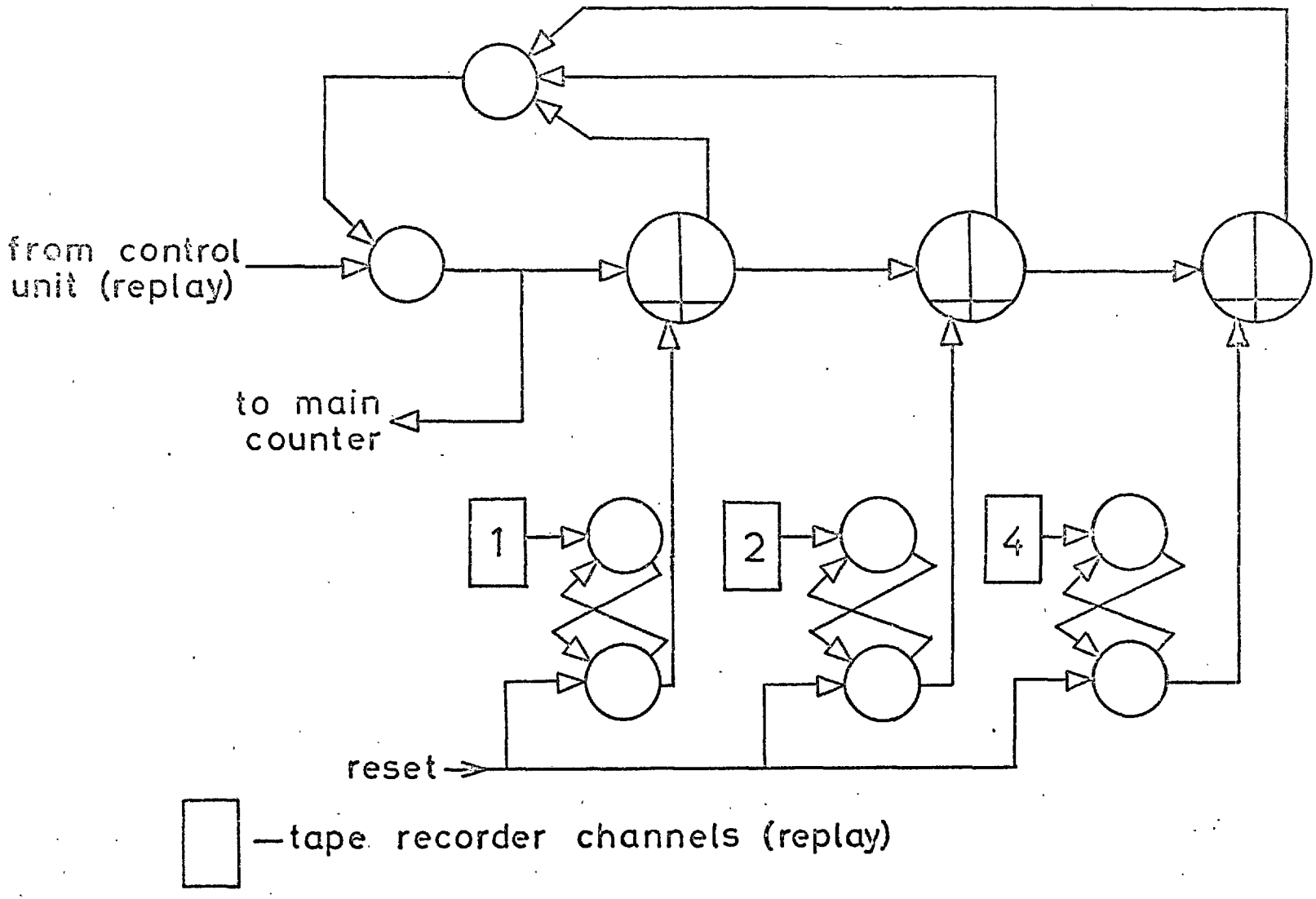

FIG. 3.10 SERIALIZER

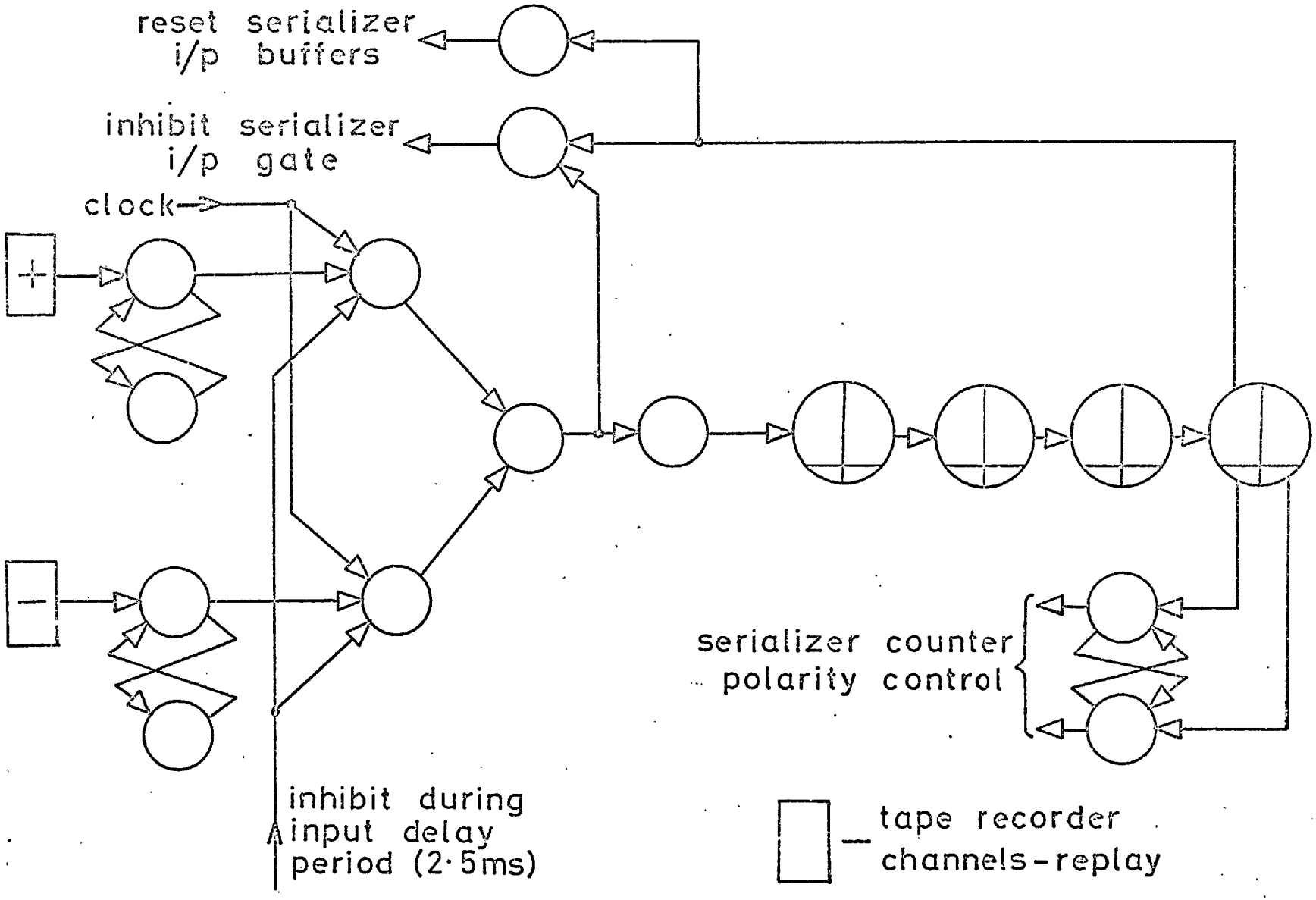

FIG. 3.11 CONTROL UNIT (REPLAY)

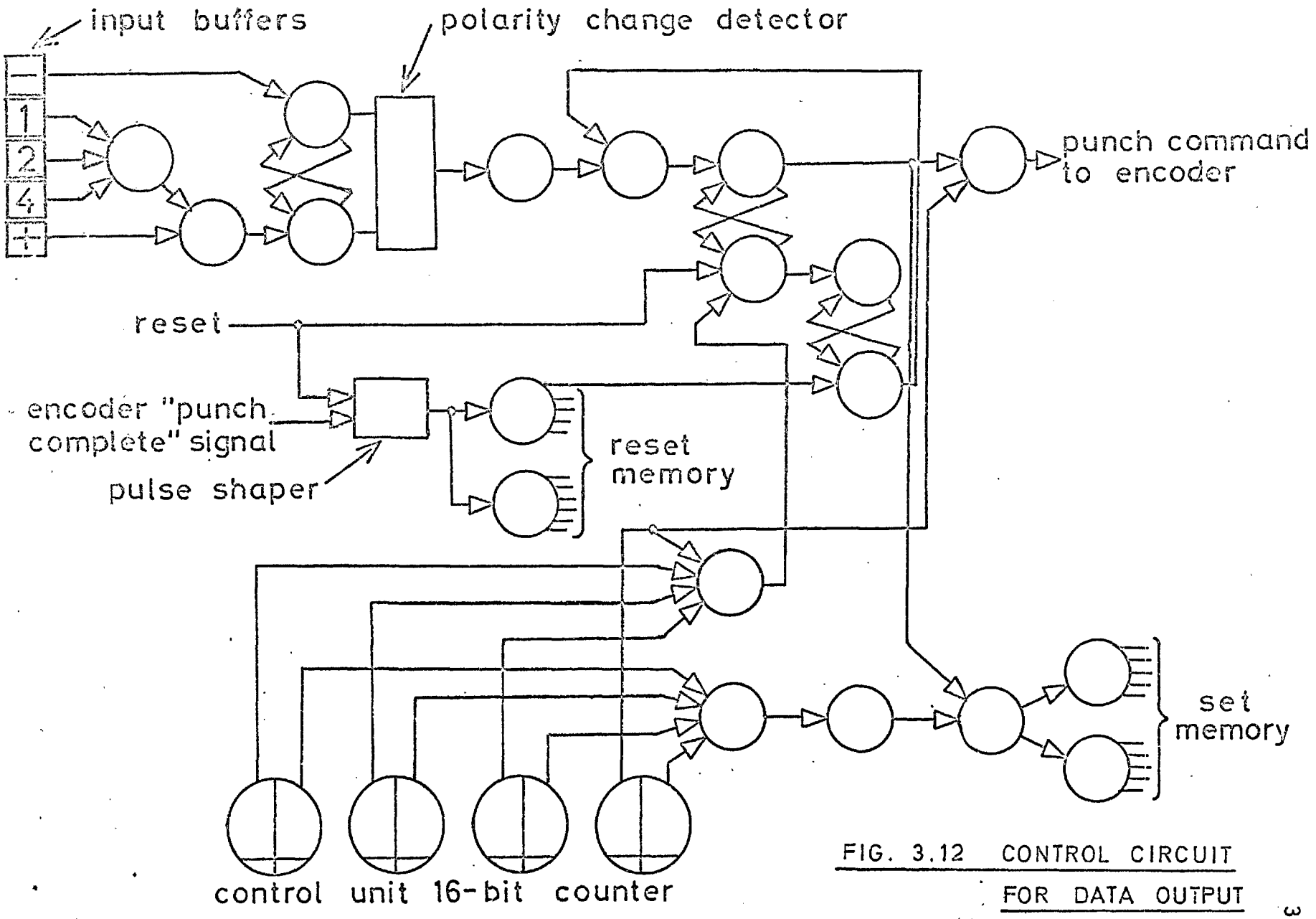

FIG. 3.12 CONTROL CIRCUIT FOR DATA OUTPUT

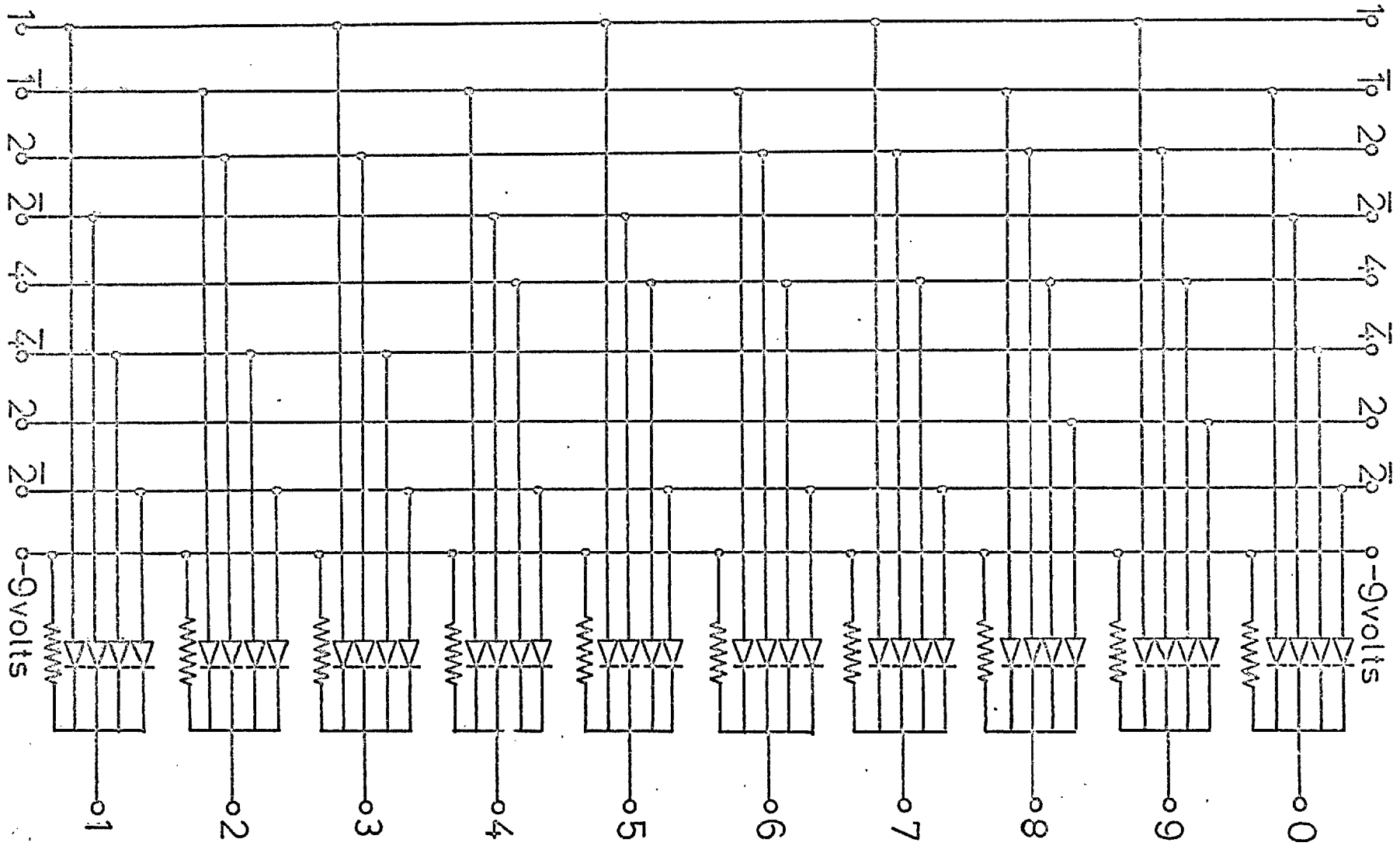

FIG. 3.13 BINARY TO DECIMAL DECODING NETWORK

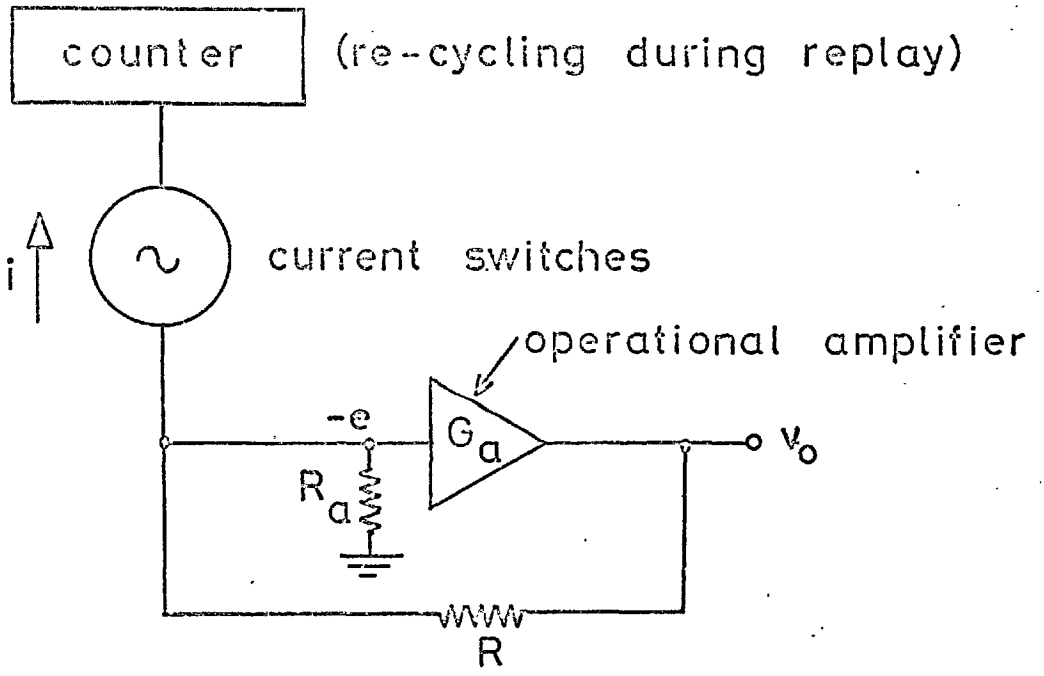

Circuit Performance

$$v_o = -G_a(-e)$$

$$i = \frac{v_o + e}{R} + \frac{e}{R_a}$$

$$\therefore v_o = \frac{i.R}{1 + \frac{1}{G_a}(1 + \frac{R}{R_a})}$$

$R = 500\ \Omega$
$R_a = 200\ K\Omega$
$G_a = 2000$

$$\therefore v_o = 0{\cdot}9995.iR$$

FIG. 3.14 RECONSTRUCTION OF ANALOGUE SIGNAL

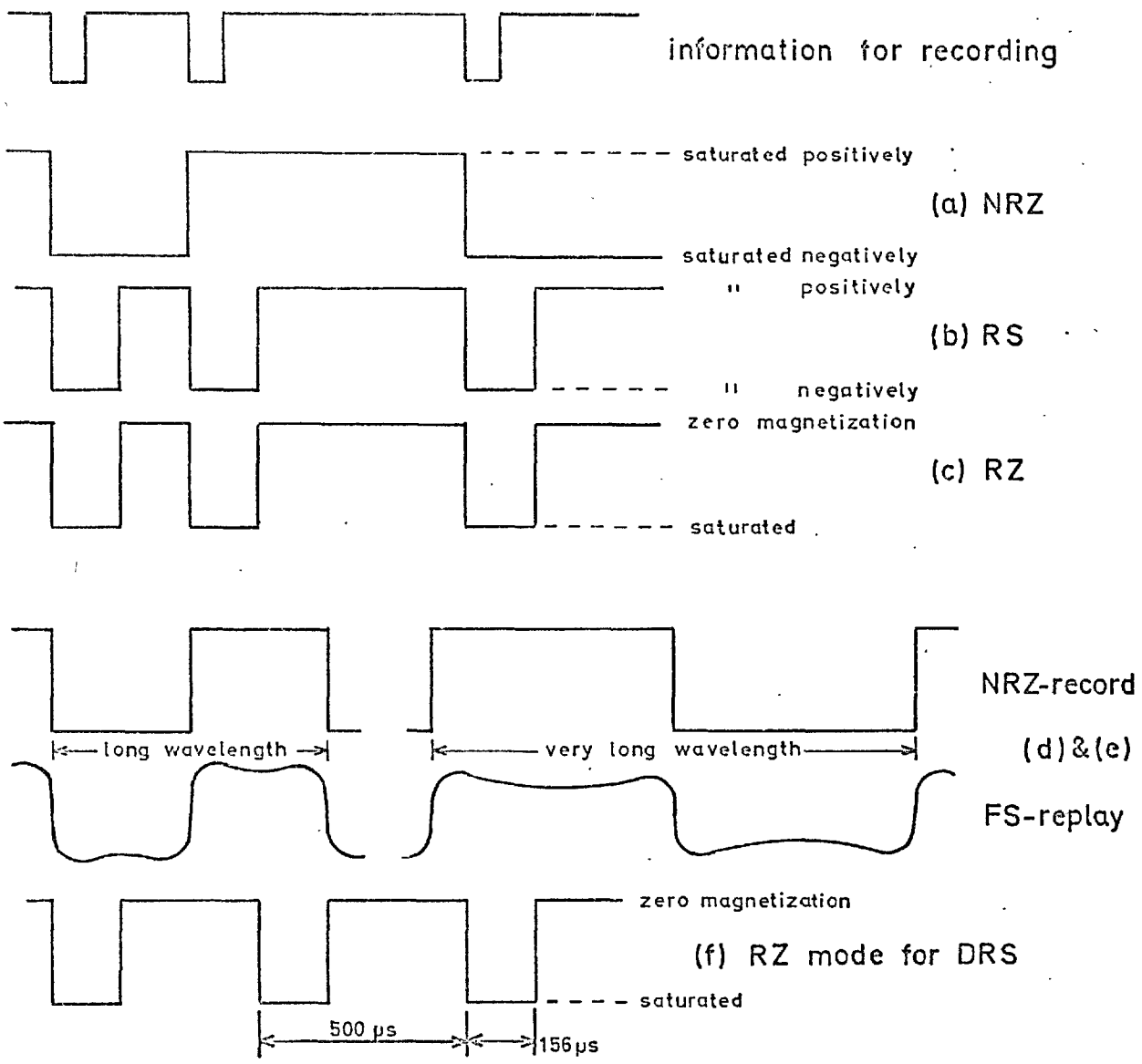

FIG. 3.15 RECORDING MODES

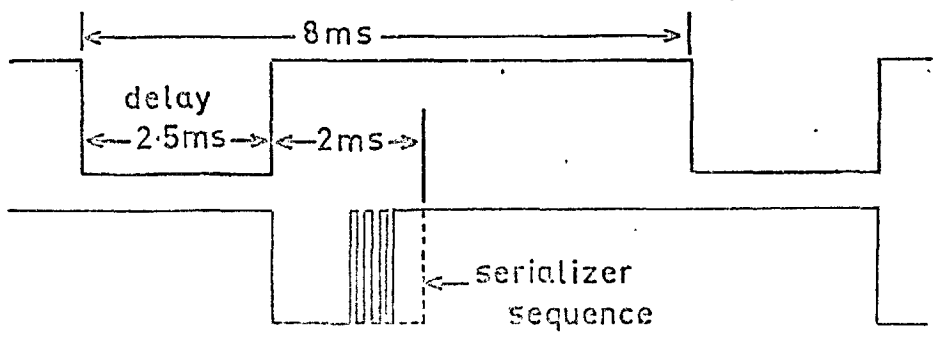

FIG. 3.16 TIMING OF REPLAY SEQUENCE

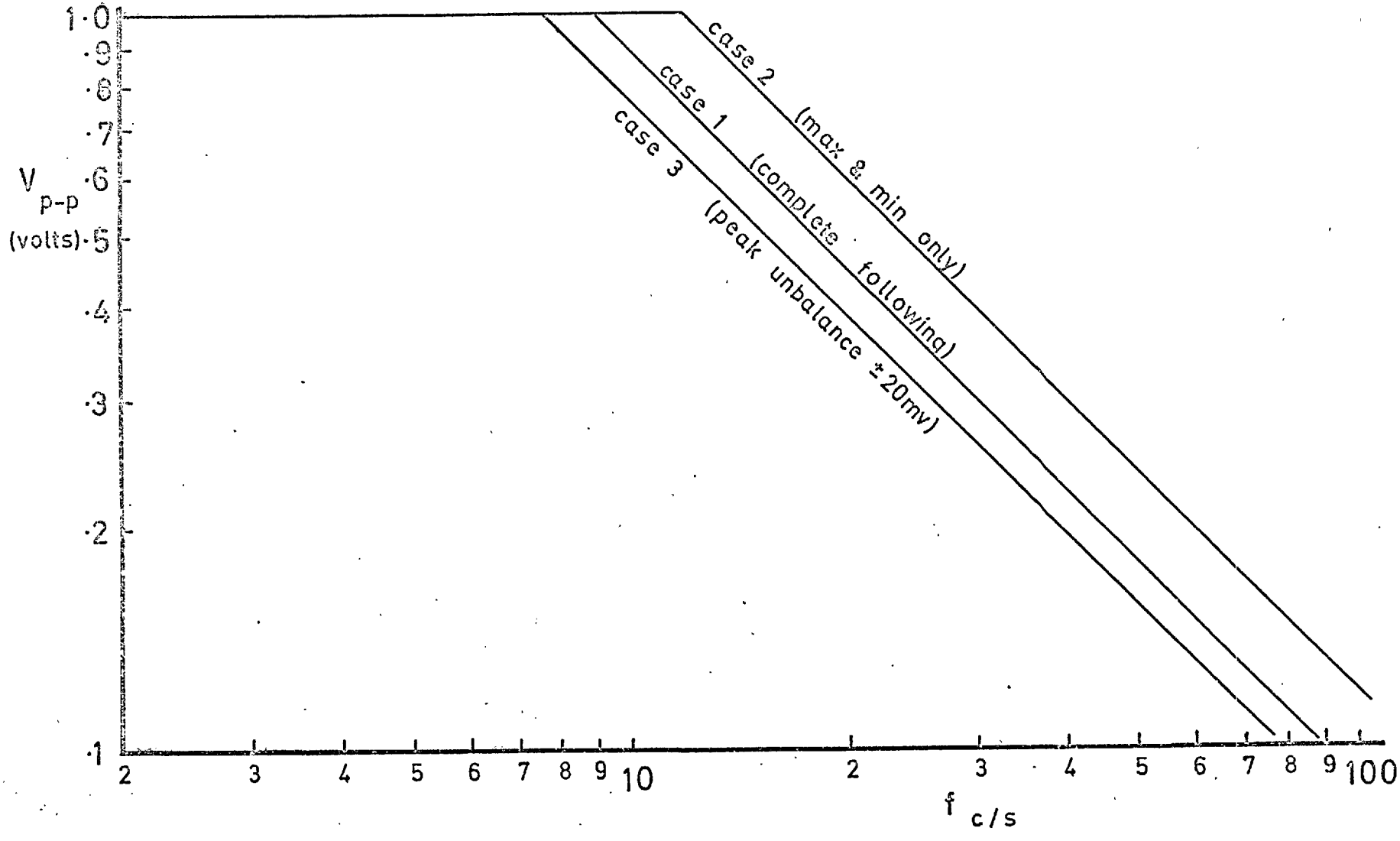

FIG. 3.17 PERFORMANCE OF D.R.S.

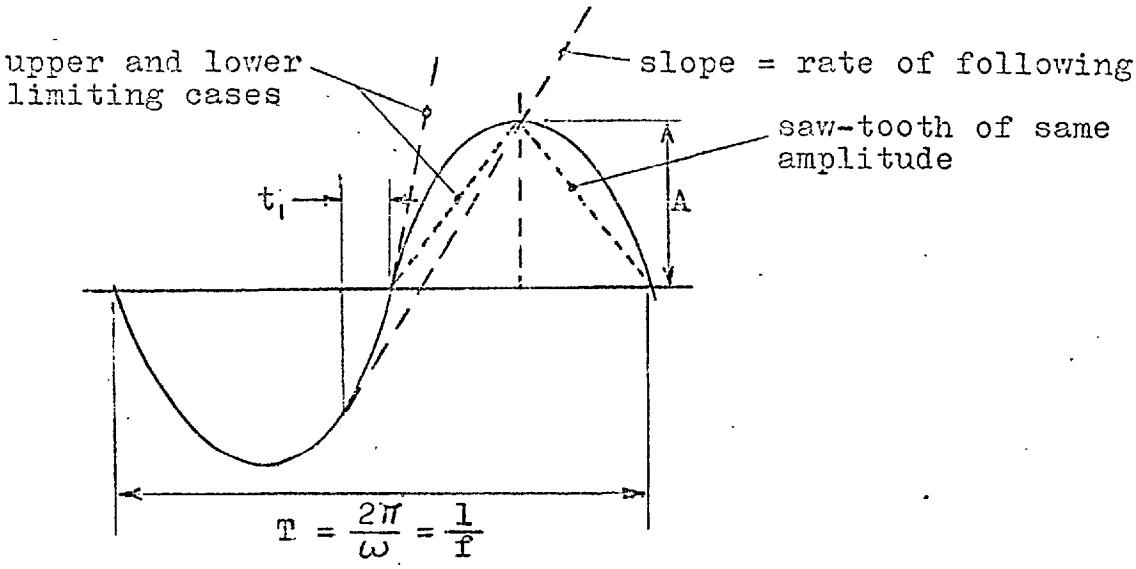

$v = A \sin \omega t$: $\frac{dv}{dt} = A\omega \cos \omega t$: $R = A\omega \cos \omega t_1$

i.e. $t_1 = \frac{1}{\omega} \cos^{-1} \frac{R}{A\omega}$: Now $(t_1 + \frac{\pi}{2\omega})R = A(\sin \omega t_1 + 1)$

But $\sin \omega t_1 = \sqrt{\omega^2 A^2 - R^2} / \omega A$

i.e. $\cos^{-1} \frac{R}{A\omega} = \sqrt{\left[\left(\frac{A}{R\omega}\right) - 1\right]} + \frac{A\omega}{R} - \frac{\pi}{2}$

i.e. $\frac{R}{A\omega} = \sin \left[\sqrt{\left(\frac{A\omega}{R}\right)^2 - 1} + \frac{A\omega}{R}\right]$

Solution must lie between $R = A\omega$ (complete following) and $R = 4Af$, ($\omega = 2\pi f$), ramp of same A and ω

i.e. between $\frac{\pi}{2} \rangle \frac{A\omega}{R} \rangle 1$

Solution (found numerically) is

$$\frac{A\omega}{R} = 0.4198\pi$$

FIG. 3.18 FOLLOWING OF MAXIMA AND MINIMA

4 RECORDINGS

4.1 Introduction

Two series of recordings are made. In the first filtered random noise is used as the signal source. In the second series recordings are made of car suspension loads for a wider bandwidth case. The results are presented and discussed in Chapter 5.

For each recording the mean value is half full-scale (corresponding to a digital value of 500), and the recording levels adjusted to give a signal standard deviation of digital value 100. Thus the crest factor (the ratio between maximum recorded peak and the standard deviation) is five. Assuming a Rayleigh distribution of peaks the probability of the signal having a maxima (or minima) outside the range of the system is therefore 1 in 270,000. For irregularity factors less than unity a signal excursion outside the range is even less likely.

4.2 Filtered Random Noise

To match the capabilities of the recording system 'white' noise over a range of approximately 2 - 25c/s is required. As no such noise generator was available at the time, one was constructed using a miniature neon light as the noise source. A band-pass filter was used to limit the bandwidth of the signal so as to obtain the required values of irregularity factor.

Two sets of recordings were made with filter settings of 2-9 and 2-25c/s respectively. The characteristics of the filter for these two settings are shown in Fig. 4.1 and tabulated in Table 4.1. The values of irregularity factor

obtained were 0.792 and 0.732 which are lower than the corresponding figures for an ideal filter (0.835 and 0.728) due to the actual characteristics of the band-pass filter. However these figures obtained do agree remarkably well with the estimates made from the filter characteristics themselves (as discussed in Chapter 5).

4.3 Loads in car suspension

For these recordings a 'Mini' belonging to the Advanced School of Automobile Engineering (A.S.A.E.) of Cranfield College of Aeronautics was used. The car instrumentation consisted of strain-gauged load cells built into various suspension points. For the recordings the car was linked by cable to another vehicle containing the recording system. A view of this instrumentation vehicle showing the digital recording system and other ancillary equipment is given in Fig. 4.2.

The tests were performed on the Belgian pavé surface of the Motor Industries Research Association (M.I.R.A.) proving ground at Nuneaton. The vehicle containing the recording equipment accompanied the test vehicle on a smooth circuit lying outside the pavé circuit. A view of the pavé surface is shown in Fig. 4.3. The 'Mini' was driven on the pavé at a constant speed of 20 m.p.h.

The recording system was powered by a static inverter. A transistorized dynamic strain gauge bridge amplifying unit (Peekel T-630) linked the load cell to the recording system. A complete description of the load cells on the 'Mini' is given in ref. 7. The data presented here was recorded from the front middle-longitudinal (FML) load cell. This cell detects fore and aft loads between the car

body and the sub-frame of the front suspension (Fig. 4.4).

The calibration of the load cell when used with the A.S.A.E. standard instrumentation (a 'SEL' unit) was supplied by A.S.A.E. (6 lb/SEL unit deflection at SEL attenuation of 24 dB). Also supplied was the SEL calibration against strain-gauge bridge out-of-balance (890 SEL units /1% unbalance at attenuation of 21 dB). Thus the variation of load against bridge % unbalance is known. As an independent check on this calibration a number of static loads were placed on the vehicle and the simultaneous SEL output and T-630 output were recorded (Fig. 4.5). The T-630 was then separately calibrated against bridge out-of-balance and this confirmed the calibrations supplied by A.S.A.E. to within 1% (Fig. 4.6). The T-630 output calibration is finally 1.48 lb/mV. (Fig. 4.6).

For these recordings a two stage R-C filter (corner frequency 160 c/s) was incorporated into the input to improve the suppression of the Peekel T-630 carrier frequency (1 kc/s). The filter resistance (500Ω) doubles the input resistance of the recording system and so the detection thresholds of the main amplifier were reset to ±5 mV, the full scale range being 2 volts. Thus the calibration for these recordings is 2.96 lb/digital unit.

The value of irregularity factor obtained was 0.460. The digital value of r.m.s. load on the first pass of the data was 91.42, or 270.6 lbs. As explained later the data was then factored by 1.094 to give a r.m.s. digital value of 100, so that the histogram grids and conditional range counts are based on the r.m.s. level. Thus the calibration for the data presented here is 2.706 lbs/digital unit.

FIG. 4.1 AMPLIFIERS AND BAND - PASS - FILTER RESPONSE

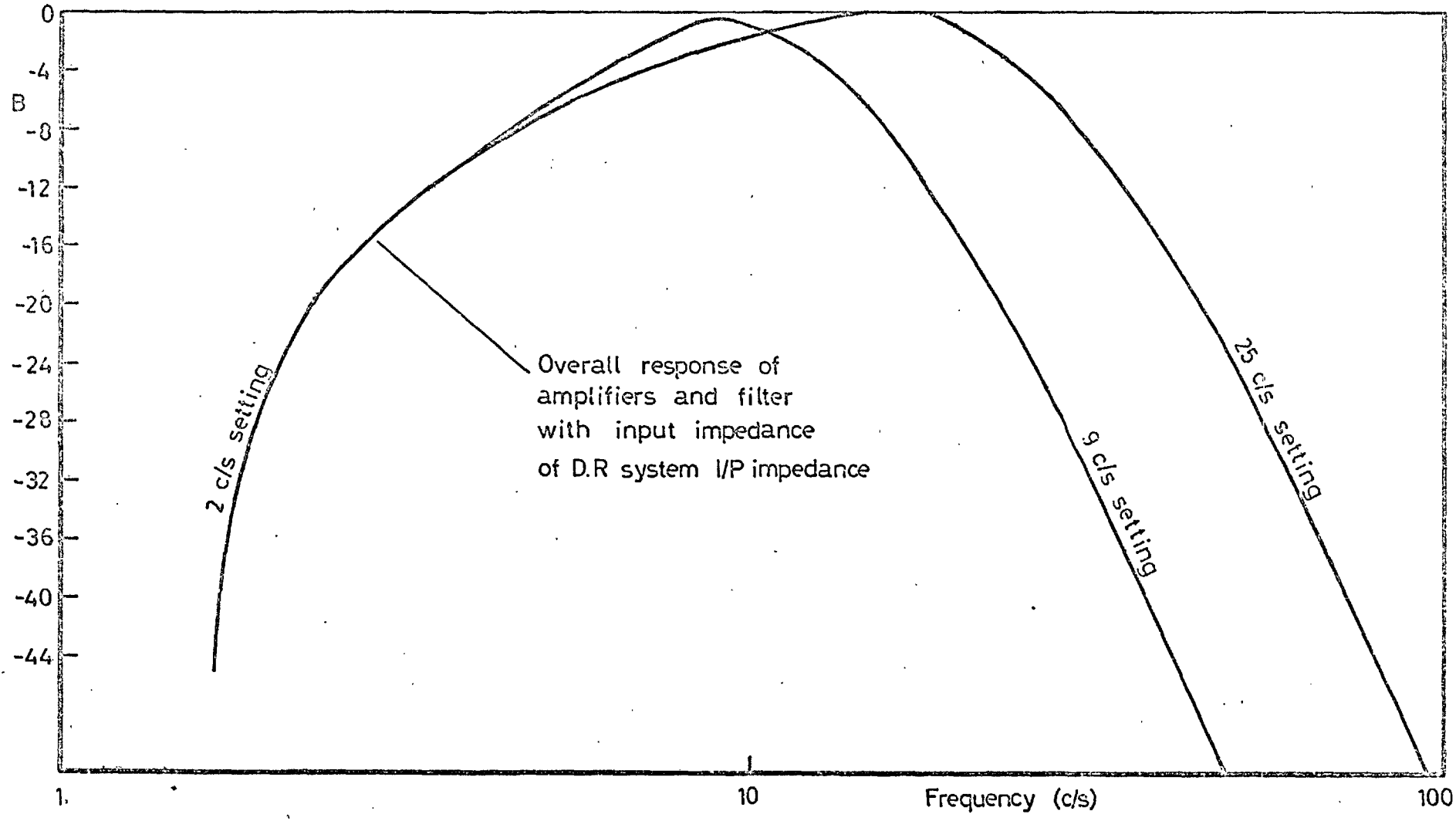

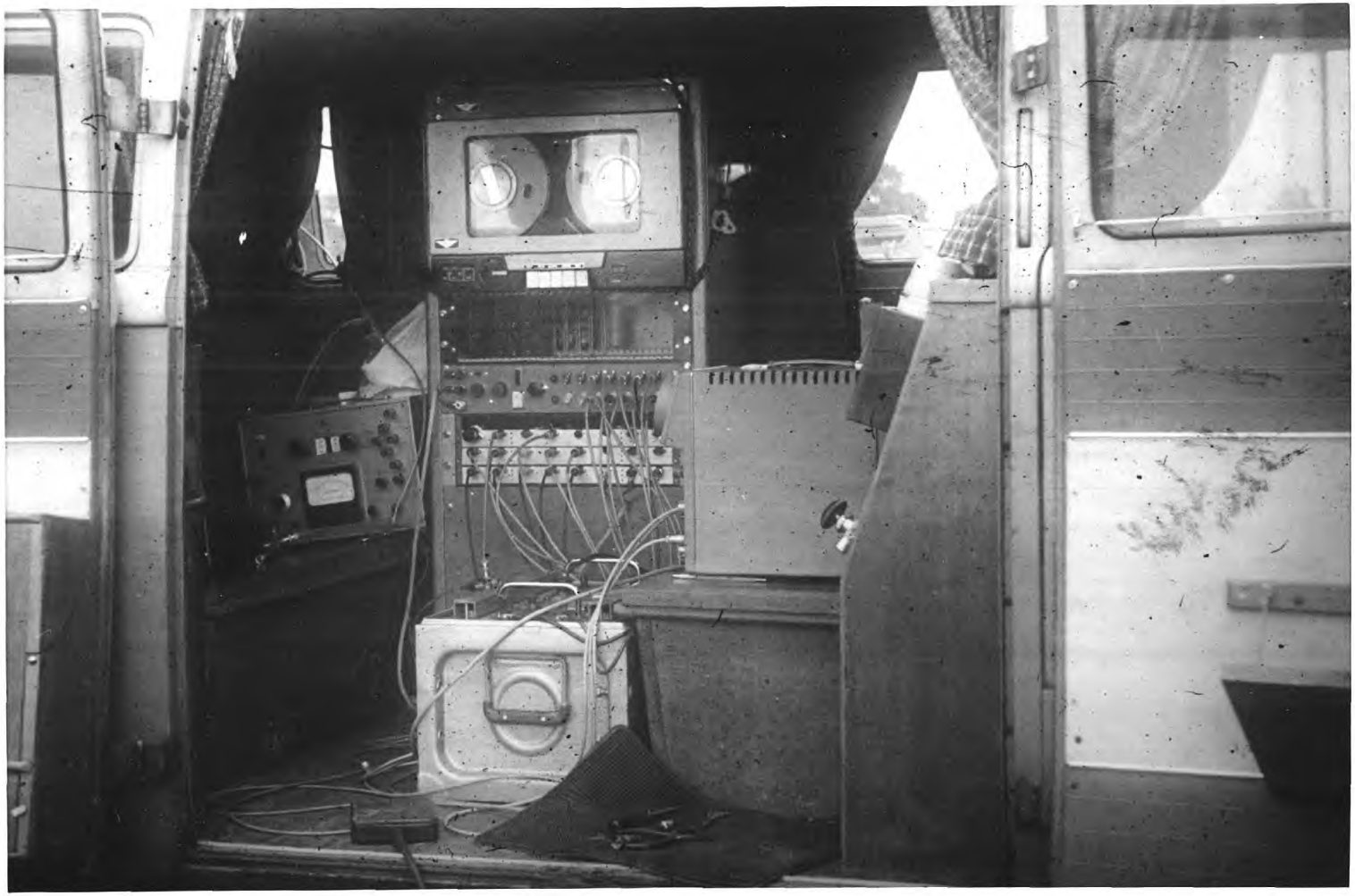

FIG. 4.2 THE INSTRUMENTATION VEHICLE

FIG. 4.3 VIEW OF PAVE SURFACE

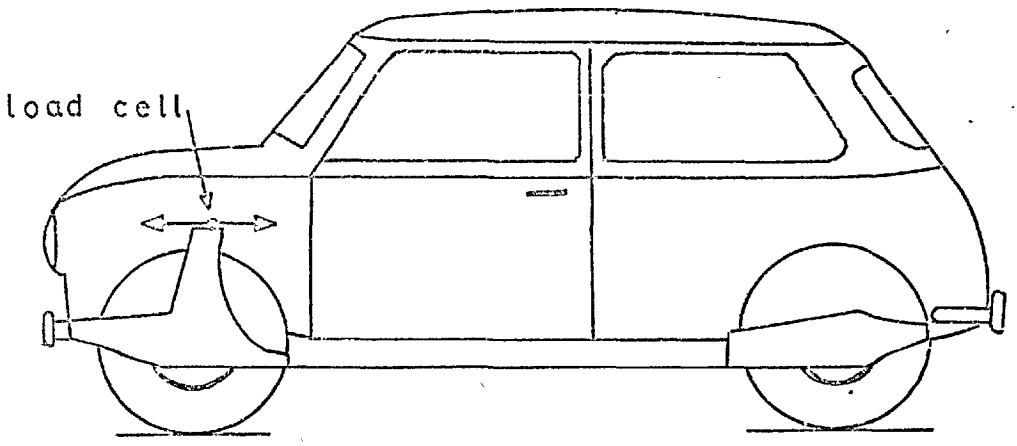

FIG. 4.4 A.S.A.E MINI

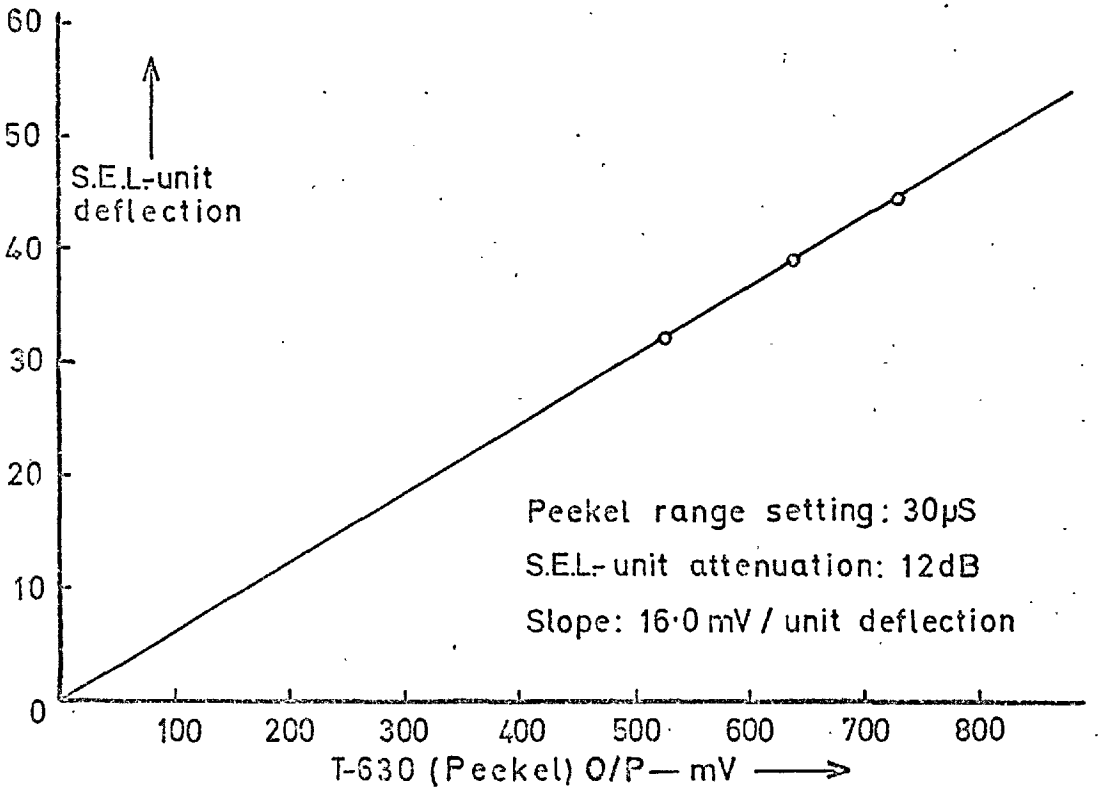

FIG. 4.5 T-630 vs S.E.L. CALIBRATION

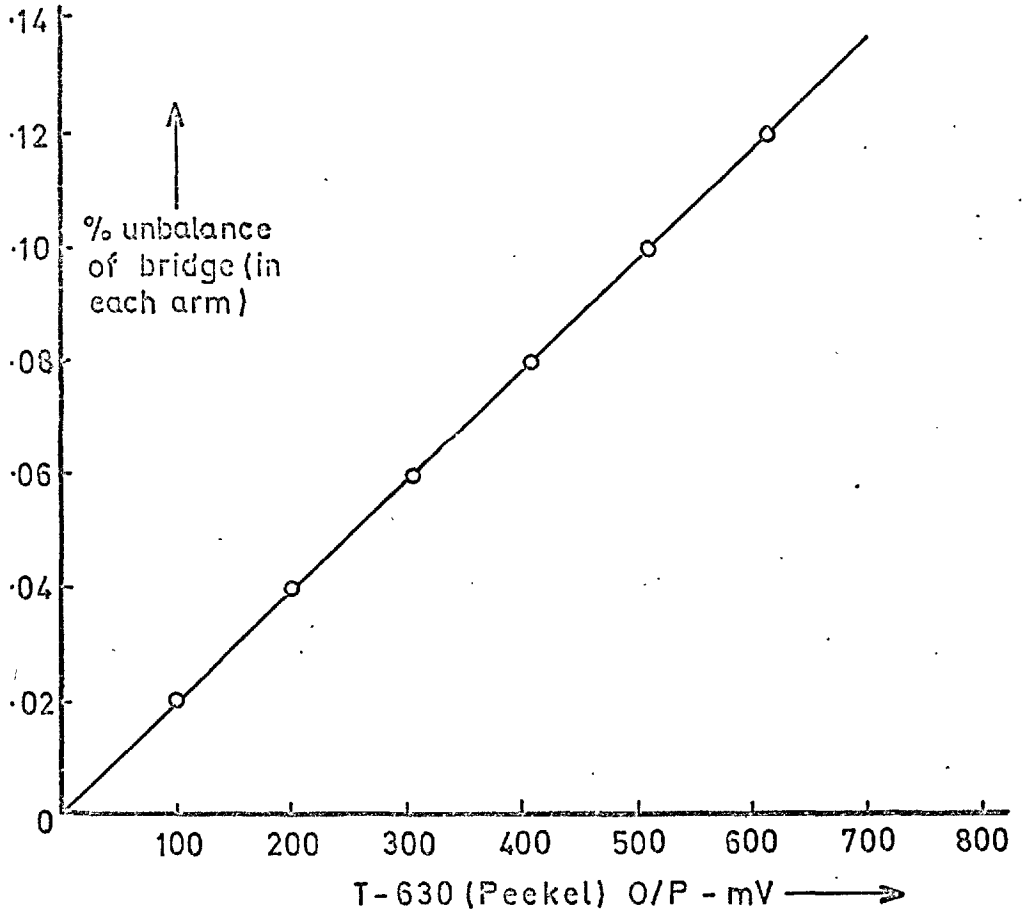

CALIBRATION CHECK

from figs. 4.5 & 4.6:

with attenuation of 12dB:

S.E.L. deflection / % unbalance = $\frac{5100}{16}$ = 318·5

∴ with attenuation of 21dB:

S.E.L deflection / % unbalance

= 318·5 x 2·818 = 898

i.e. checks calibration supplied (890) to 1%

hence Peekel-T630 O/P calibration is

load (lb) / mV = 6·0 x 890 x 1·414 / 5100

= 1·48

FIG. 4.6 PEEKEL T-630 CALIBRATION

TABLE 4.1 BAND PASS FILTER CHARACTERISTICS

Setting: 2-25c/s

c/s	2	4	6	8	10	12	14	16	18	20
dB	26	9.6	5.2	2.9	1.6	0.8	0.2	0.0	0.2	1.0
c/s	22	24	26	28	30	32	34	36	38	40
dB	2.3	3.7	5.0	6.3	7.9	9.6	11.4	12.8	14.4	16
c/s	41.5	43.5	45.5	47.5	49.5	51.5	53.5	55.5	57.5	59.5
dB	17.2	18.6	20.5	22	23.6	25.1	26.4	28.2	29.5	31
c/s	63	68	73	78	83					
dB	33.2	36.6	39.6	42.6	45.3					

Setting: 2-9c/s

c/s	2	4	6	8	10	11	12	13	14	15
dB	26	9.6	4.0	1.1	0.9	1.6	2.7	4.0	5.4	6.9
c/s	16	17	18	19	20	22	24	26	28	30
dB	8.7	10.4	12	13.6	15.3	18.4	21.4	24.5	27.5	30.5
c/s	31.5	33.5	35.5	37.5	39.5					
dB	32.8	35.3	38	40.6	42.6					

5 RESULTS

5.1 Analysis of Recordings

The data from each recording series was analysed using the University Atlas Computer. Histograms were constructed using the following counting methods - Peak, Mean-Crossing-Peak and Range-Mean counts. The Range-Mean counts were performed with five different minimum range values. The counting methods are described in Appendix 2, and the data analysis programmes given in Appendix 3.

In order to relate the minimum ranges of the conditional range counts to the standard deviation of the signal the data analysis was performed twice. On the first pass the standard deviation of the signal was obtained and on the second the data was factored (relative to the overall mean value) to obtain a standard deviation of 10% full scale. In the recordings themselves the recording levels were adjusted to give approximately this standard deviation and in the data analysis only very small adjustments were necessary. The standard deviation of 10% full scale means that the numerical grid is also related to the signal standard deviation.

The data itself consists of successive maxima and minima. The continuous signal standard deviation has therefore to be calculated from the peak (discrete value) standard deviation using the relationship given in Chapter 2.

The tabulations of the data for the counting methods are given in Appendix 5, together with the data corresponding to the probability density distributions referred to in this Chapter. The cumulative distributions corresponding to each counting method are shown in Fig. 5.1-5.3 for the three recordings (Noise 2-9c/s; Noise 2-25c/s;

car suspension loads). The computed values of irregularity factor for the three cases are 0.792; 0.732; 0.460 respectively.

As expected the counting methods lead to essentially similar results for the narrowest bandwidth case (I.F. = 0.792). As the bandwidth widens the counting methods diverge. The peak based methods give essentially different results to the range based methods.

In the random noise analysis it has beenassumed that the instantaneous values of the signal have a Gaussian distribution. The distribution of peaks may be used to ascertain whether or not the distribution of the signal is in fact Gaussian. In Figs. 5.4-5.6 are presented the probability density distributions of peaks. The measured distributions agree closely with the expected (theoretical) distributions based on the measured values of irregularity factor. This implies of course that the signal is indeed Gaussian.

Next, comparisons are made between measured values of irregularity factor and the expected (theoretical) values. The expected irregularity factor is given by

$$n = \frac{\int_0^\infty E(\sigma) \cdot \sigma^2 \cdot d\sigma}{\left[\int_0^\infty E(\sigma)\, d\sigma \cdot \int_0^\infty E(\sigma) \cdot \sigma^4 \cdot d\sigma\right]^{\frac{1}{2}}}$$

where $E(\sigma)$ is the energy spectrum of the signal, σ being frequency (see chapter 2). The noise generator is assumed to produce 'white' noise ($E_1(\sigma)$ = constant) so that filtering with a filter of receptance $A(i\omega)$ produces a signal with a new energy spectrum $E_2(\sigma)$ given by

$$E_2(\sigma) = \left|A(i\omega)\right|^2 \cdot E_1(\sigma)$$

Since only the modulus of the receptance is used the term $|A(i\omega)|^2$ is obtained directly from the filters response curve (Fig. 4.1). The filter curve is obtained over sufficient bandwidth so that the integrations can be completed accurately.

The expected value of I.F. for the 2-9 filter setting is 0.803 (compared to the measured value of 0.792). For the 2-25 setting it is 0.742 (measured 0.732). Both values are within 1.5% which shows that if the spectral density is known sufficiently well, very accurate estimates can be made of the irregularity factor. In the case of the car suspension loads the spectrum presented in ref. 8 is not defined over sufficient bandwidth to perform the integrations

In Figs. 5.7-5.9 are presented the mean-crossing peak distributions. For comparison these distributions are related to the total peak count. In each case the two distributions converge at high peaks (as expected) and also at very small peaks. In the limiting case all amplitudes giving peaks at or near the mean also cross the mean.

In Figs. 5.10-5.12 are presented the range distributions for both the conditional and unconditional counting methods. For comparison the distribution of peaks is also shown in each case. The unconditional distributions are discussed in detail in Chapter 6. The variation of the range counts with the different minimum ranges is clearly evident, even in the narrowest bandwidth case. The great difference between the unconditional range counts and the corresponding peak count is striking. As expected the distributions converge as the irregularity factor approaches unity.

Figs. 5.13 and 5.14 show the overall distributions

of mean values, where the probability densities are related to the standard deviation of the continuous signal. These distributions are shown to be normal in Chapter 6. In addition the distributions of means for each value of range are also normal as pointed out by Schijve (ref. 6). As expected the smaller the bandwidth the closer the individual mean values are grouped around the overall mean (Fig. 5.15)

It is noteworthy that for the widest bandwidth case (I.F. = 0.46) 50% of all ranges have mean values lying outside the limits $\pm 0.5\sigma$, and 20% outside $\pm\sigma$. In the other two cases the corresponding figures are 38 and 10% (for I.F. = 0.73) and 28 & 7% (for I.F. = 0.79). (Thus the established procedure of neglecting mean value variations in programme fatigue testing based directly or indirectly on range counts is questionable for wider spectrums).

5.2 Linear Cumulative Damage Estimates

In order to see quantitavely what effects the irregularity factor may have on estimates of fatigue life, a range of typical S-N curves have been selected. Linear cumulative damage estimates have been made using the data from each of the various counting methods. Such estimates are simple to perform as such form the basis of many design studies, particularly in early project stages. The author considers it relevant to point out further shortcomings in this practice.

Very simple S-N curves have been used ($S = aN^b$) which have been derived from R.Ae. Soc. data sheets (ref. 7). The derivation of the curves is given in detail in Appendix 4, where is also explained the relationship between the numerical grid and the stress scale. Because of the particular type

of S-N curve selected, the comparisons between estimates from differing counting methods depend only on the slopes of the log log S-N curves (to within 10%) - see Appendix 4.

Three log log S-N curve slopes have been used; a high-slope (corresponding to a lug with interference), a medium-slope (lug without interference), and low-slope (al-alloy in bending). In making the comparisons between fatigue life estimates the following points are considered;

(i) the effect of mean stress variations (Range c.f. Range/Mean)
(ii) the effect of omitting small amplitudes in the conditional range counts (Range c.f. Range (P > o))
(iii) the difference between range based counts and peak based counts (Range c.f. M-C-P)
(iv) the difference between Peak and M-C-P

Finally since all the data is derived from signals with the same standard deviation it is interesting to see if they lead to similar cumulative damage rates. The estimated lives based on m-c-p counts and referred to the same number of zero-crossings is evaluated. The m-c-p method is used here because it is one of the most commonly used methods (see for example ref. 12).

Table 5.1 tabulates the above comparisons in the form of ratios between each pair of lives being compared.

The difference between Range and Range-Mean estimates is low, ranging from ratios of 1.0 to 1.7. For the higher slope log log S-N curve the difference is in fact completely insignificant so that measurements of mean values in addition to ranges is not justifiable for range based estimates.

The omission of small ranges when making a range count has a surprisingly small effect. With the low-slope S-N curve and the widest bandwidth the life-ratio approaches 1.6 when the smallest detected range (P) is equal to the standard deviation. For the more typical case of $P = \frac{1}{4}\sigma$ the effect is completely insignificant even for the widest bandwidth.

Another surprising effect is the vast difference between range based and peak based estimates. The life ratios between m-c-p and range results vary up to 17 depending on slope and bandwidth.

The comparison of peak and m-c-p estimates leads to completely insignificant differences. It appears that the extra complication in obtaining m-c-p results for life estimates is unwarranted - although in programme testing, the testing time is reduced.

The estimated lives based on m-c-p data (referred to the same number of zero crossings) are given in Table 5.2. The figures can be assumed to be measures of life on an arbitrary scale when exposed to each signal in turn. For each S-N curve the lives are very approximately the same.

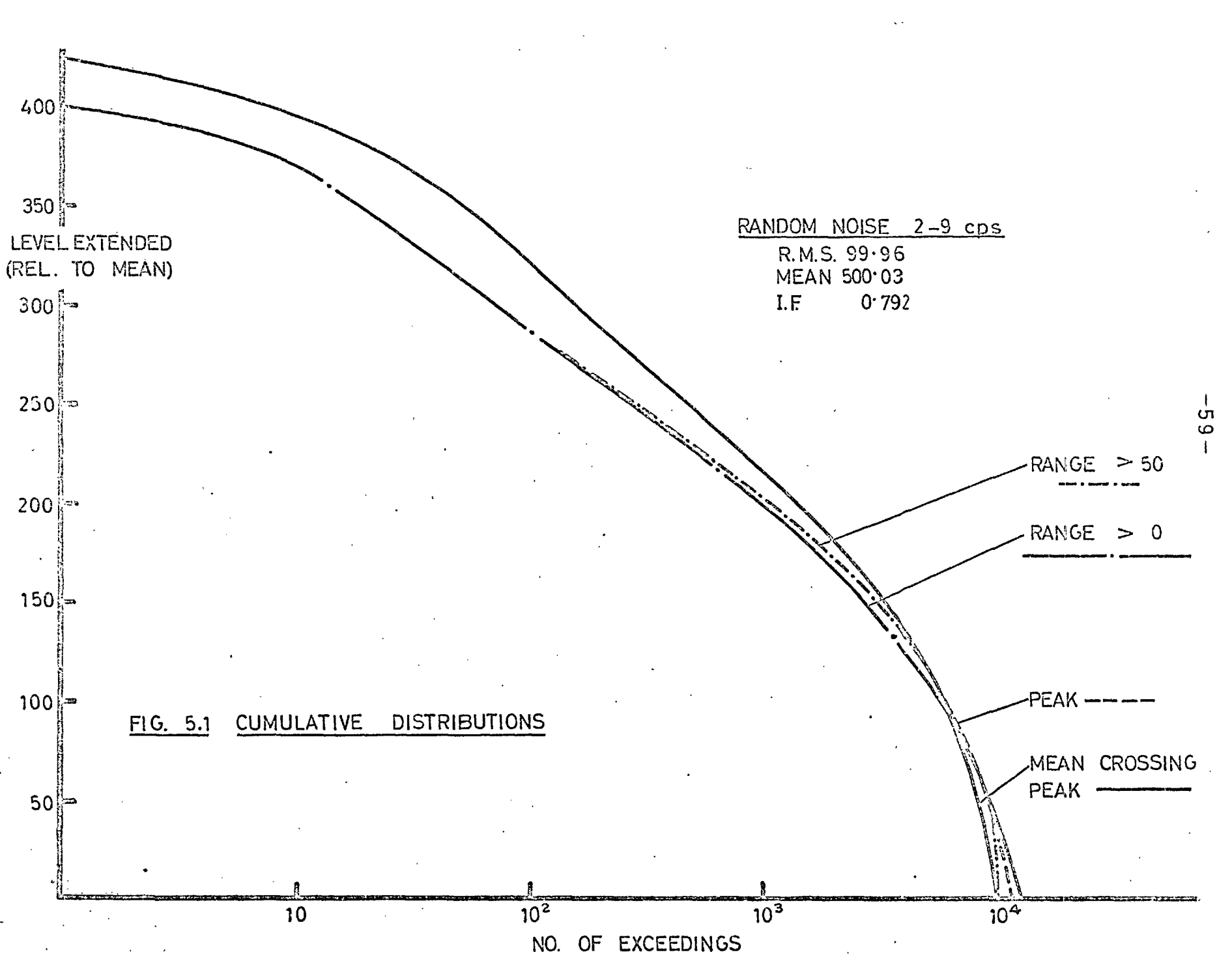

FIG. 5.1 CUMULATIVE DISTRIBUTIONS

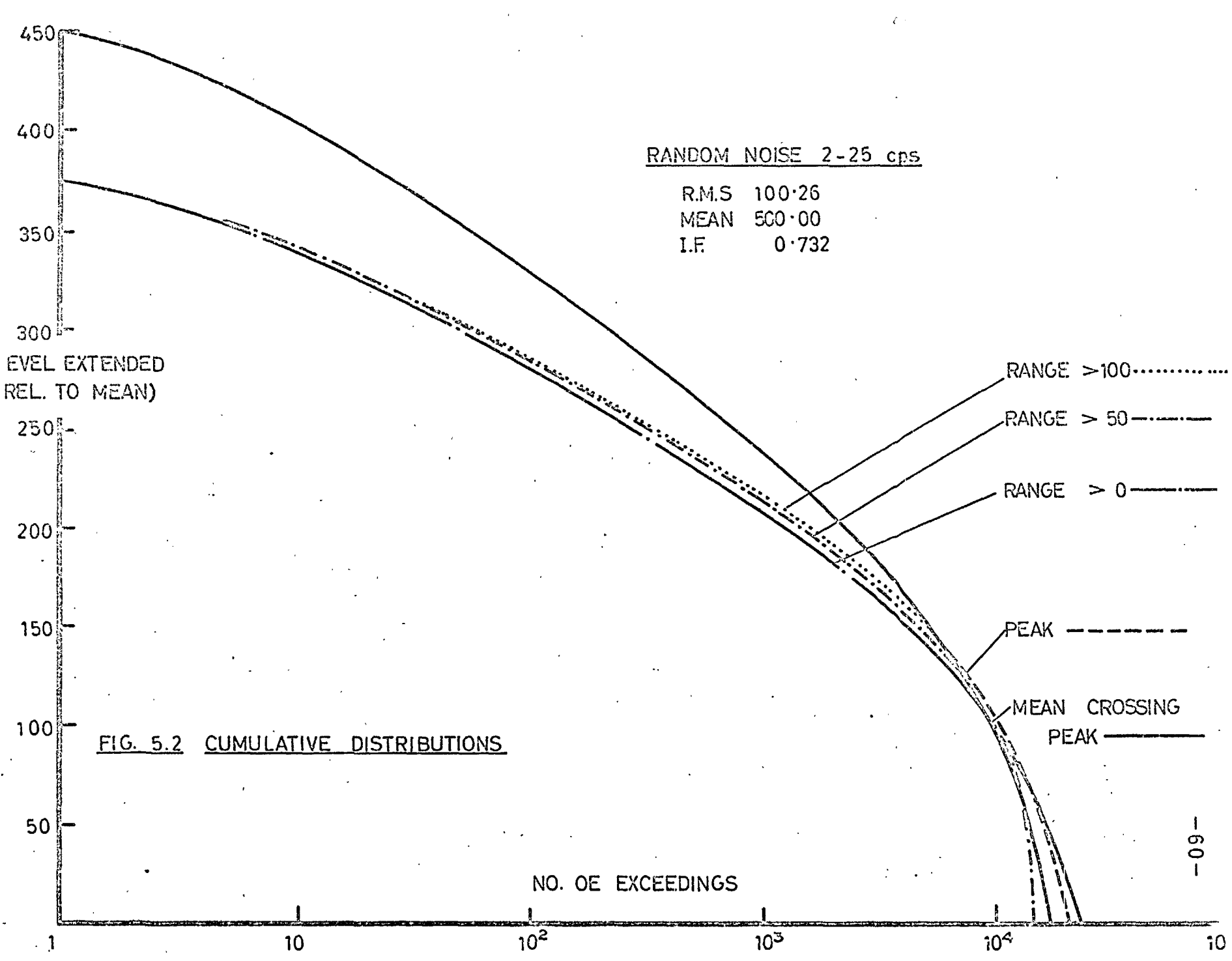

FIG. 5.2 CUMULATIVE DISTRIBUTIONS

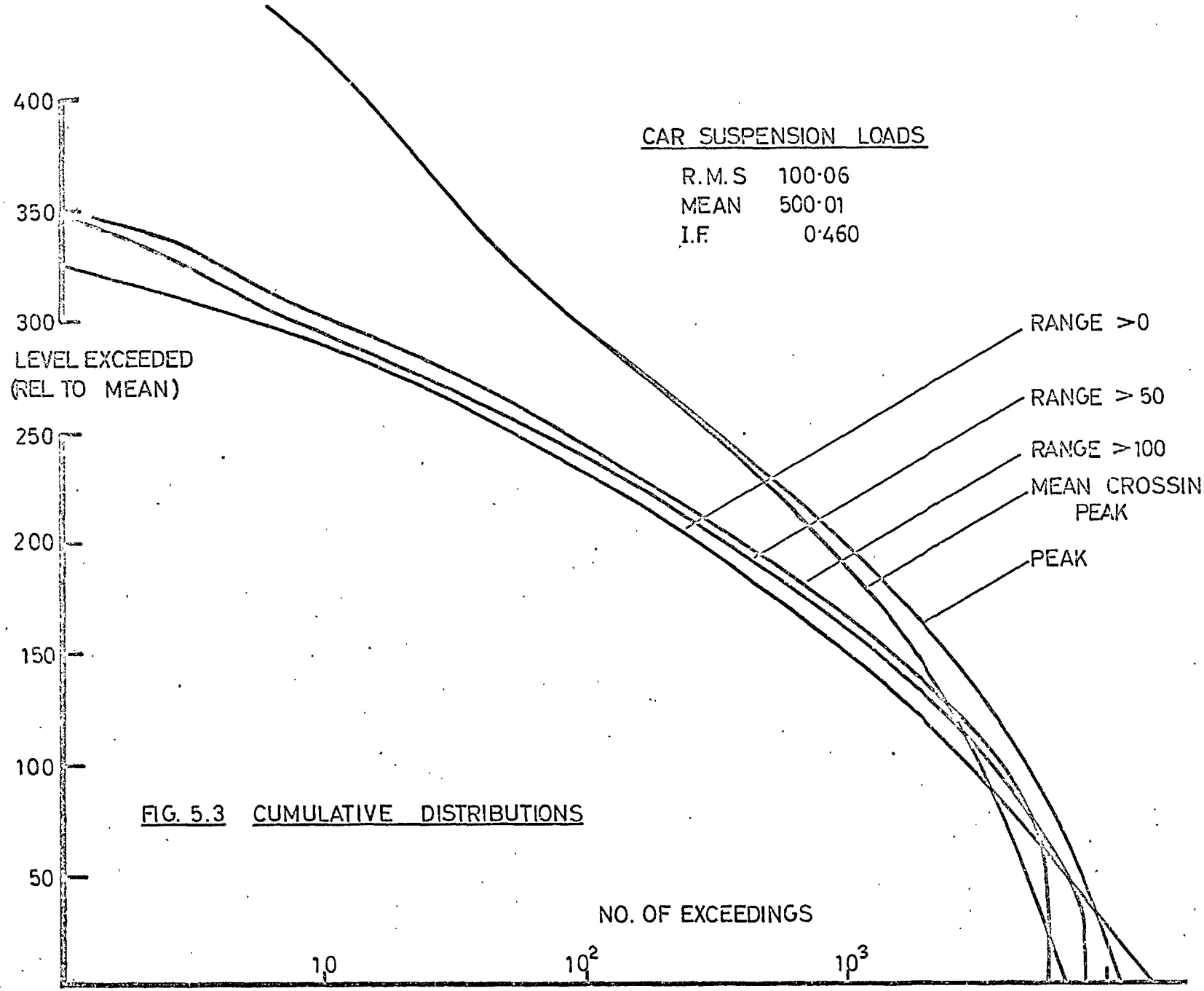

FIG. 5.3 CUMULATIVE DISTRIBUTIONS

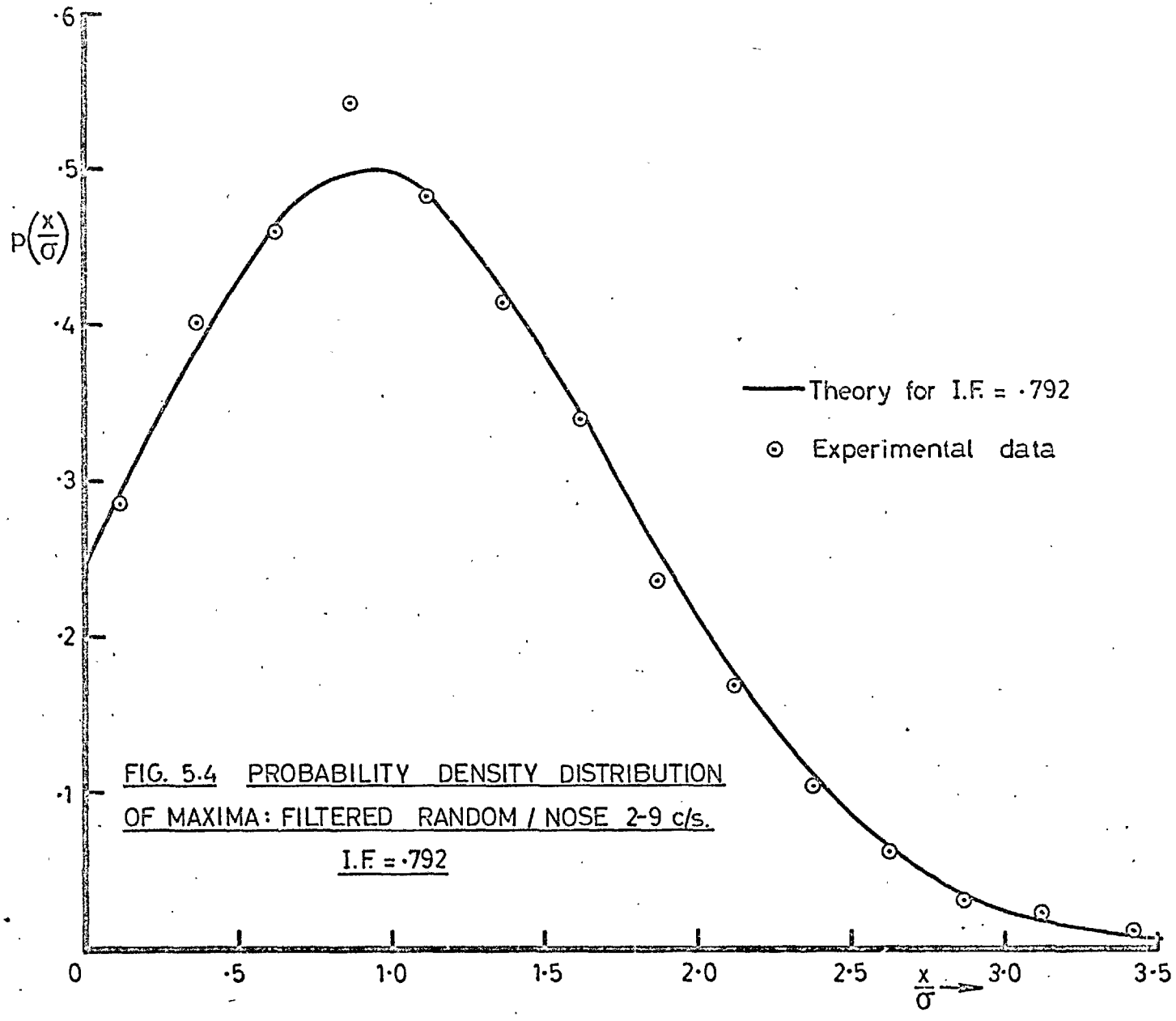

FIG. 5.4 PROBABILITY DENSITY DISTRIBUTION OF MAXIMA: FILTERED RANDOM / NOSE 2-9 c/s. I.F. = ·792

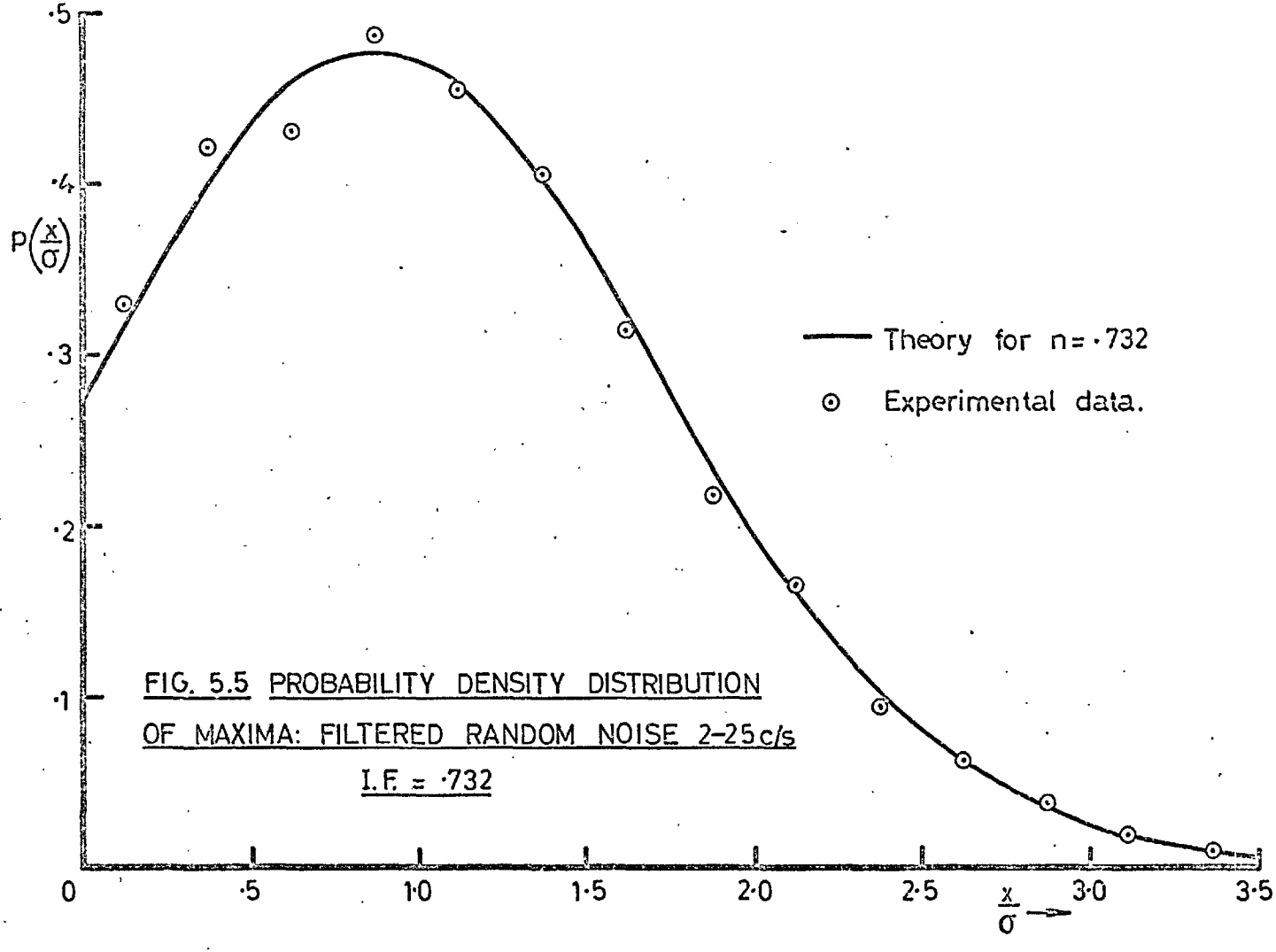

FIG. 5.5 PROBABILITY DENSITY DISTRIBUTION OF MAXIMA: FILTERED RANDOM NOISE 2–25 c/s I.F. = ·732

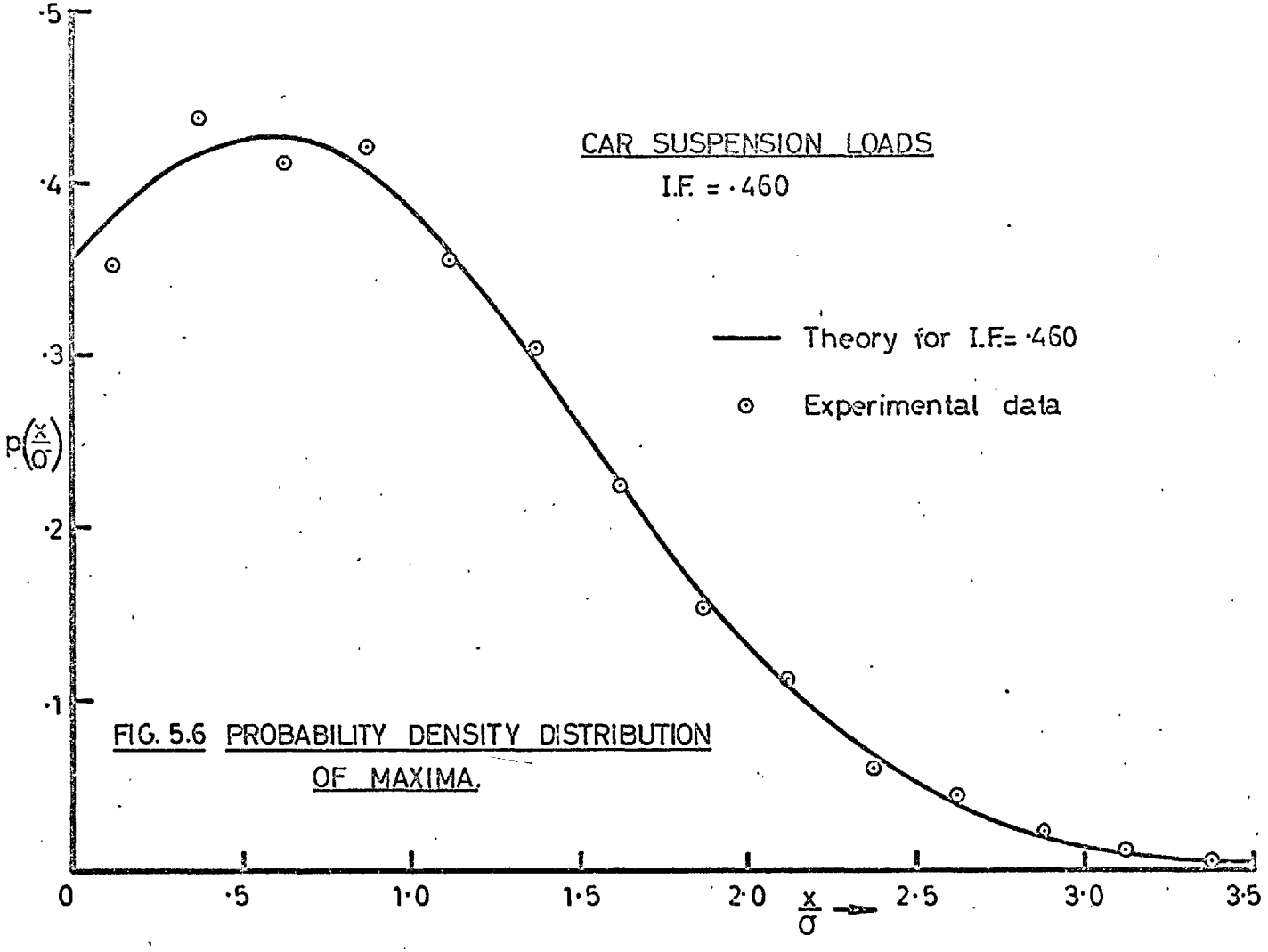

FIG. 5.6 PROBABILITY DENSITY DISTRIBUTION OF MAXIMA.

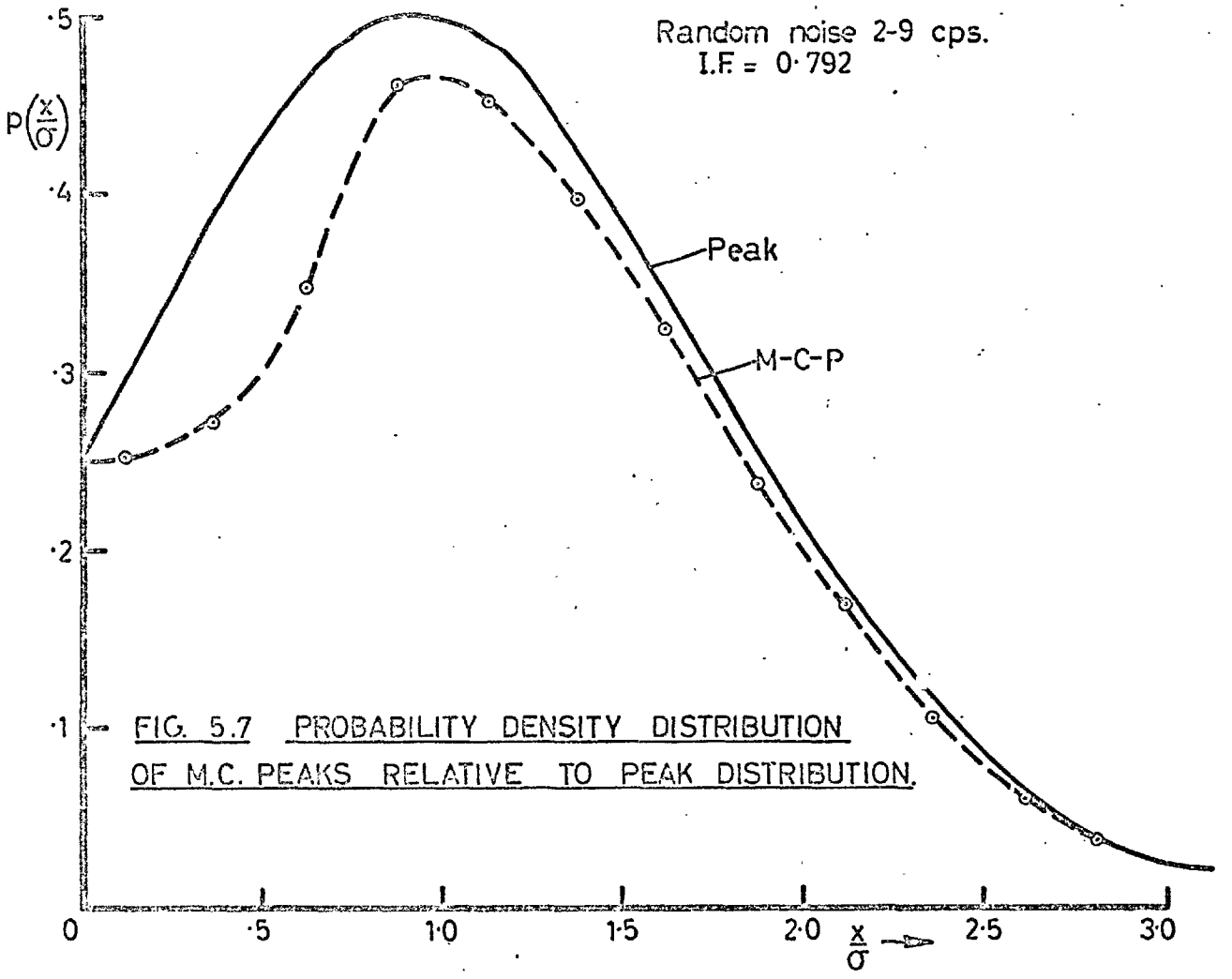

FIG. 5.7 PROBABILITY DENSITY DISTRIBUTION OF M.C. PEAKS RELATIVE TO PEAK DISTRIBUTION.

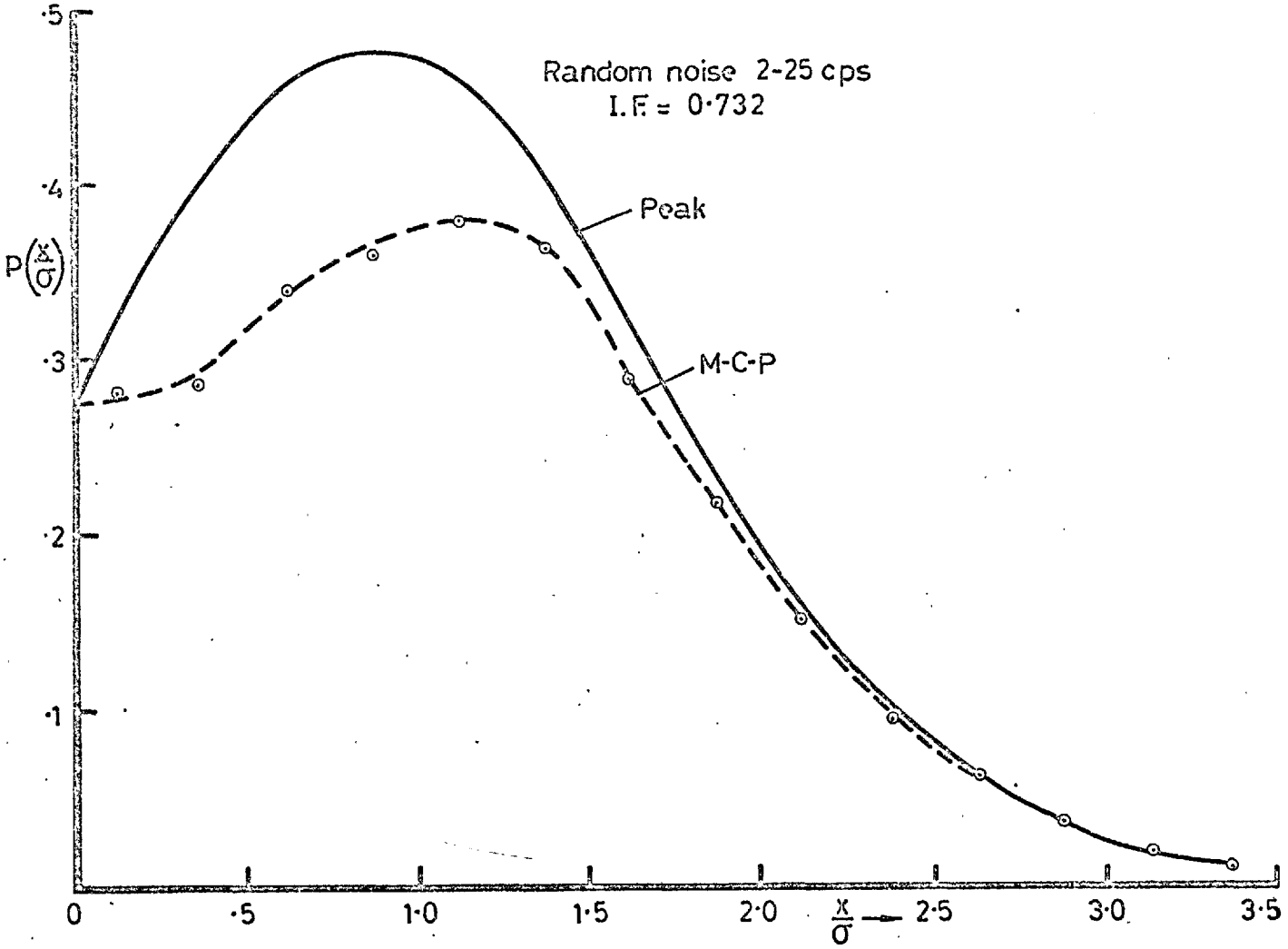

FIG. 5.8 PROBABILITY DENSITY DISTRIBUTION OF M.C. PEAKS RELATIVE TO PEAK DISTRIBUTION

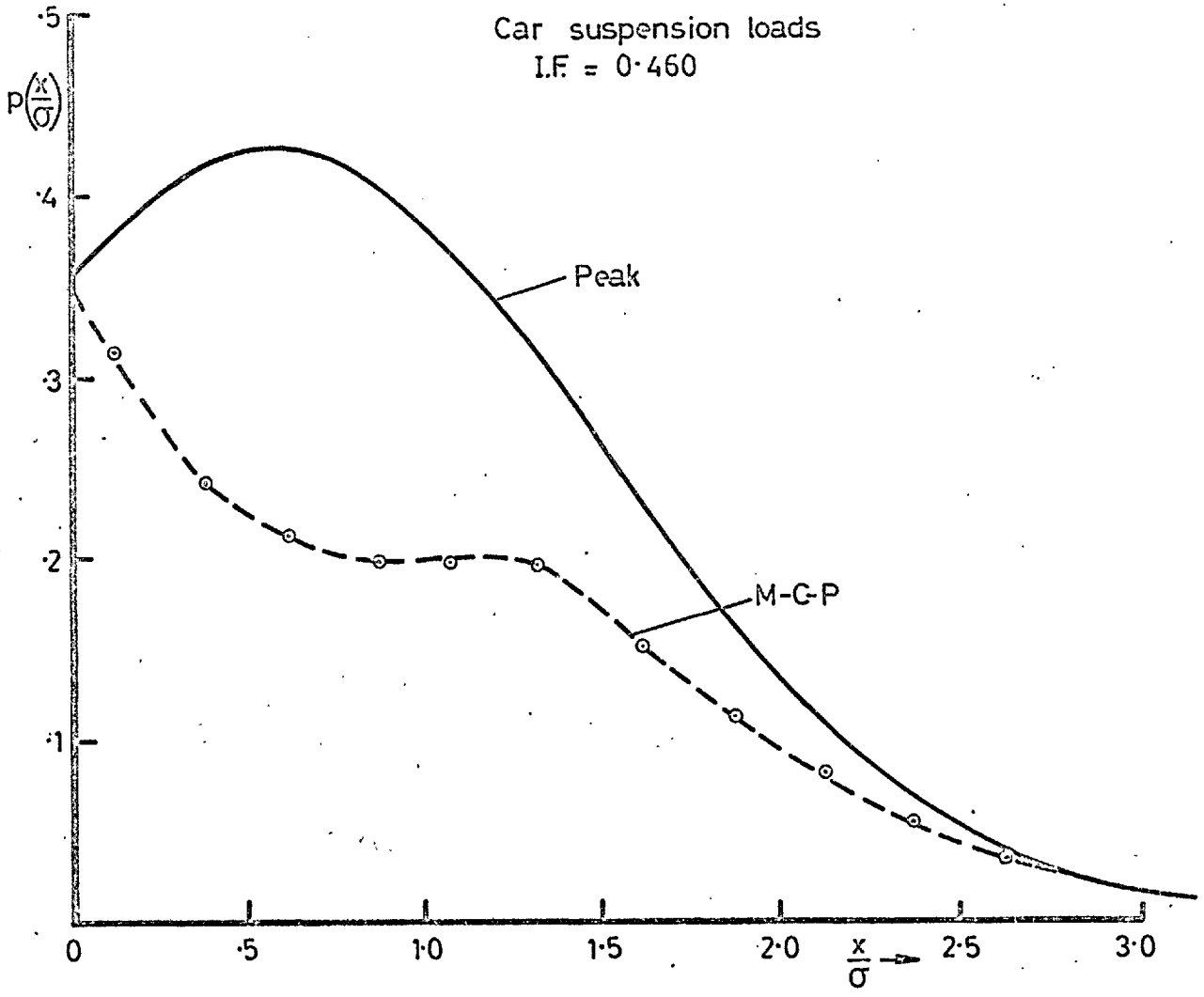

FIG. 5.9 PROBABILITY DENSITY DISTRIBUTION OF M.C. PEAKS RELATIVE TO PEAK DISTRIBUTION

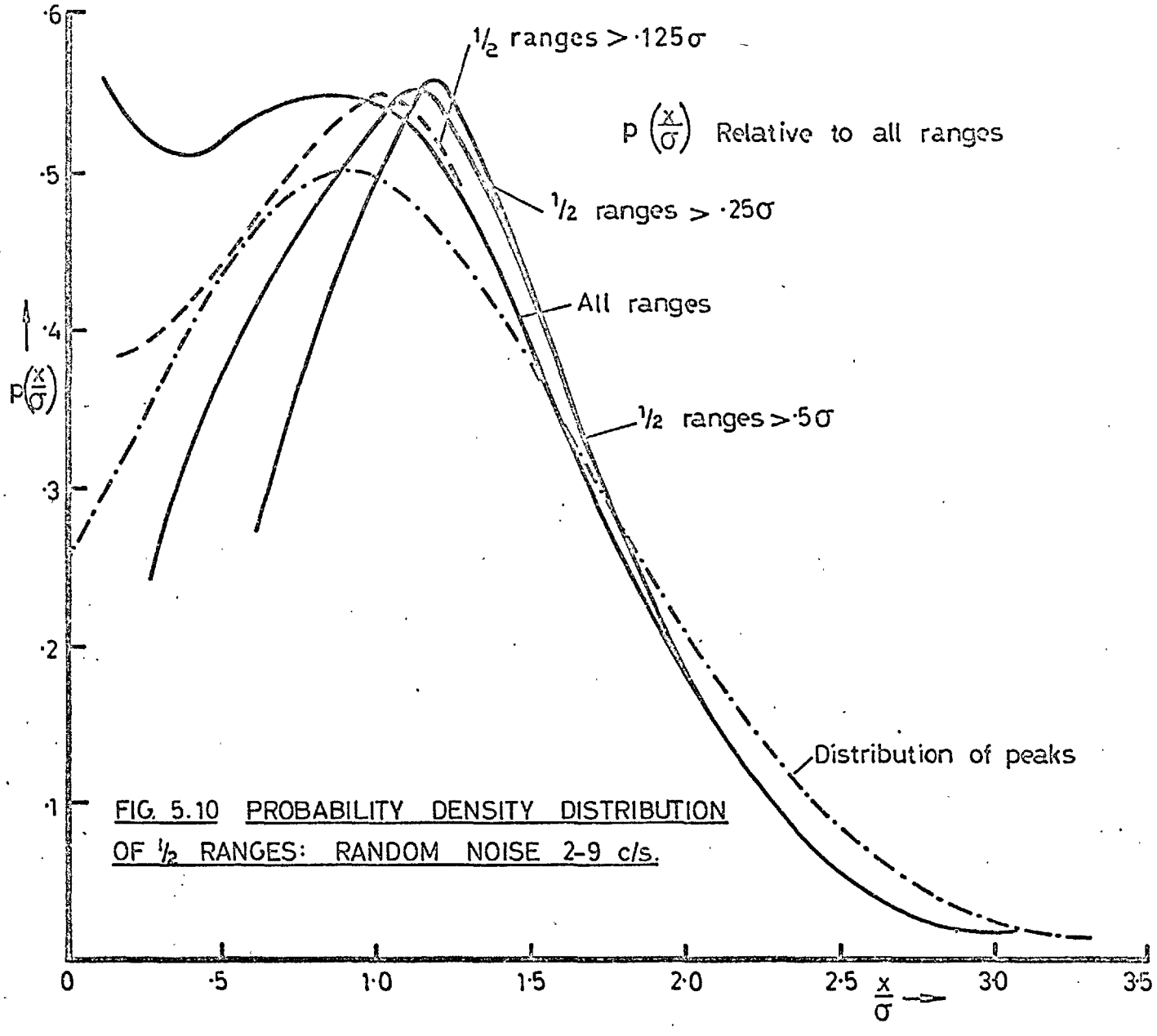

FIG. 5.10 PROBABILITY DENSITY DISTRIBUTION OF ½ RANGES: RANDOM NOISE 2-9 c/s.

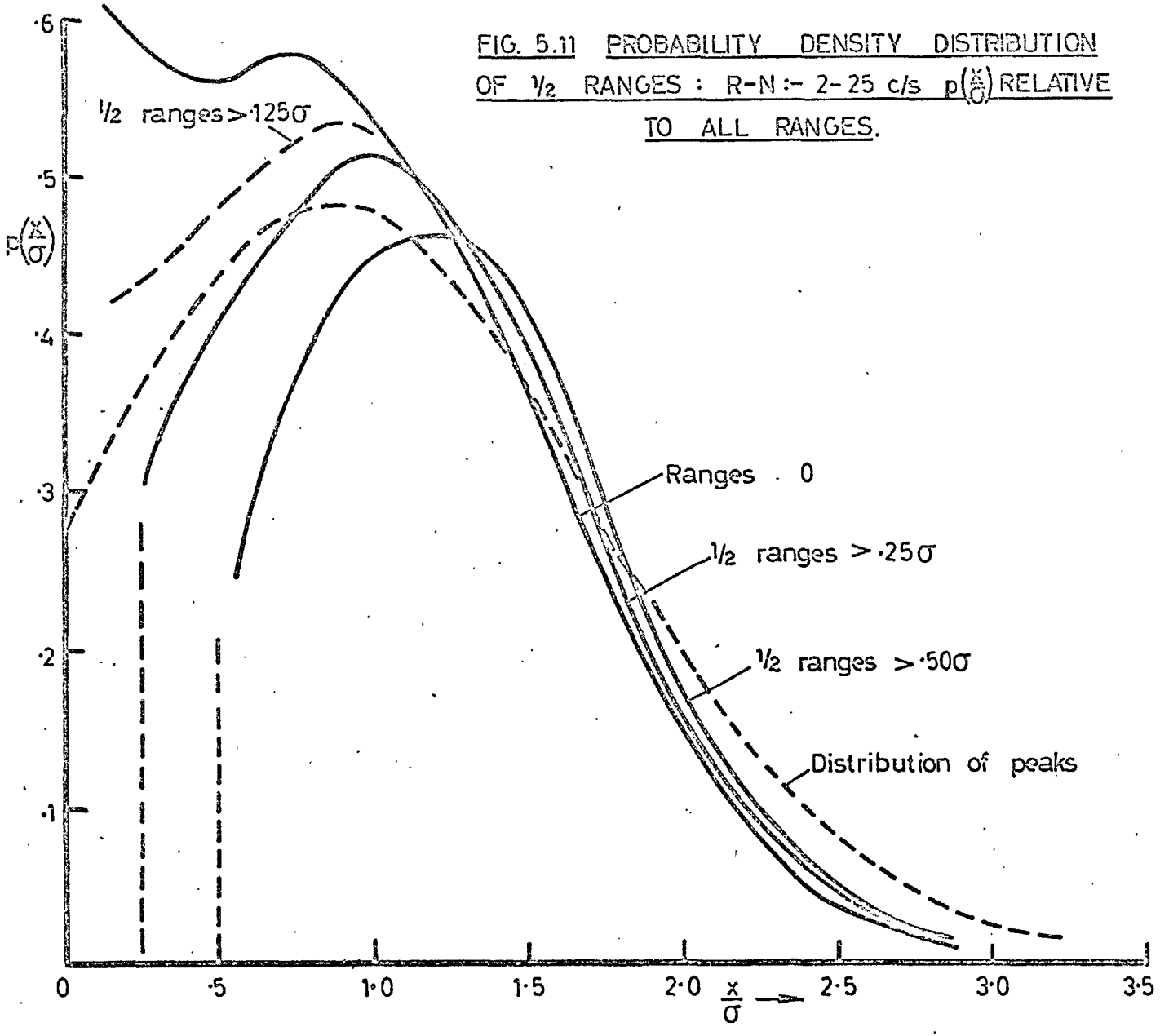

FIG. 5.11 PROBABILITY DENSITY DISTRIBUTION OF ½ RANGES : R-N :- 2-25 c/s $p(\frac{x}{\sigma})$ RELATIVE TO ALL RANGES.

FIG. 5.12 PROBABILITY DENSITY DISTRIBUTION OF ½ RANGES. $p\left(\frac{x}{\sigma}\right)$ RELATIVE TO ALL RANGES.

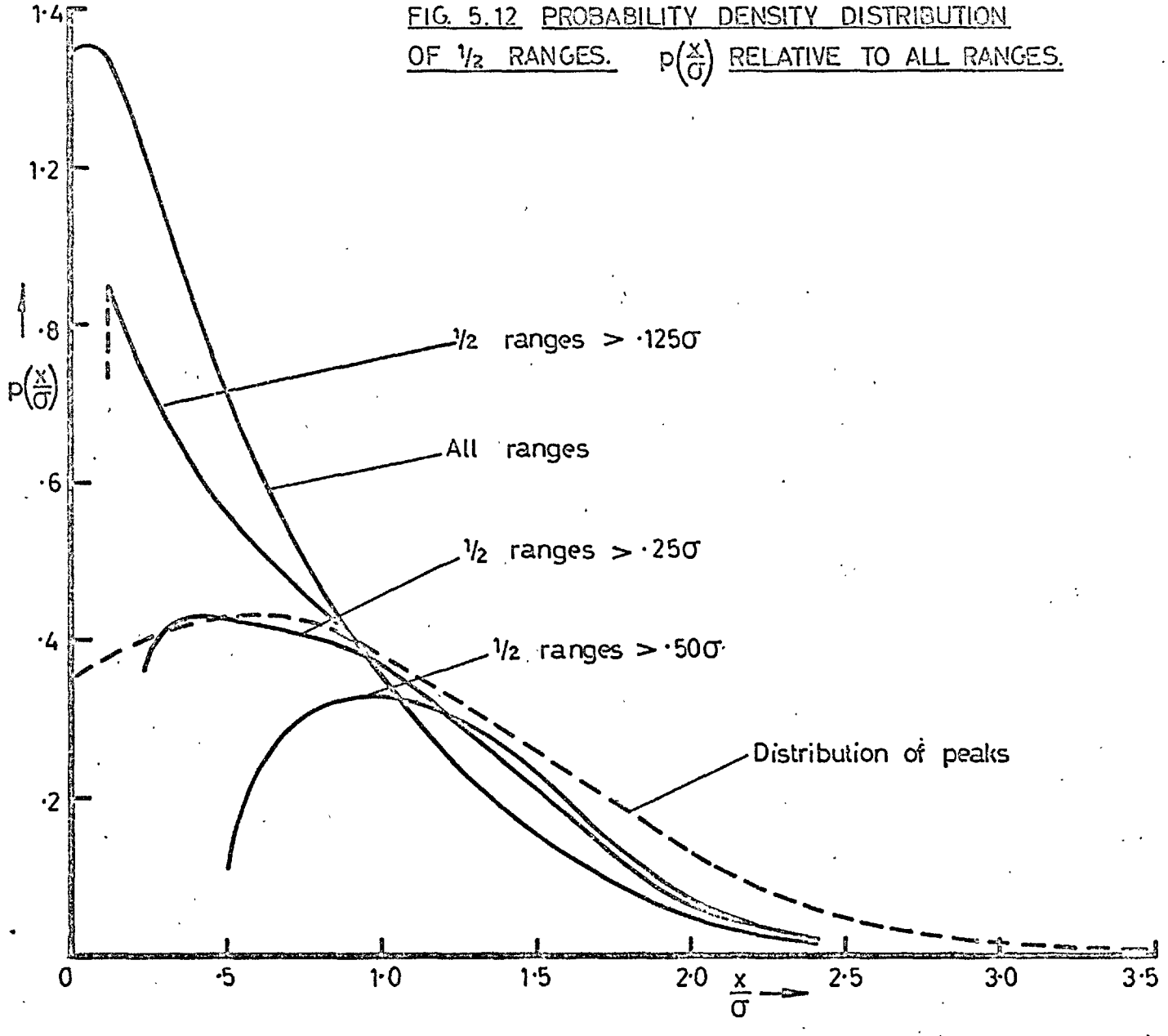

σ = R.M.S. FUNCTION

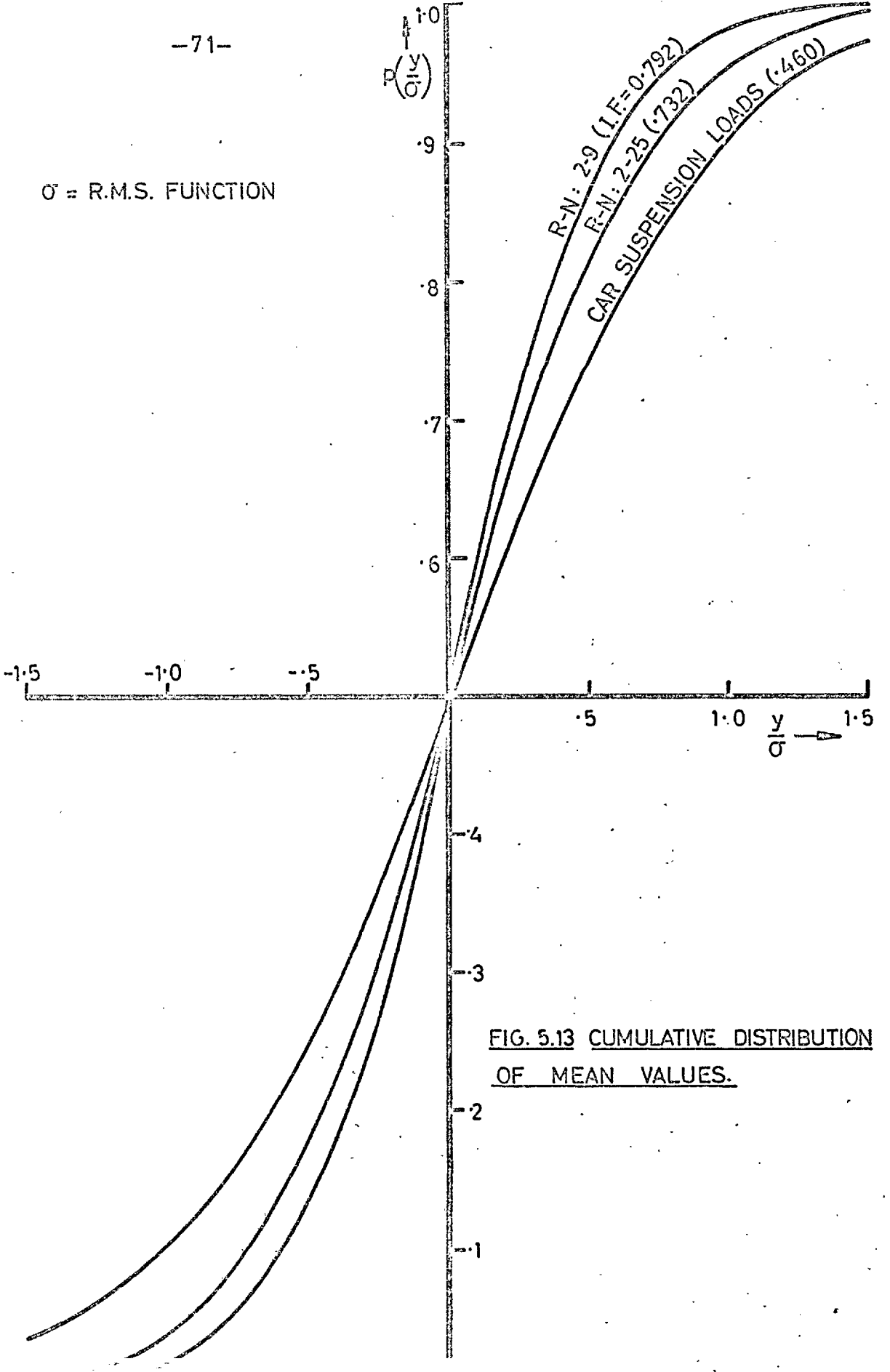

FIG. 5.13 CUMULATIVE DISTRIBUTION OF MEAN VALUES.

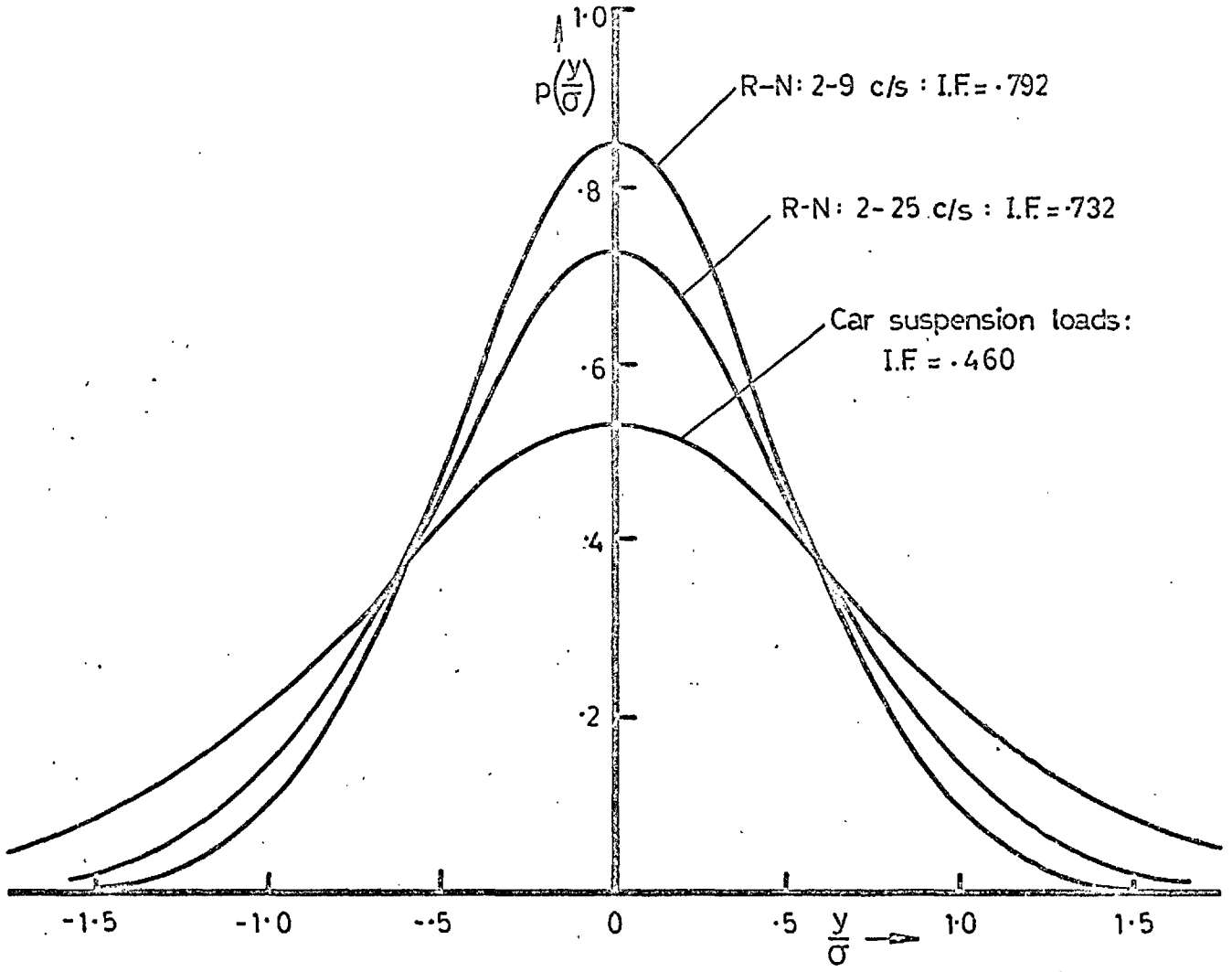

FIG. 5.14 PROBABILITY DENSITY DISTRIBUTION FOR MEAN VALUES (σ=R.M.S. FUNCTION).

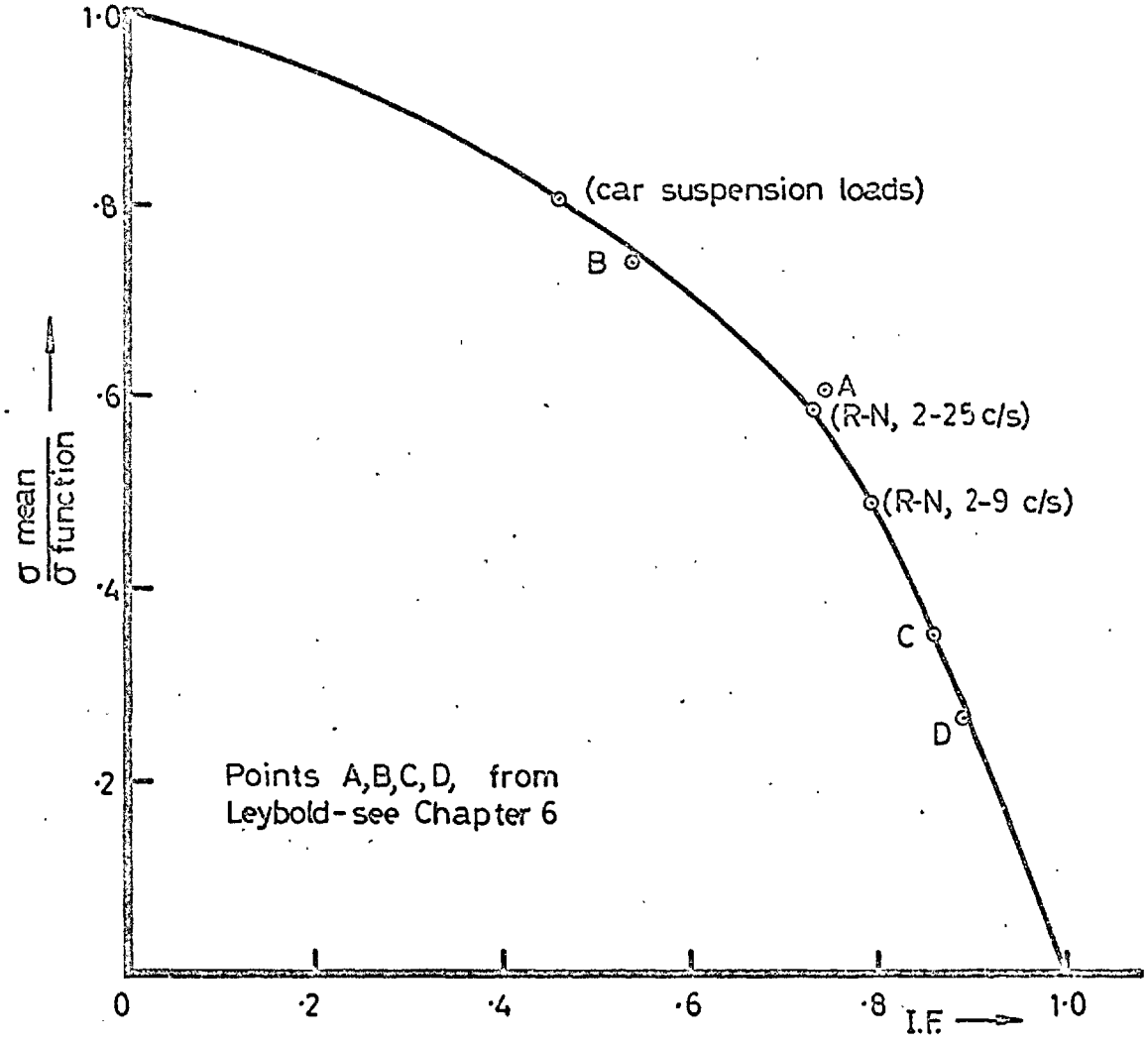

FIG. 5.15 EFFECT OF IRREGULARITY FACTOR ON R.M.S. VALUE OF MEANS

TABLE 5.1 COMPARATIVE LINEAR CUMULATIVE DAMAGE ESTIMATES

Ratio	Case	I.F.	SN1 Low-slope	SN2 Medium-sl	SN3 Hi-slope
L_r/L_{rm}	CAR	0.460	1.72	1.23	1.05
	2-25	0.732	1.59	1.18	1.04
	2-9	0.792	1.18	1.09	1.02
L_r/L_{mcp}	CAR	0.460	17.0	5.47	1.94
	2-25	0.732	5.19	2.70	1.47
	2-9	0.792	2.46	1.84	1.28
L_{rm}/L_{mcp}	CAR	0.460	9.90	4.44	1.95
	2-25	0.732	3.37	2.29	1.41
	2-9	0.792	2.09	1.69	1.25
L_{mcp}/L_p	CAR	0.460	1.08	1.13	1.29
	2-25	0.732	1.0	1.0	1.0
	2-9	0.792	1.0	1.0	1.0
RANGE;	$L_{p=o}/L_{p=o}$				
$p=.25\sigma$	CAR	0.460	1.16	1.14	1.12
$p=.50\sigma$	CAR	0.460	1.30	1.25	1.20
$p=.75\sigma$	CAR	0.460	1.35	1.32	1.25
$p=1.0\sigma$	CAR	0.460	1.56	1.44	1.30

NOTE:

$$L_r/L_{rm} = \frac{\text{Life based on RANGE}}{\text{Life based on RANGE-MEAN}}, \text{ETC.}$$

and p = PEAK

mcp = MEAN-CROSSING PEAK

TABLE 5.2 EFFECT OF IRREGULARITY FACTOR ON MCP ESTIMATES

	CASE	CAR	2-25	2-9
	I.F.	0.460	0.732	0.792
Effective Lives	High slope	9662.0	12711.	11279.
	Med. slope	1461.0	1537.0	1404.0
	Low slope	95.5	84.5	82.4

6 DISTRIBUTION OF RANGES.

To find the empirical distribution of ranges three independent noise sources have been used. These are (i) filtered random noise (two cases), (ii) car suspension loads (one case) and (iii) filtered random numbers (data from Leybold and Naumann - five cases - refs. 9 and 10).

It is the author's submission that the distribution of ranges has not been suggested previously because results have been obscured by the resolution of the counting systems. As is well known range counts are highly sensitive to the smallest range detectable. Figs. 6.1 - 6.3 show the effect on the range distribution of ignoring $\frac{1}{2}$-ranges of size 0.125σ and 0.25σ (for the three recordings of the author's) compared with that for 'all' ranges (0.025σ). In each case the new distributions have the characteristic shape of the Rayleigh distribution, a fact which may have led to the belief that for fairly high values of irregularity factor (eg. above 0.8) the range distribution was Rayleigh (the distribution for I.F. of unity). All recording systems have, of course, a finite resolution - in this case (of 0.025σ), it is assumed that relatively few ranges are omitted.

To find the range distribution the distribution of all ranges (regardless of mean value) is first considered. Following this an attempt is made to correlate the distributions for each mean value with this overall distribution. The grounds for attempting this are that the distribution of mean values has already been found (by Schijve ref.6) to be normal, independent of the value of range (that is constant standard deviation for all values of range).

A difficulty in finding probability density distributions is that the data consists of histograms,

that is areas of columns under the probability density curve. Where the gradations of range are reasonably small, distributions can be constructed accurately even in the region of maxima and minima, by bearing in mind that it is the area under the curve that is known. It has to be assumed there are no points of inflexion. It is impossible, of course, to assess the distribution in the immediate neighbourhood of the vertical axis.

However, these results are based on samples and it would be unrealistic to assume the distributions are the true ones. Hence for the purpose of illustrating the following discussion the points have merely been joined by smooth curves, truncated at the data point nearest the vertical axis. The histograms have been tabulated separately. Note that Naumann substitutes a new case D for Leybold's original case D. This new case is referred to as case E. Fig. 6.4 gives the distributions for the eight cases of irregularity factor. Clearly case A and E do not fit into the general pattern, having the familiar Rayleigh characteristic shape. The remainder of the curves appear to be part of the same family (Fig. 6.10).

All the Leybold/Naumann data is based on filtered random numbers, where the numbers are considered as equally timed samples of a stationary random process. However, the criteria used by Leybold in selecting his random number generator was to choose a generator which gave low correlation between numbers. Clearly this is equivalent to making the sample time-interval longer. In each case the data is based on the same set of approximately 160,000 random numbers. Linear filtering is used to obtain various 'bandwidth' cases (or different spectral density shapes). In the five cases the number of maxima and minima obtained are; 52827, 36561, 43850, 44765 and 106426

This amounts to having sampled the random process at the following average number of times per ½-cycle; 3.0, 4.4, 3.7, 3.6, 1.5.

It is submitted that for cases A and E the sampling interval is too long and that the data for these cases is unrepresentative of the assumed spectral shape. This submission can be checked by examining whether the peak distributions lie close to the theoretical distributions. Figs. 6.5-6.9 give the theoretical distribution of peaks for each case together with the corresponding experimental points. For cases B and C the agreement is remarkably good. For the cases A, D and E the agreement is poor, especially case E. The distribution for case E (and to a lesser extent cases A and D) lies completely outside the family of classical distributions for all values of irregularity factor. Thus this certainly supports the hypothesis that the data for cases A and E is unrepresentative, but also indicates that the data for case D must be marginal.

The distributions for the remaining six cases are shown in Fig. 6.10. It is now immediately apparent that these curves lie in the same family. There is a continuous trend away from the Rayleigh distribution (I.F. = 1.0) with decreasing irregularity factor. There is an increasing proportion of smaller ranges and decreasing proportion of larger ranges as the spectrum widens. The proportion in the neighbourhood of .75σ stays roughly constant until the I.F. gets below 0.5. Note that for case D the range distribution departs very slightly from the trend of the remainder of the family, having a relatively higher peak. This clearly indicates that the equivalent sampling interval for case D is marginal.

Another significant feature of the family of distributions is that the data (as stated previously) is derived from completely different sources, indicating that the overall distribution of ranges (like that of peaks) may depend only on the spectrum width parameter (or irregularity factor).

Examined next is the likelihood of the distribution of ranges for each value of mean being independent of the mean value. In Figs. 6.11 - 6.16 is given the distributions for each value of mean compared with the overall distribution for each case. The departure from the overall distribution is fairly small in all cases. Note here that the data for the relatively higher values of mean (depending on I.F.) is omitted on the grounds that the samples for these are too small. However the data presented here in the figures includes about 95% of all ranges - that is the ignored data is about one twentieth of the total.

Finally the distribution of the mean values is examined. As found previously by Schijve (ref. 6) the distributions are normal for the six cases (Figs. 6.17 - 6.19) The variation of the standard deviation of the means with irregularity factor is shown in Fig. 6.20.

In conclusion it is submitted that an adequate model for the distribution of ranges is that represented by the family given in Fig. 6.10, with the distributions independent of mean value and dependent only on the irregularity factor. The proportion of ranges at each mean is known from the normality of the distribution of mean values, using the empirical relation between mean r.m.s. and the function r.m.s. given in Fig. 6.20.

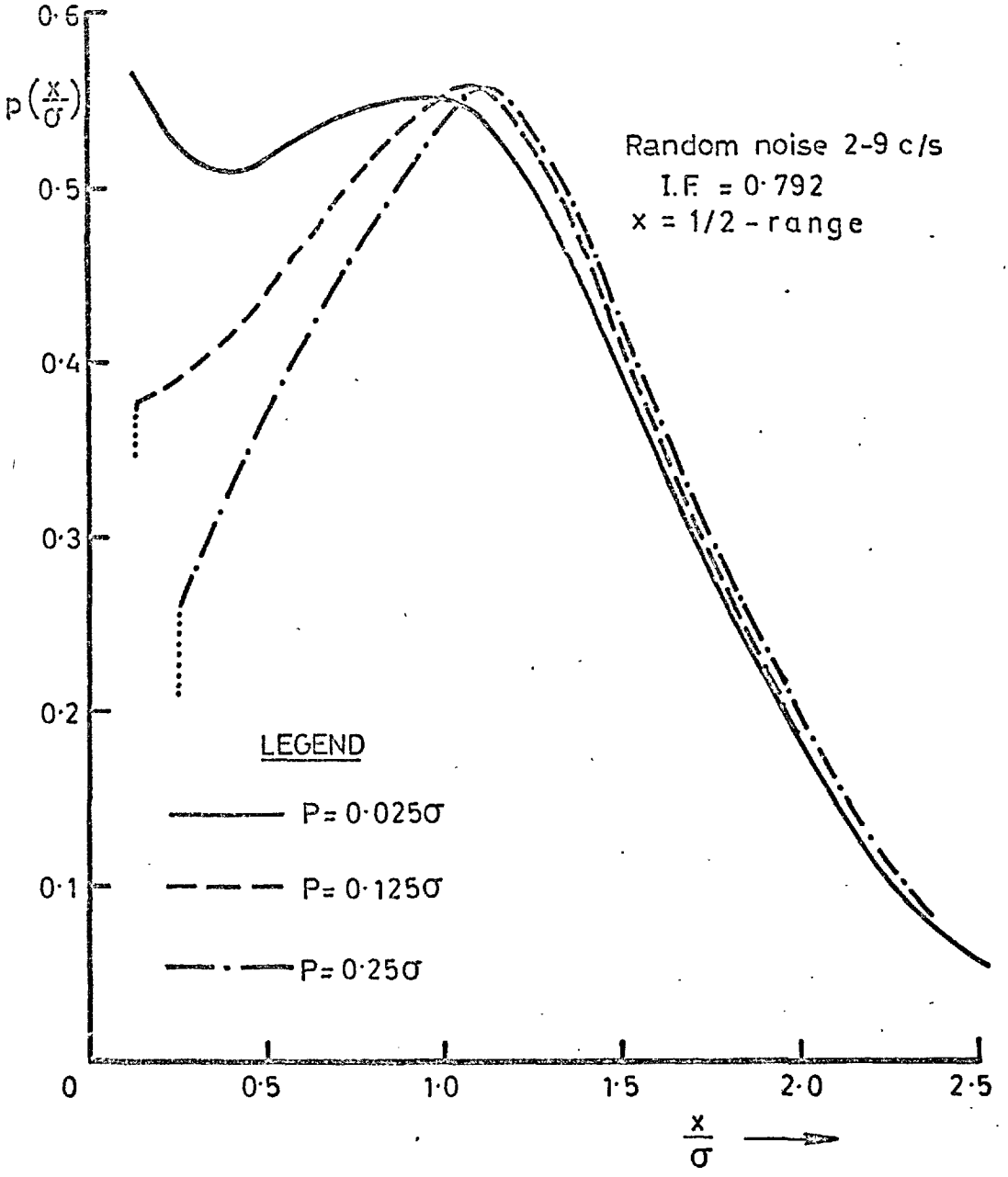

FIG. 6.1 EFFECT ON RANGE DISTRIBUTION OF IGNORING 1/2 - RANGES LESS THAN P (P = ·025σ, ·125σ, ·25σ).

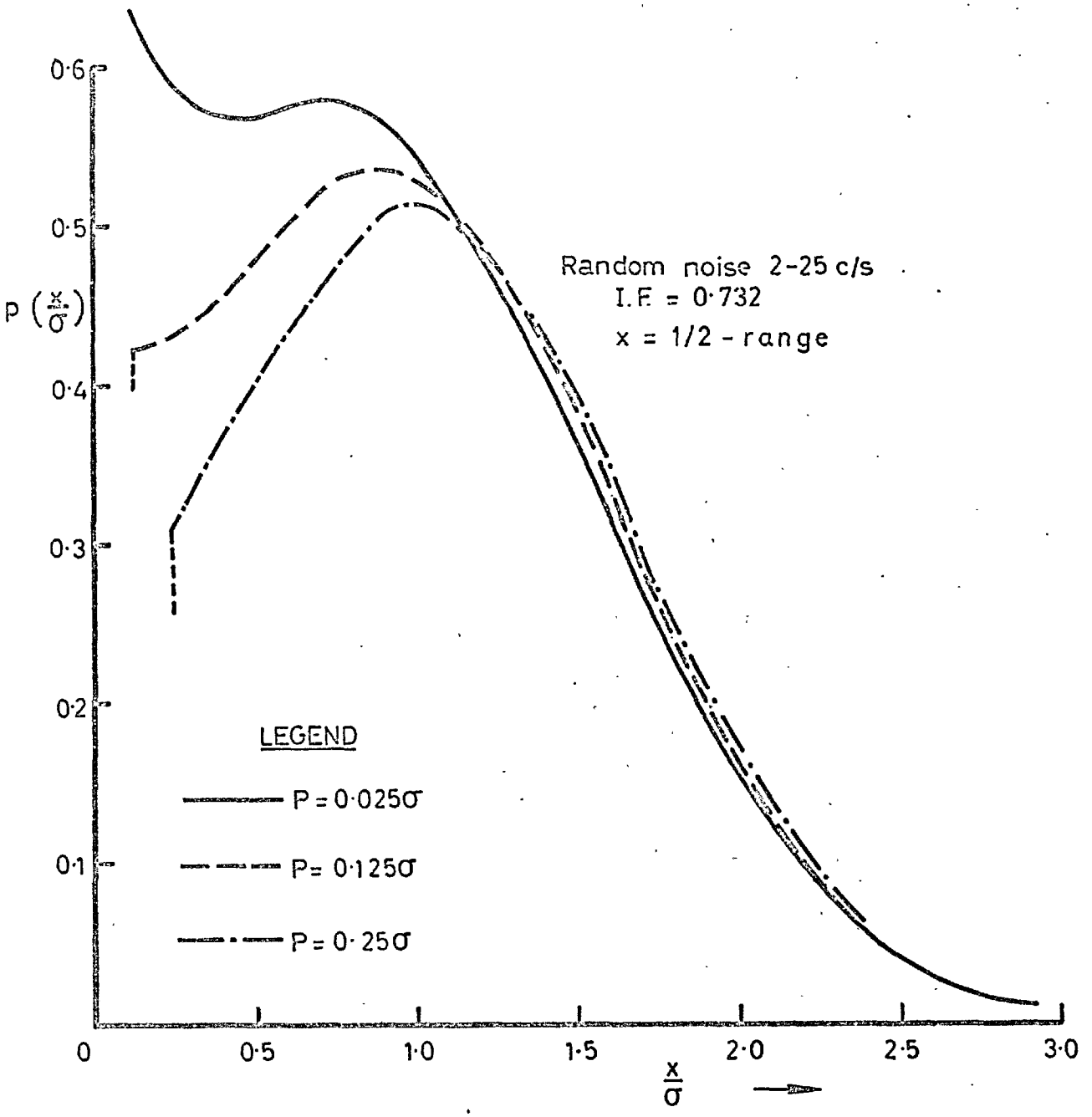

FIG. 6.2 EFFECT ON RANGE DISTRIBUTION OF IGNORING 1/2-RANGES LESS THAN P (P = ·025σ, ·125σ, ·25σ).

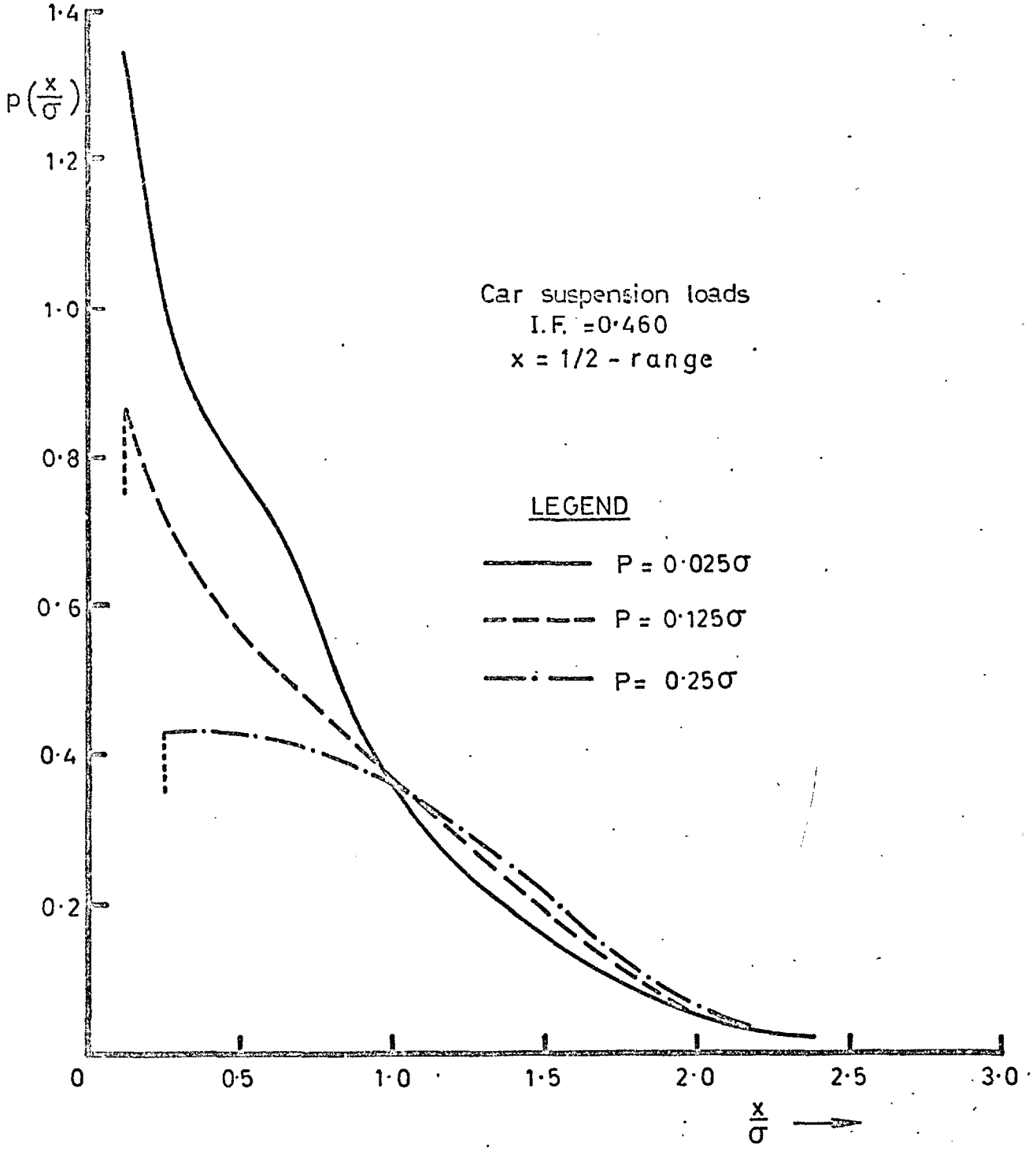

FIG. 6.3 EFFECT ON RANGE DISTRIBUTION OF IGNORING $\frac{1}{2}$RANGES LESS THAN P (P=·025σ, 0·125σ, 0·25σ).

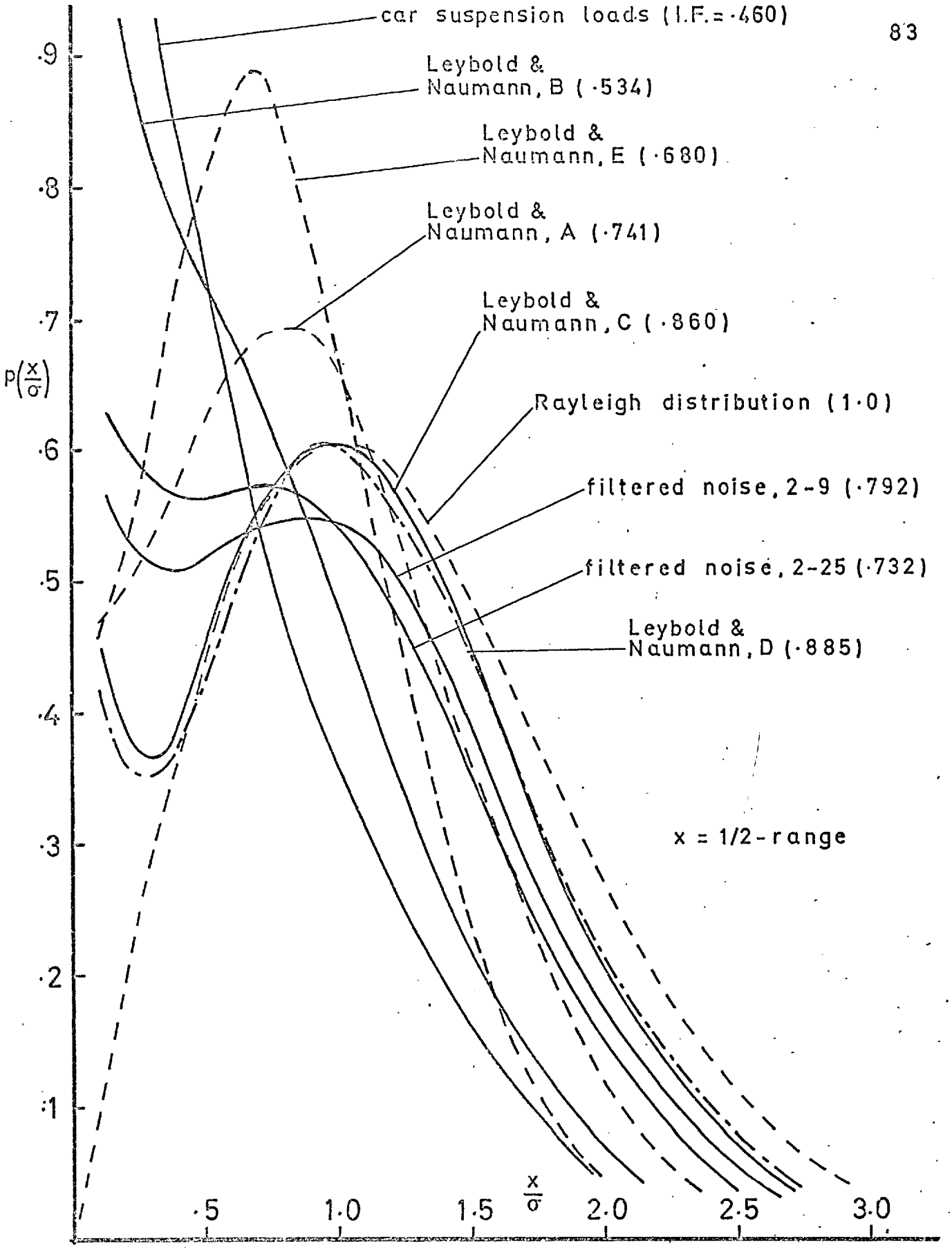

FIG. 6.4 RANGE DISTRIBUTIONS – ALL CASES

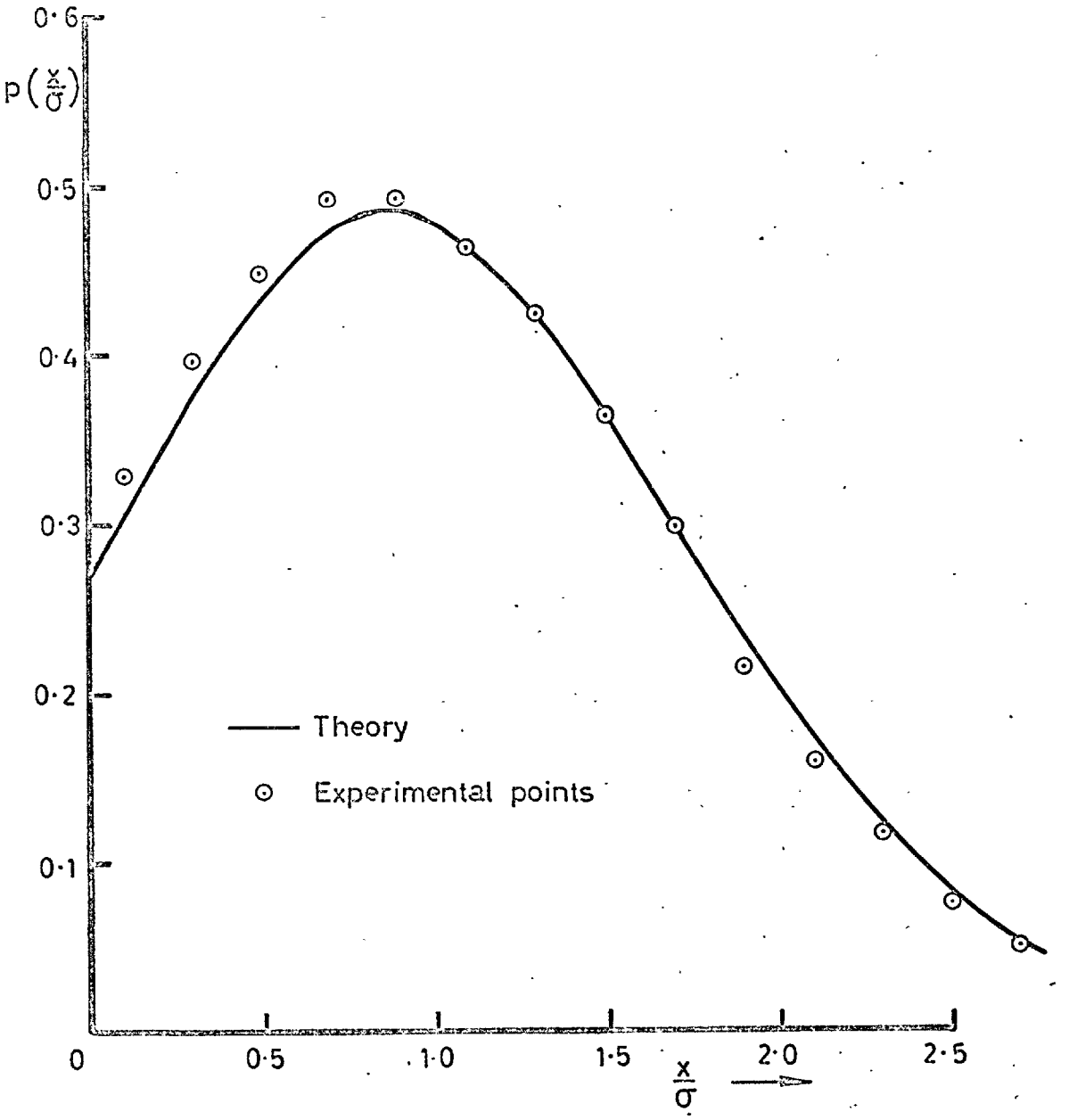

FIG. 6.5 PEAK DISTRIBUTION CURVE : A n = 0·74.

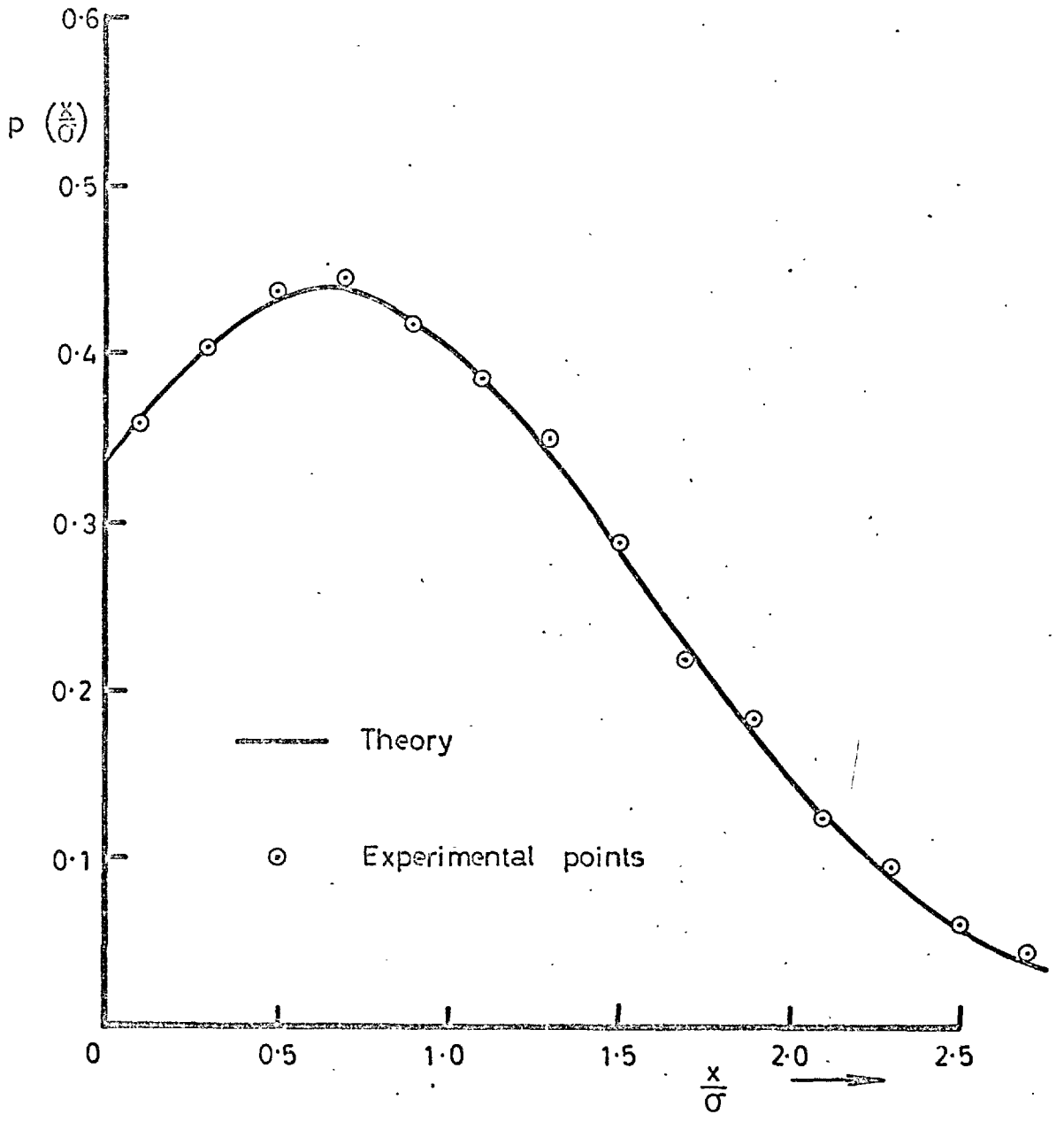

FIG. 6.6 PEAK DISTRIBUTION CURVE : B n = 0·53

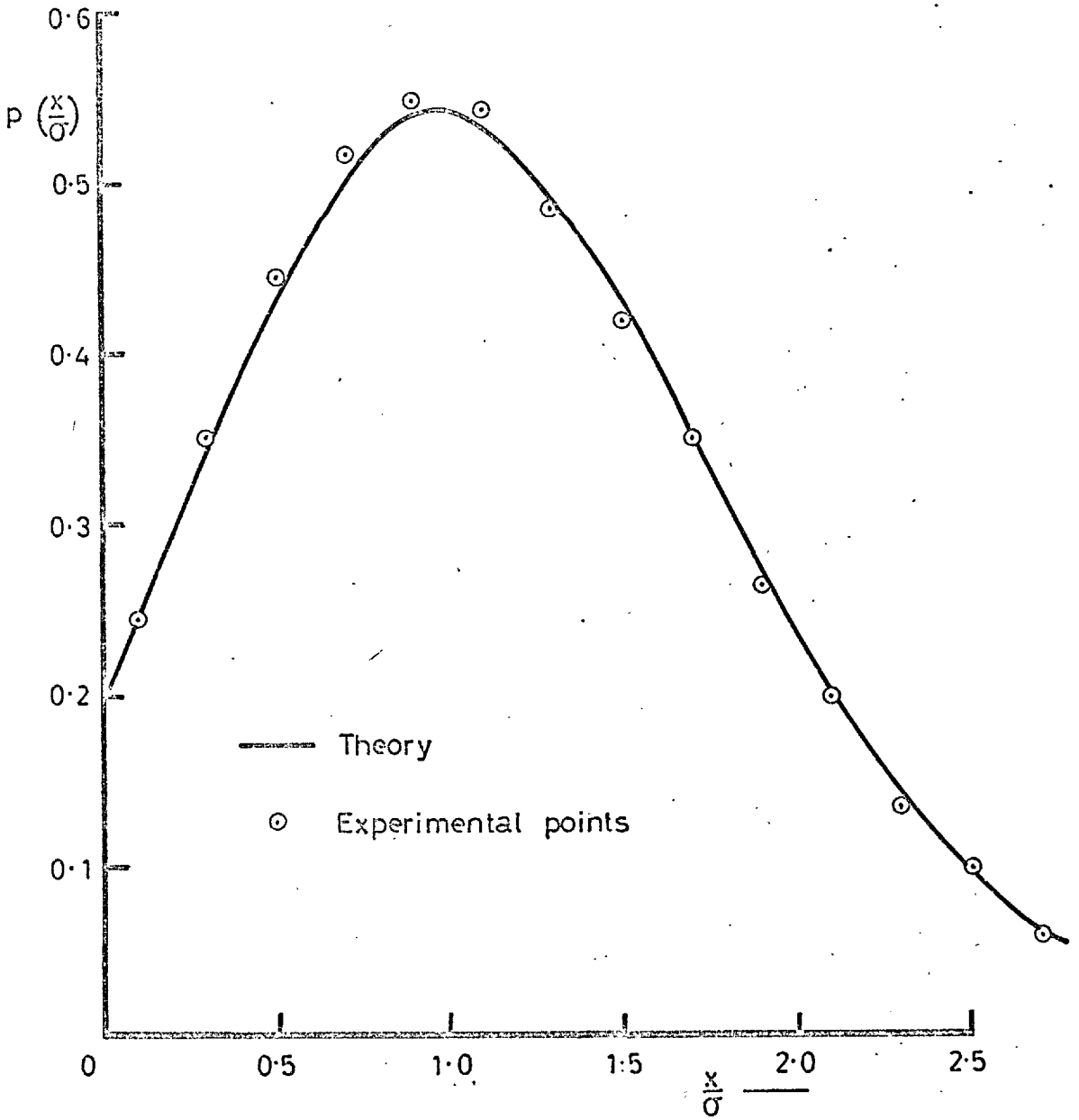

FIG. 6.7 PEAK DISTRIBUTION CURVE C n = 0·88

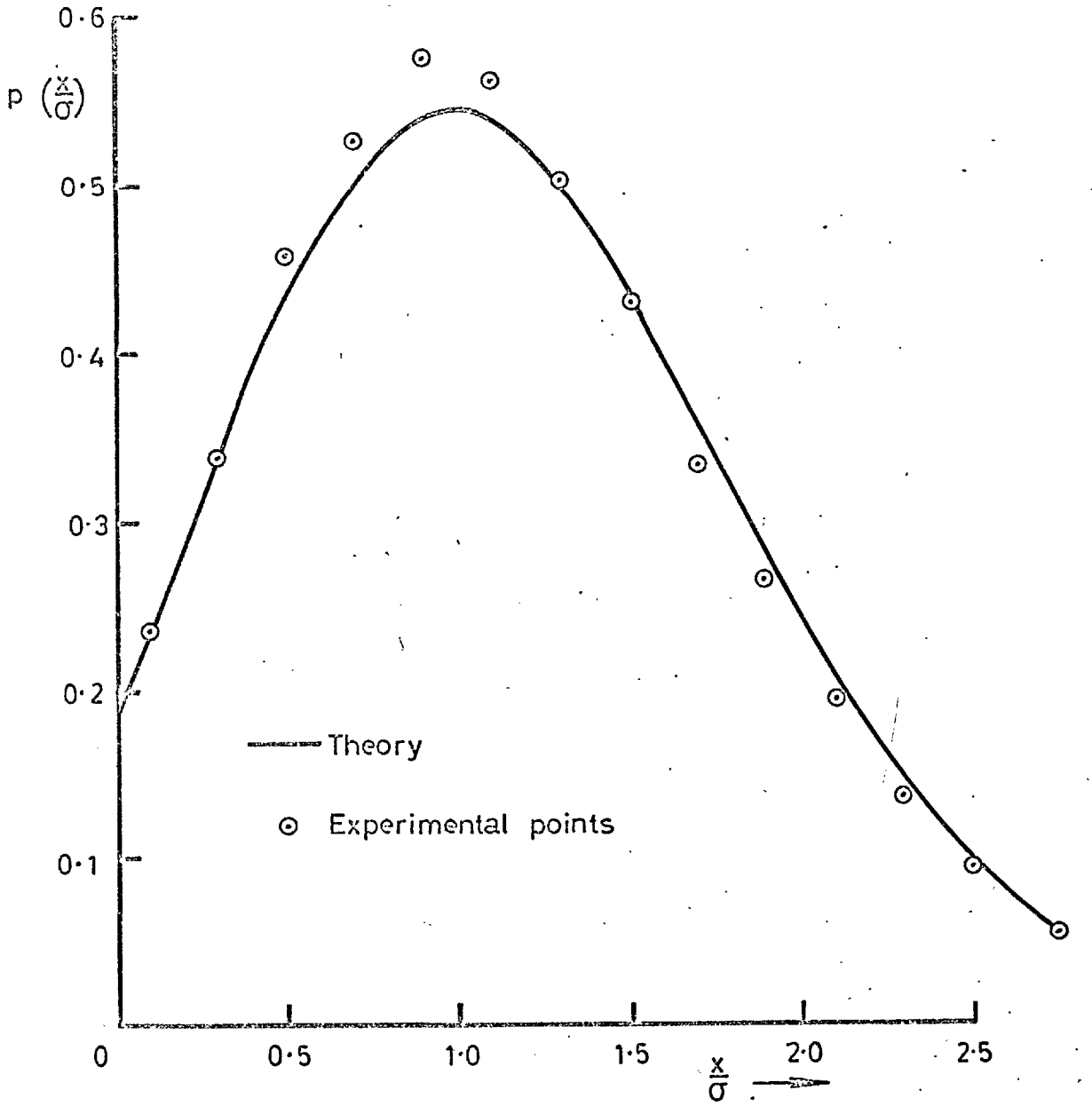

FIG. 6.8 PEAK DISTRIBUTION CURVE D n = 0·89

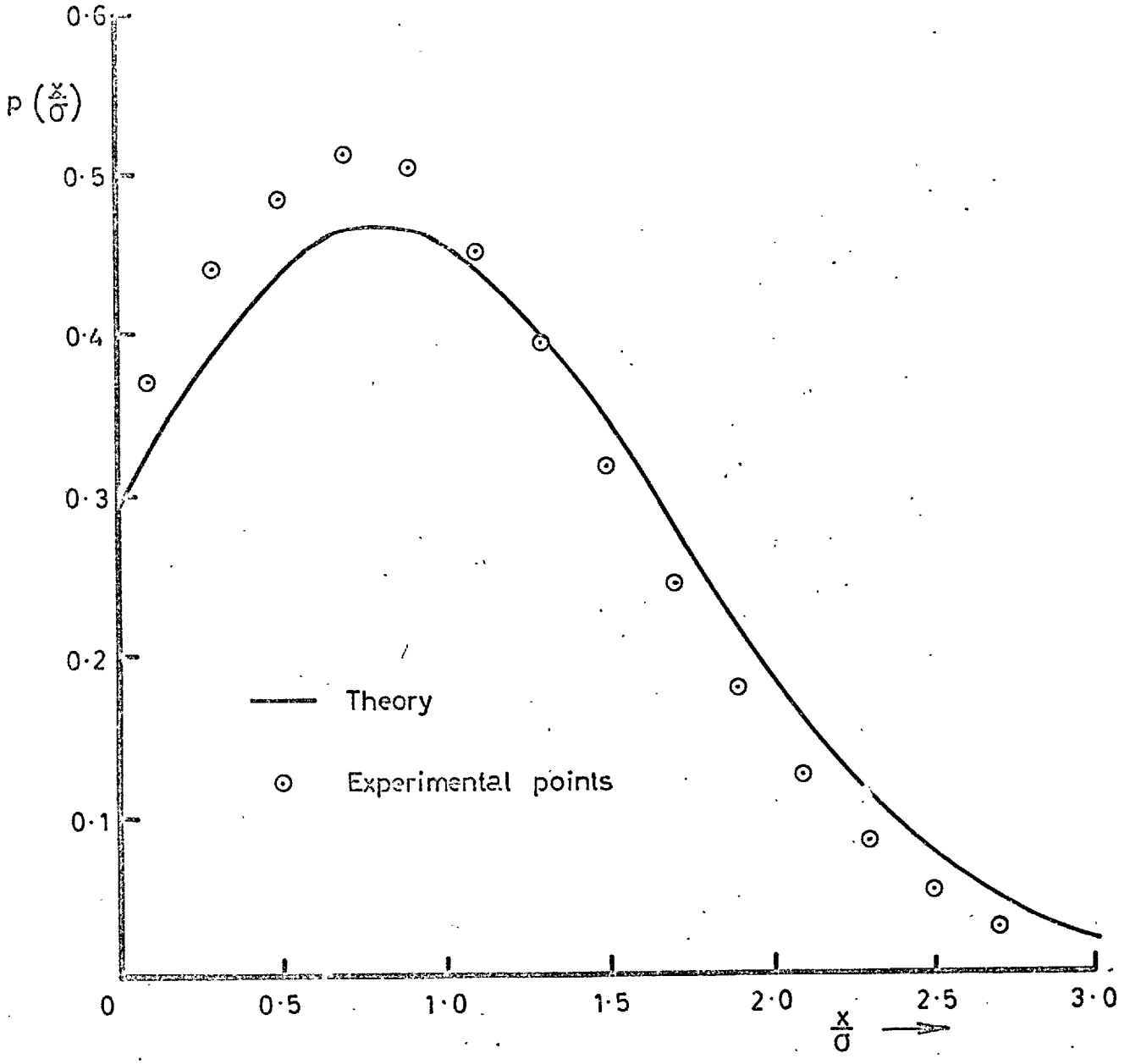

FIG. 6.9 PEAK DISTRIBUTION CURVE E n = 0·68.

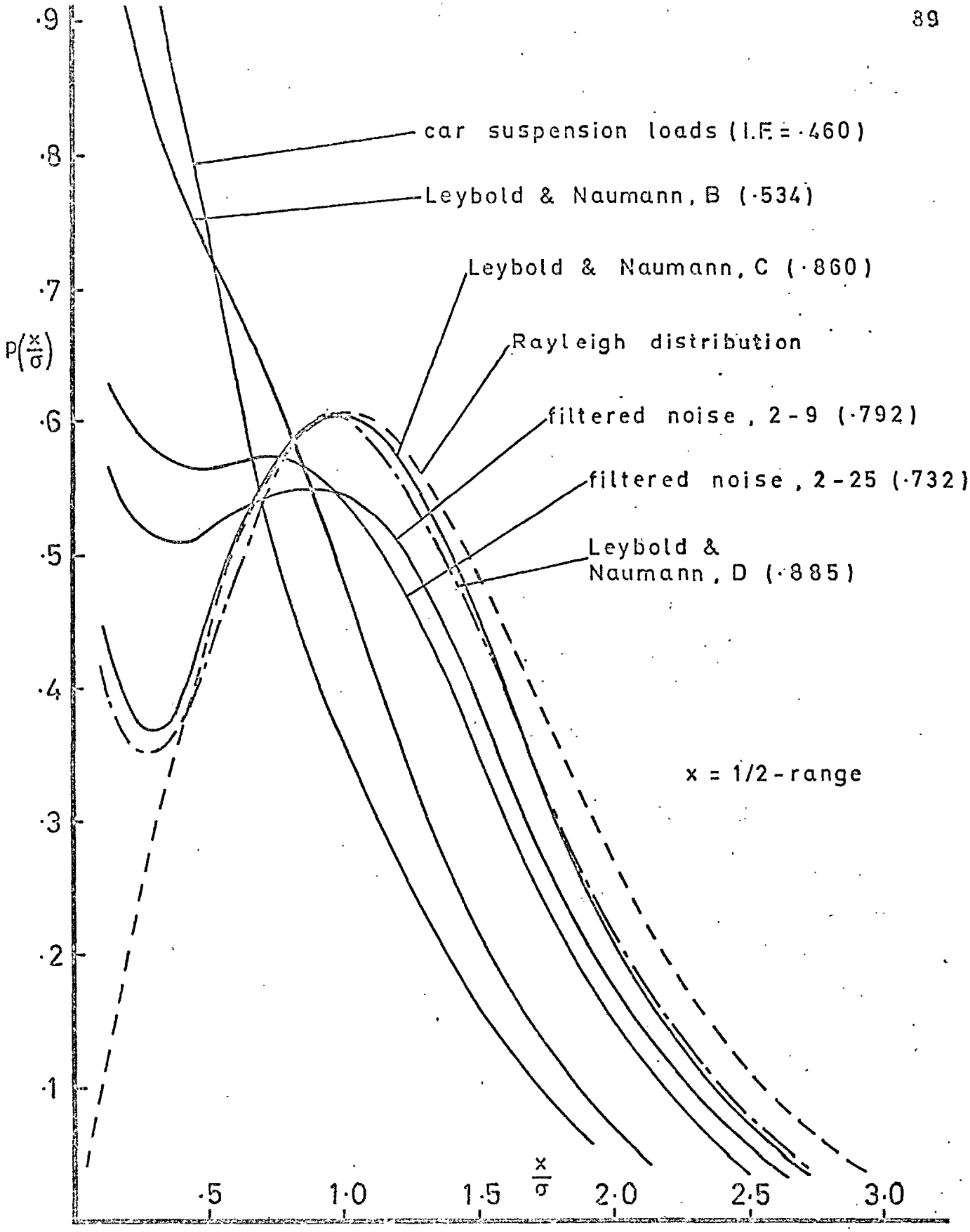

FIG. 6.10 RANGE DISTRIBUTIONS – ACCEPTED CASES

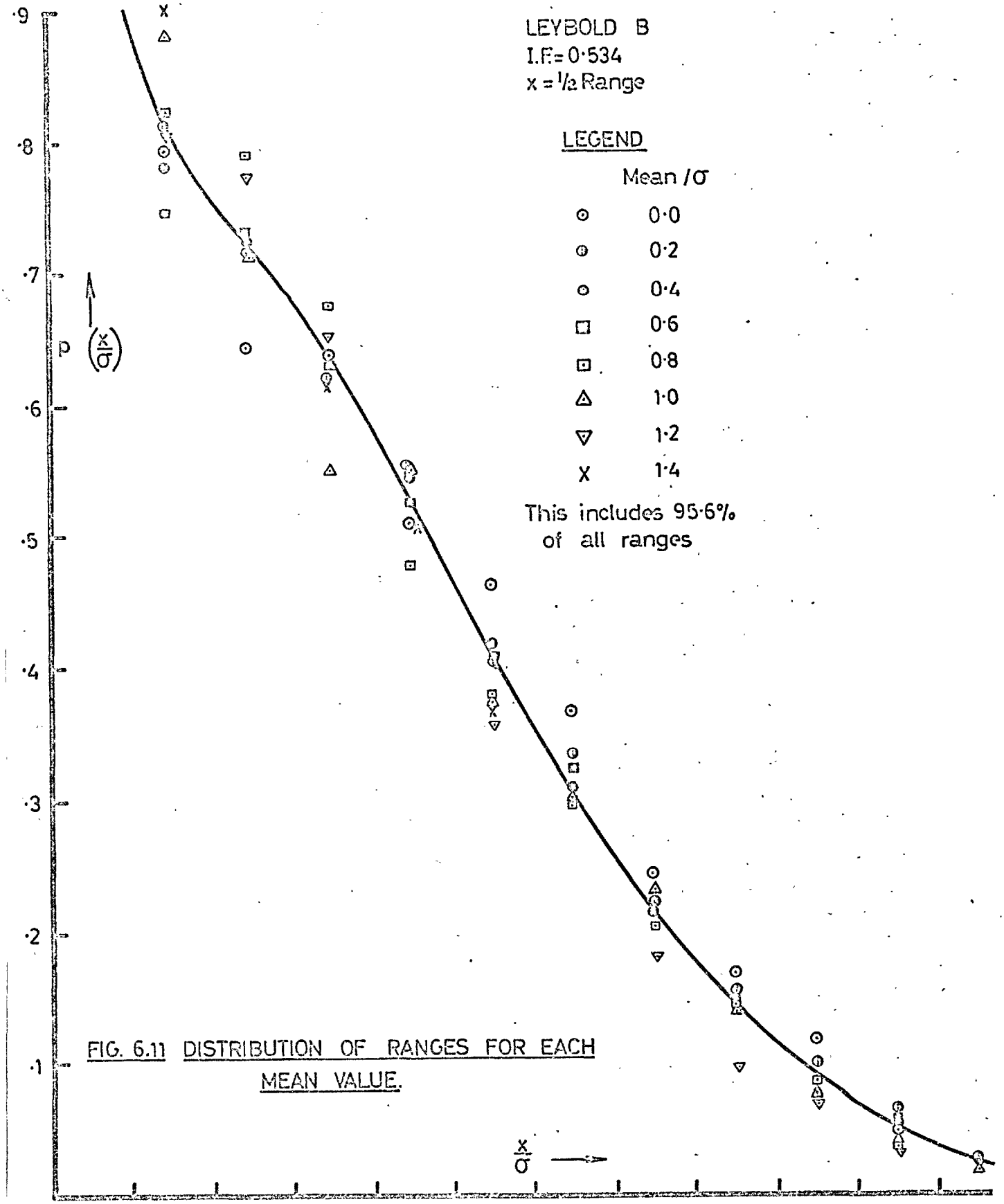

FIG. 6.11 DISTRIBUTION OF RANGES FOR EACH MEAN VALUE.

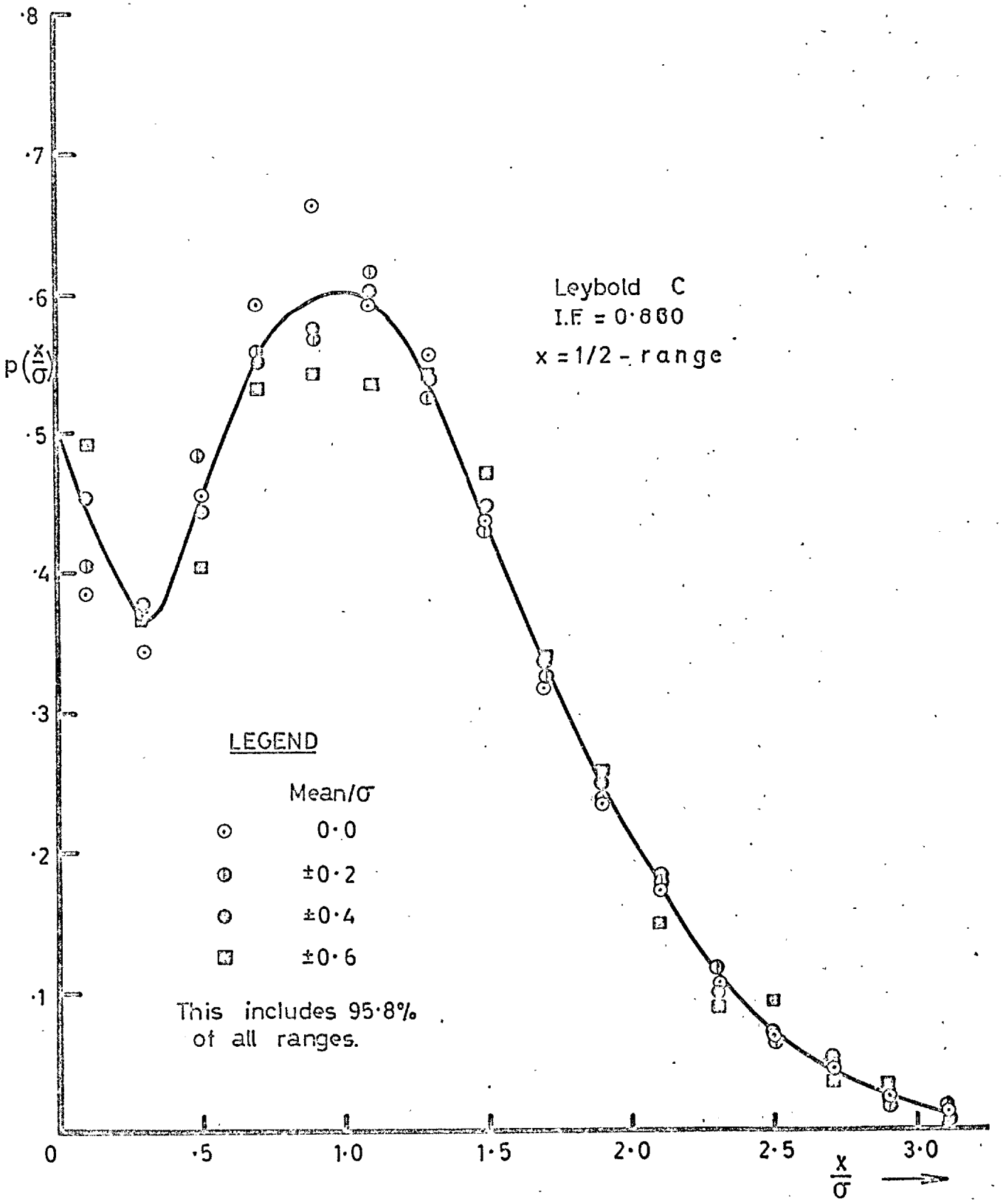

FIG. 6.12 DISTRIBUTION OF RANGES FOR EACH MEAN VALUE.

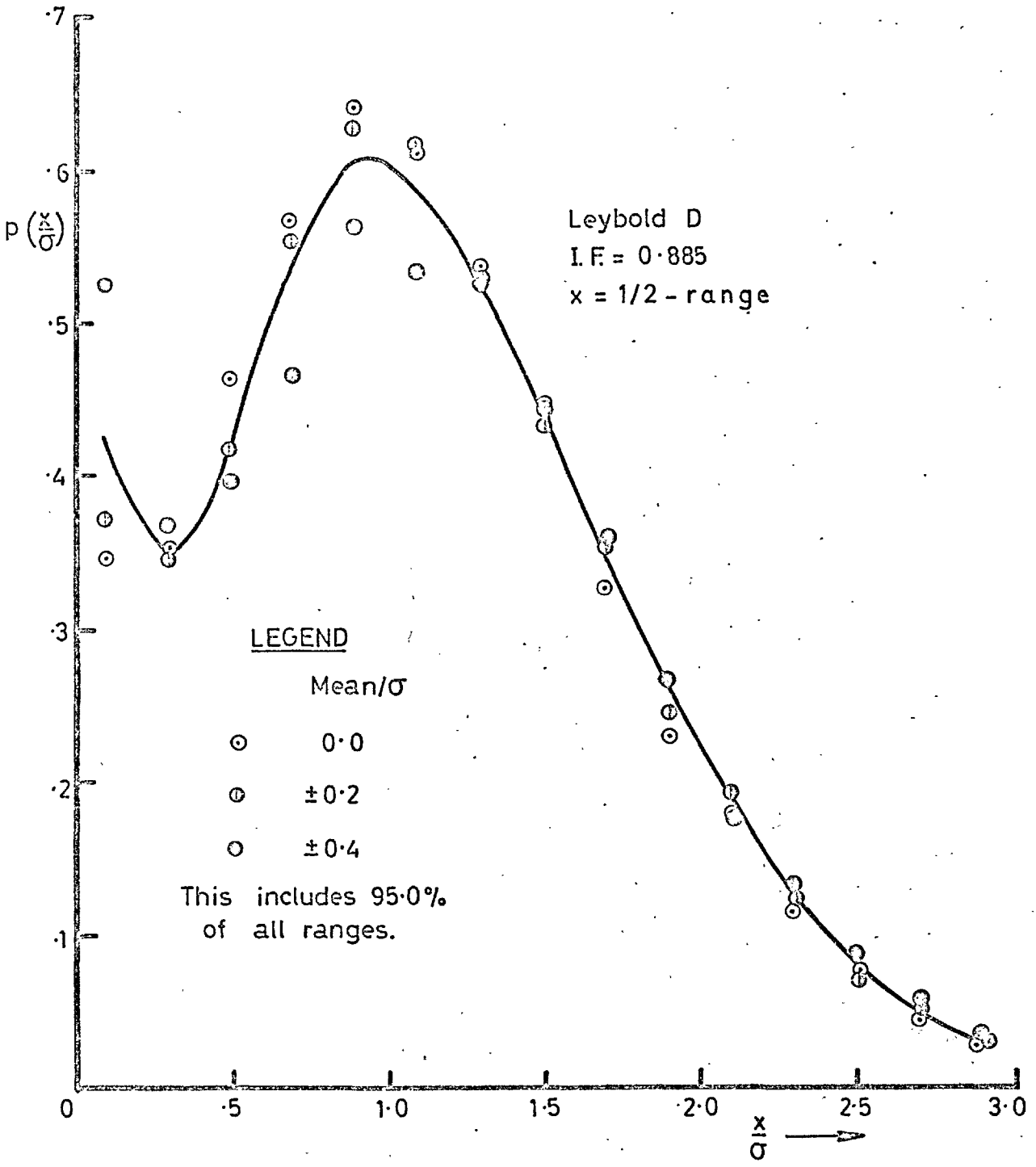

FIG. 6.13 DISTRIBUTION OF RANGES FOR EACH MEAN VALUE.

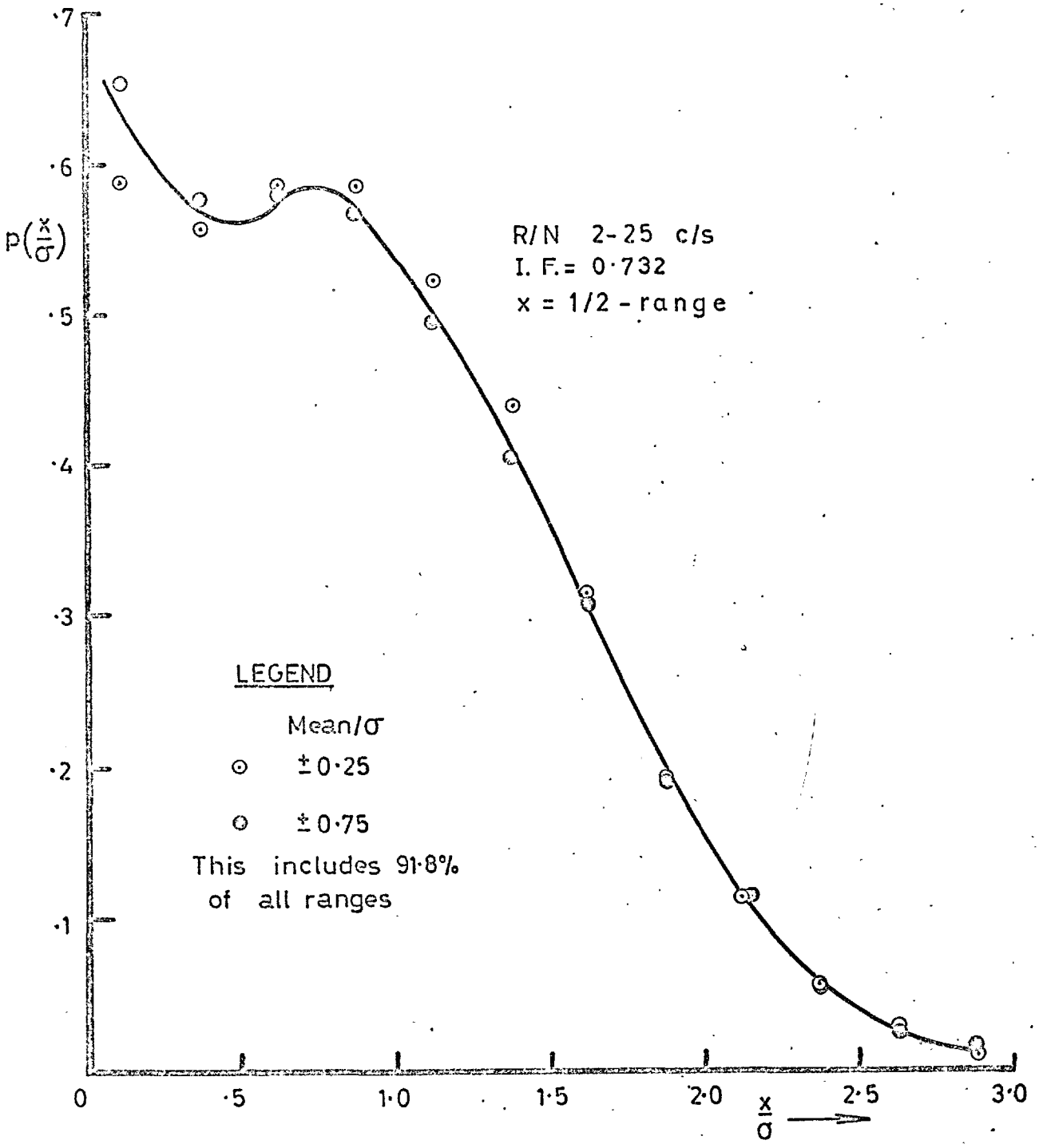

FIG. 6.14 DISTRIBUTION OF RANGES FOR EACH MEAN VALUE

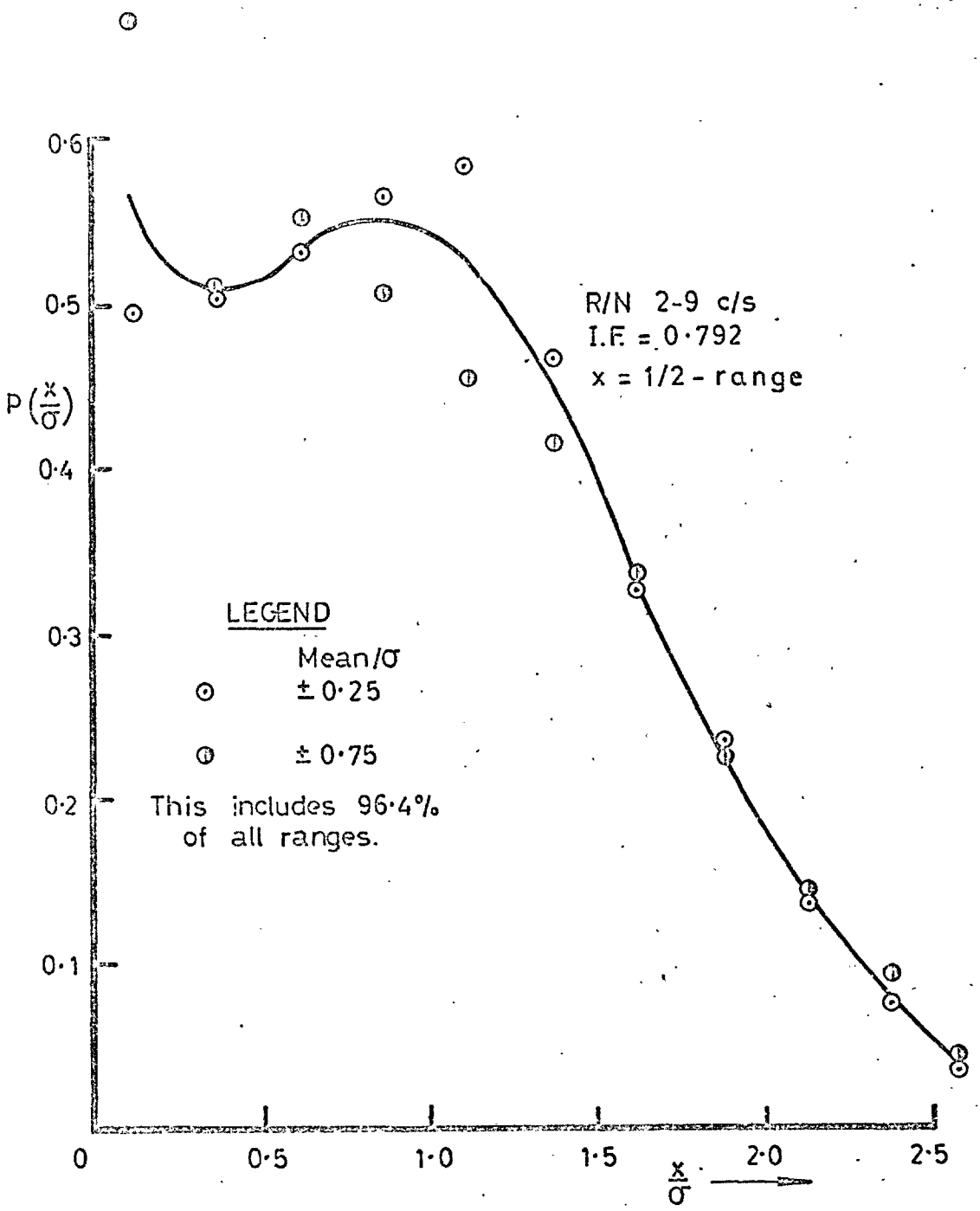

FIG. 6·15 DISTRIBUTION OF RANGES FOR EACH MEAN VALUE

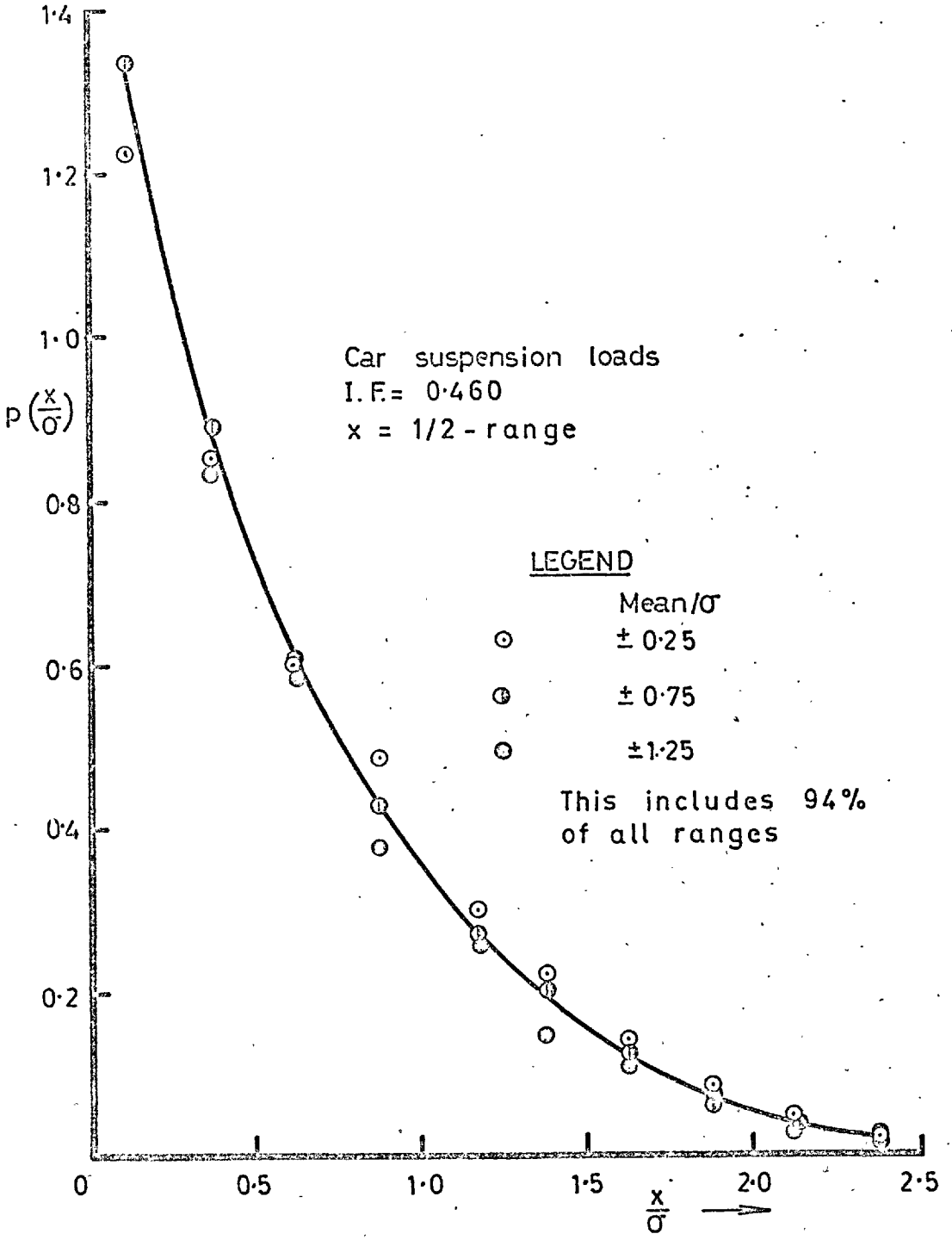

FIG. 6.16 DISTRIBUTION OF RANGES FOR EACH MEAN VALUE

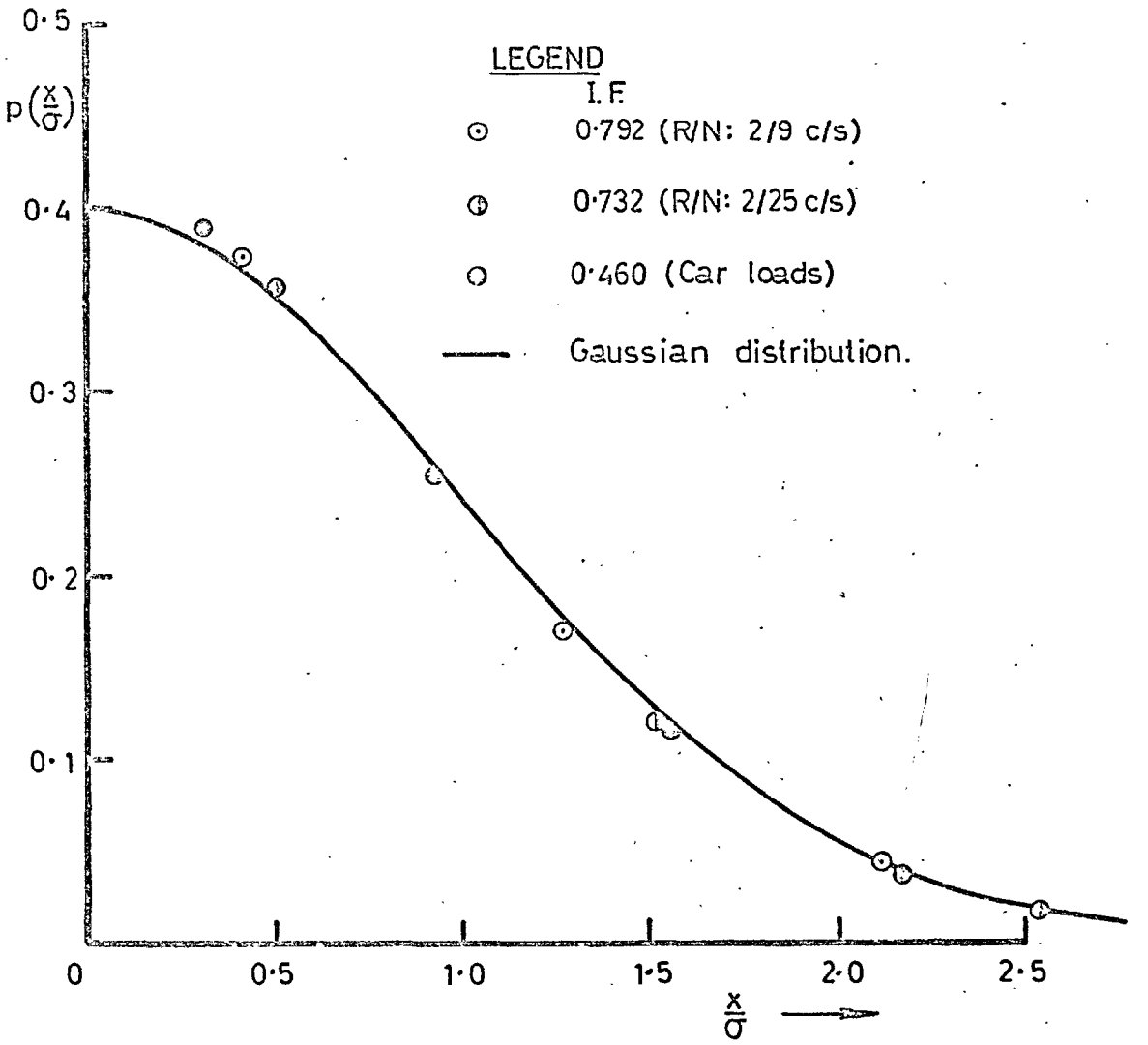

FIG. 6.17 DISTRIBUTION OF MEANS

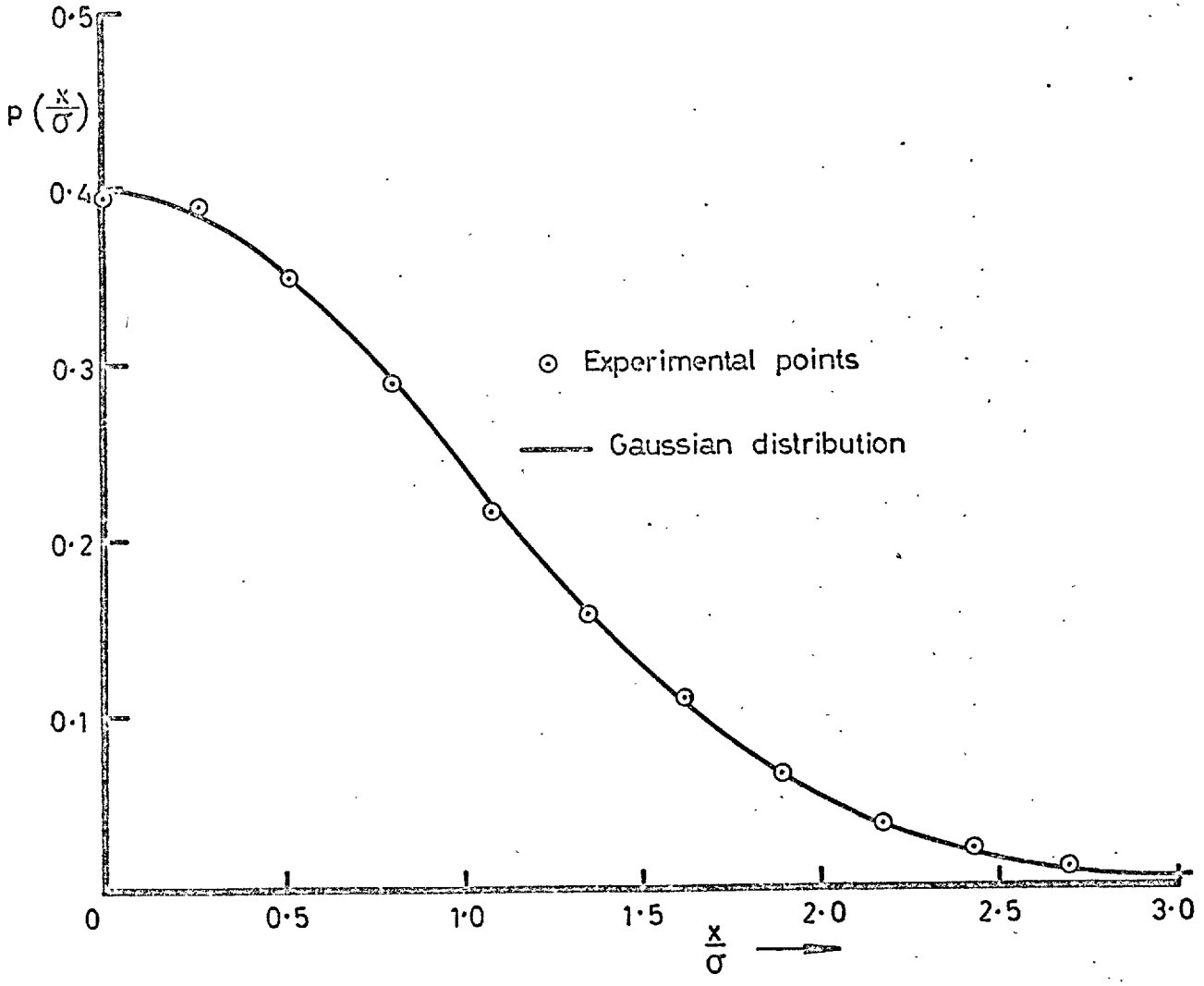

FIG. 6.18 DISTRIBUTION OF MEANS LEYBOLD – CURVE B

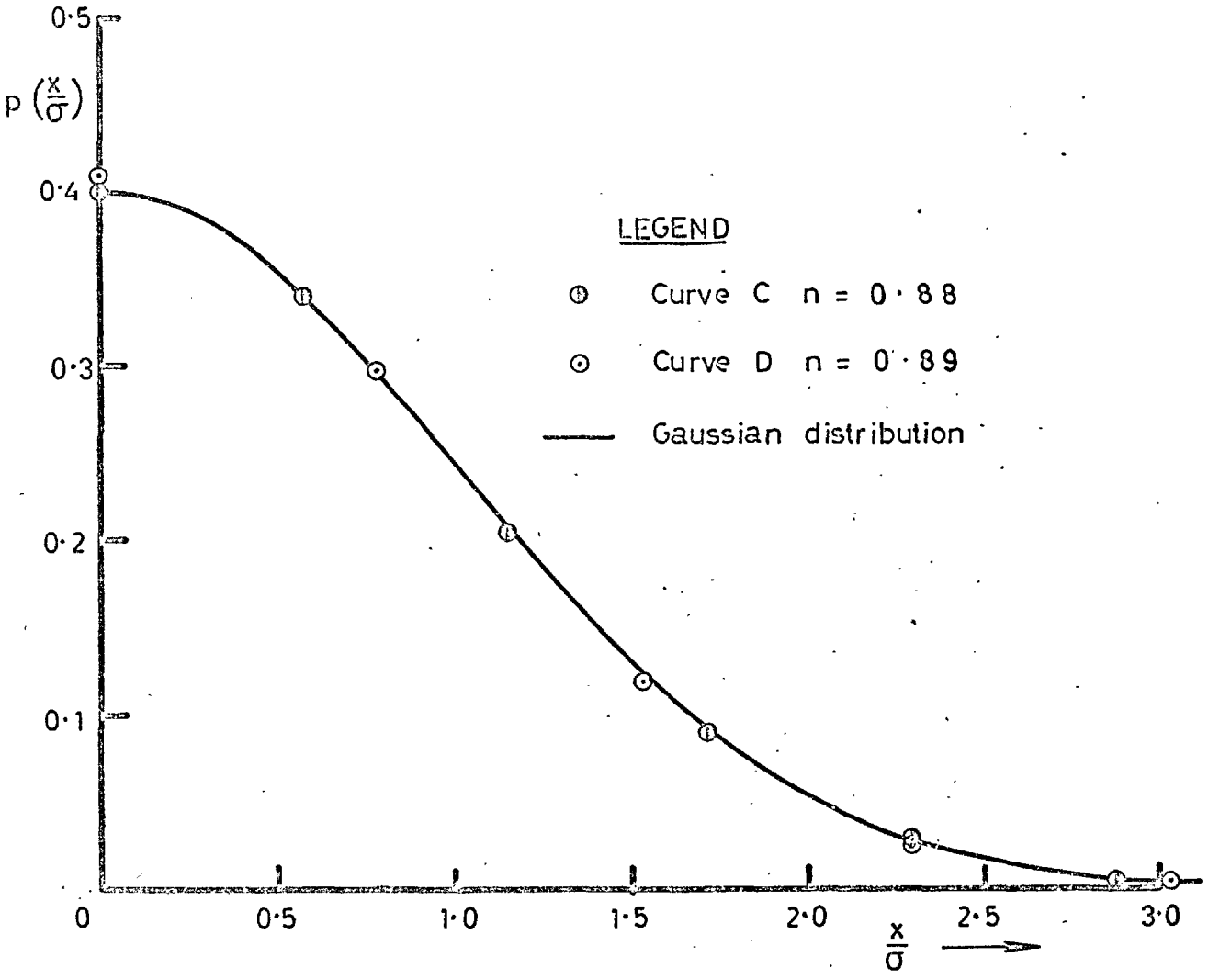

FIG. 6.19 DISTRIBUTION OF MEANS LEYBOLD CURVES C & D.

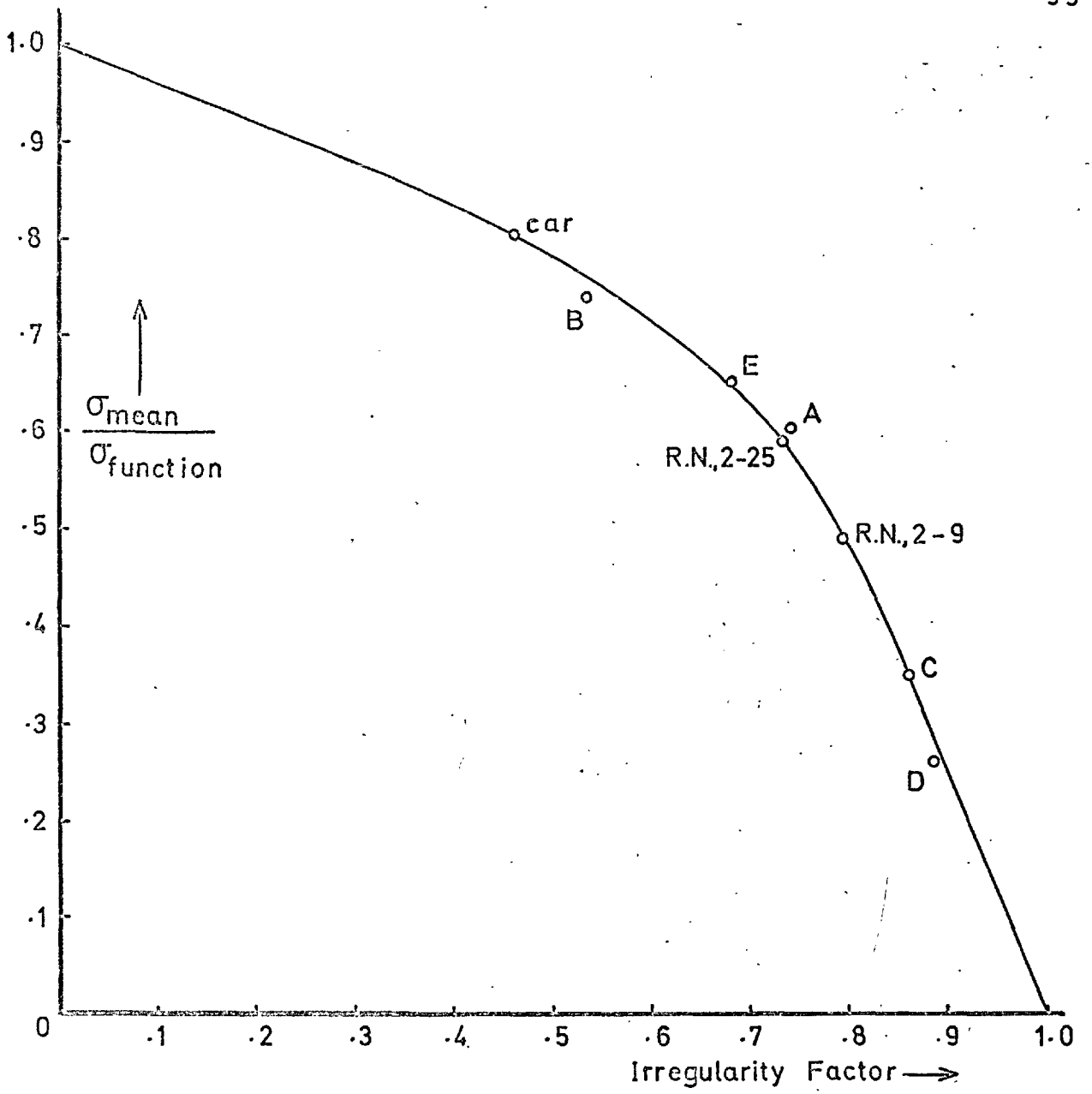

FIG. 6.20 VARIATION OF R.M.S. MEANS WITH I.F.

SOURCE	2-9	2-25	CAR	A	B	C	D	E
I.F.	·792	·732	·460	·741	·534	·860	·885	·680
σ_m/σ_f	·492	·590	·804	·604	·741	·350	·262	·654

7 REVIEW OF RANDOM FATIGUE TESTS

The irregularity factor describes the distribution of peaks, and has been demonstrated to be the major parameter in a model of the distribution of ranges. It is an obvious step to investigate its role in random fatigue testing. Random testing has been performed at several research establishments, and a comprehensive bibliography can be found in ref. 3. There follows a brief investigation into the published work to establish any consistent trends in the effect of the irregularity factor.

The fatigue process incorporates several mechanistic phases. Principally these are the crack initiation phase and the crack propagation phase. The initiation phase may be subdivided into a shear crack initiation phase and shear crack propagation phase, leading to the direct (tensile) stress crack propagation. Thus it may seem unlikely that any one general trend of the effect of irregularity factor will exist.

However the fatigue condition in aircraft is usually high values of stress concentration and relatively high mean loads, so that the fatigue process will be essentially direct stress crack propagation. Secondly random testing may interact the mechanistic phases. For an example, Forsyth's terminology of Stage I (slip plane growth) and Stage II (propagation on plane perpendicular to maximum tensile stress ref. 14) will be used. The transition from Stage I growth to Stage II growth may possibly be delayed owing to periodic low stress cycling during the random sequence which may cause sections of an incomplete crack front to revert to Stage I growth, thus reducing the effectiveness of the crack front

as a stress raiser to subsequent higher tensile loads. Such an effect could take place over a range of values of r.m.s. loading.

Another example of the interaction effect could be explained in terms of residual stresses, where earlier higher loads in the random sequence cause residual stresses which reduce the effect of subsequent lower stress cycles. A further example of random loading effects is that brittle striations are very often found in service loading failures, whereas in constant amplitude or programme tests they are not as common (Jacoby, ref. 16). This indicates a certain uniqueness about random loading, as also does the fact that crack propagation rates are highest for random loading tests (Schijve, ref. 17).

In accordance with current practice, fatigue life is considered in the following discussion in terms of counts of zero-crossings as a function of r.m.s. stress. Only work which includes the testing of similar specimens with at least two different types of random loading is discussed.

Clevenson and Steiner (ref. 13) performed tests on 2024-T4 round bars with a circular notch, with a stress concentration factor of 2.2 at zero mean stress. Although the tests are classed as axial the stress distribution will clearly not be axial (except for axial symmetry) due to the shape of the specimen. Clevenson and Steiner studied the effect of the spectrum shape on fatigue life and concluded that the spectral shape and irregularity factor have only a secondary effect. However, two-thirds of their tests were performed with values of irregularity factor between 0.8 and 1.0. Only 20% of the tests were performed with an irregularity factor of less than 0.75.

Clearly this invites the proposition that spectral shape is irrelevant provided the irregularity factor is approximately constant; that is that the irregularity factor (together with r.m.s. stress) is the controlling parameter in random tests. Their results have therefore been separated into two groups corresponding to irregularity factor bands of 1.0 to 0.8 and 0.8 to 0.6. In the first group (say irregularity factor = 0.9) are 48 specimens, and in the second group (say irregularity factor = 0.7) are 26 specimens. A linear regression has been performed for both groups to find the log S v log N relation.

The two groups regress onto two almost parallel, but distinctly separate, straight lines (fig. 7.1). The lives for the wider spectrum group (irregularity factor = 0.7) are systematically less than those for the narrower spectrum group (irregularity factor = 0.9) by a factor of about 1.8. The co-efficients of linear correlation for the two groups are 0.98 (larger group, irregularity factor = 0.9) and 0.95 (smaller group, irregularity factor = 0.7) compared with a value of 0.96 in a single regression of all the results. Thus the improvement in the correlation of the larger group is only barely significant. The correlation for the smaller group is still good, but note that there is a greater amount of scatter in the results for the smaller group (irregularity factor = 0.7) at the lower stress levels. The statistical significance of the groupings can be further examined from the plots of the results. The line corresponding to the linear regression of the larger group (0.9) corresponds to the 85% confidence line for the smaller group (0.7) and the line for the smaller group (0.7) corresponds to the 15% confidence line for the larger group (0.9).

This does not necessarily mean that the effect of

irregularity factor is negligible, as the authors concluded. It surely indicates a need for further empirical data before making an assessment of the effect of irregularity factor, more tests particularly in the wider spectrum group are really necessary. Secondly it may be possible that still lower values of irregularity factor may have an appreciable effect.

Swanson (ref. 11) performed tests on axially loaded 2024-T4 unnotched bars with a mean stress of 16000 psi. These tests were performed using both a single degree of freedom system and a two degree of freedom system to obtain two spectral shapes. The values of irregularity factor obtained were 0.96 and 0.57. Fig. 7.2 shows the effect of r.m.s. stress on endurance measured in zero-crossings. For lives below 6.10^5 the wider spectrum has an appreciably more severe effect, the spectrums becoming equally severe at that life. These results have therefore a degree of consistency with the more liberal interpretation of Clevenson and Steiner's results in spite of the fact that the testing conditions (mean stress and notching of specimen) are so different.

Naumann (ref. 9) performs individual cycle randomization tests on 2024-T3 notched sheet specimens with a stress-concentration factor of 4 and mean stress of 17.4ksi. The specimens are loaded to successive maximum and minimum values of the random signals, whose sources are sequences of random numbers. Thus the time scale when compared to a true continuous random signal has been altered. Secondly when selecting maximum and minimum values, variations (i.e. ranges) less than 20% of the r.m.s. value of the signal are omitted.

As explained in Chapter 6, these sequences of random numbers are equivalent to periodic samples of a

continuous function. The more maxima and minima that there are in a given sequence of numbers, the more poorly is the function represented by these numbers (the equivalent sampling intervals being longer). It is shown in Chapter 6 that the samples A and D (as referred to by Naumann) are severly limited in this respect, and give results inconsistent with the continuous signals they are supposed to represent.

The samples B (irregularity factor = 0.534) and C (irregularity factor = 0.856) give average fatigue lives (again based on zero-crossings) almost exactly equal (B; 80800, C; 80400) for the same r.m.s. loading. However in considering these results, the time scale limitation must be borne in mind. Although Jacoby (ref. 18) has found that for 2024-T3 clad notched specimens, the triangular-shaped load cycle and sine-wave load cycle lead to similar endurances, the rectangular shaped load cycle of the same amplitude leads to shorter endurances, particularly at higher stress levels. Evidently a time dependent mechanism is present. This may be creep at the higher stresses.

Another possible time dependent mechanism is cleavage (Forsyth, ref. 14). Thus it may be argued that a triangular-shaped cycle should lead to longer endurances than in the case of sine-wave cycles, and that the frequency effect should be greater than that observed by Schijve (ref. 20) However cleavage fracture is not found in metals with a face-centred cubic (FCC) structure, but in those with either body-centred cubic or close packed hexagonal structures (Schijve, ref. 21). It is significant that tests performed to find the effects of cycle shape (Jacoby, ref. 18) and frequency (Schijve, ref. 20) have been done with either 2024 or 7075 alloys, both having FCC structures. However, such a time dependent mechanism should not affect Naumann's results

(2024 alloy), but triangulization of the loading may affect the endurance obtained for other alloys in this way.

Fuller (ref. 19) performed bending tests on 2024-T3 sheets with a stress concentration of 1 using three random traces with differing spectra, which produced very similar endurances. The values of irregularity factor quoted by Fuller are 0.96 (trace A), 0.75 (B) and 0.95 (C). These values are based on electronic counts of zero-crossings and hand counts of peaks.

The values of irregularity factor for cases B and C however do not agree with those estimated theoretically from the known power spectral density distributions. These estimates are 0.95 (A), 0.89 (B) and 0.81 (C). It is significant however that the number of zero-crossings (counted electronically) agree remarkably well with the estimates in all three cases. It is the discrepancies in the expected number of peaks causing the disagreement in irregularity factor. However the counts of peaks were not only done by hand but were based on samples which in Fuller's own estimate were small.

In addition the examples of traces that Fuller shows add to the confusion. The bandwidth for case C appears from the sample to be a lot wider than the empirical value of irregularity factor (0.96) would allow. Indeed an estimate from this sample is 0.59 - so that by either standard (p.s.d. estimate or empirical) it must be an unrepresentative sample.

A further check is the ratio between r.m.s. value of peaks and the r.m.s. of the continuous trace. This ratio is a simple function of irregularity factor. For the three cases the ratios correspond to the following values of

irregularity factor; 0.834 (A), 0.720 (B), 0.925 (C). Thus the measured irregularity factors for cases B and C are substantiated. However case A - apparently the one least in doubt, is not.

It is clear then that any conclusions regarding the effect of irregularity factor on endurance cannot be made in this case. In fairness to Fuller it must be pointed out that his work deals with far more broader problems in random fatigue than just the effects of spectrum width. His comments on this particular aspect are really minor facets of a very comprehensive treatise.

It may be concluded therefore, from this review of random testing, that the commonly held view that spectrum shape has no effect on endurance is not substantiated. Indeed there are indications that for axial tests on 2024-T4 specimens wider spectra lead to lower endurances, with the effect increasing with overall mean stress level. This trend could be explained on the grounds of favourable residual stresses. For narrow bandwidth loading there is a greater proportion of high loads than for ~~narrower~~ wider bandwidth loading at the same r.m.s. level. This fact coupled to higher overall mean stresses may account for a trend of this kind.

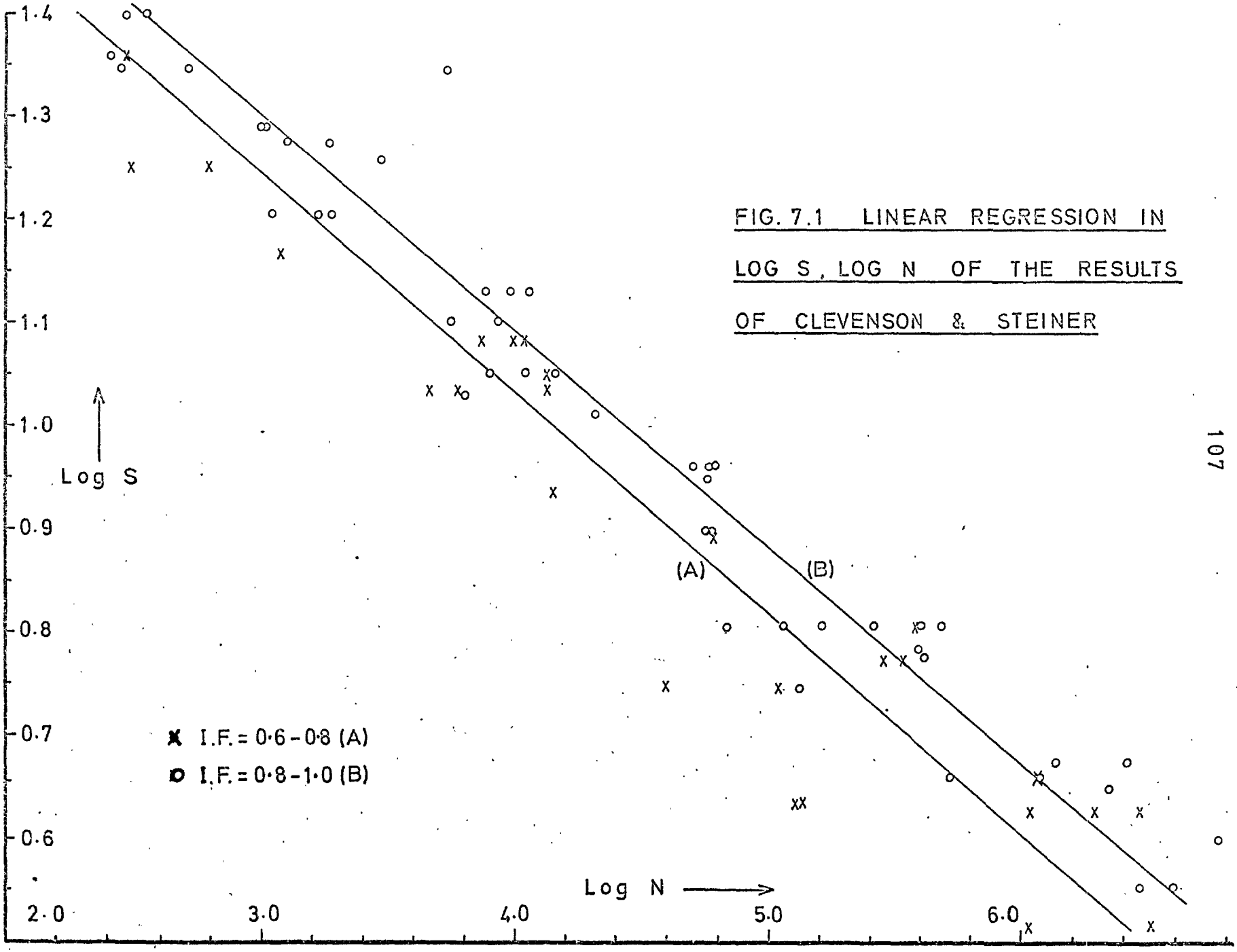

FIG. 7.1 LINEAR REGRESSION IN LOG S, LOG N OF THE RESULTS OF CLEVENSON & STEINER

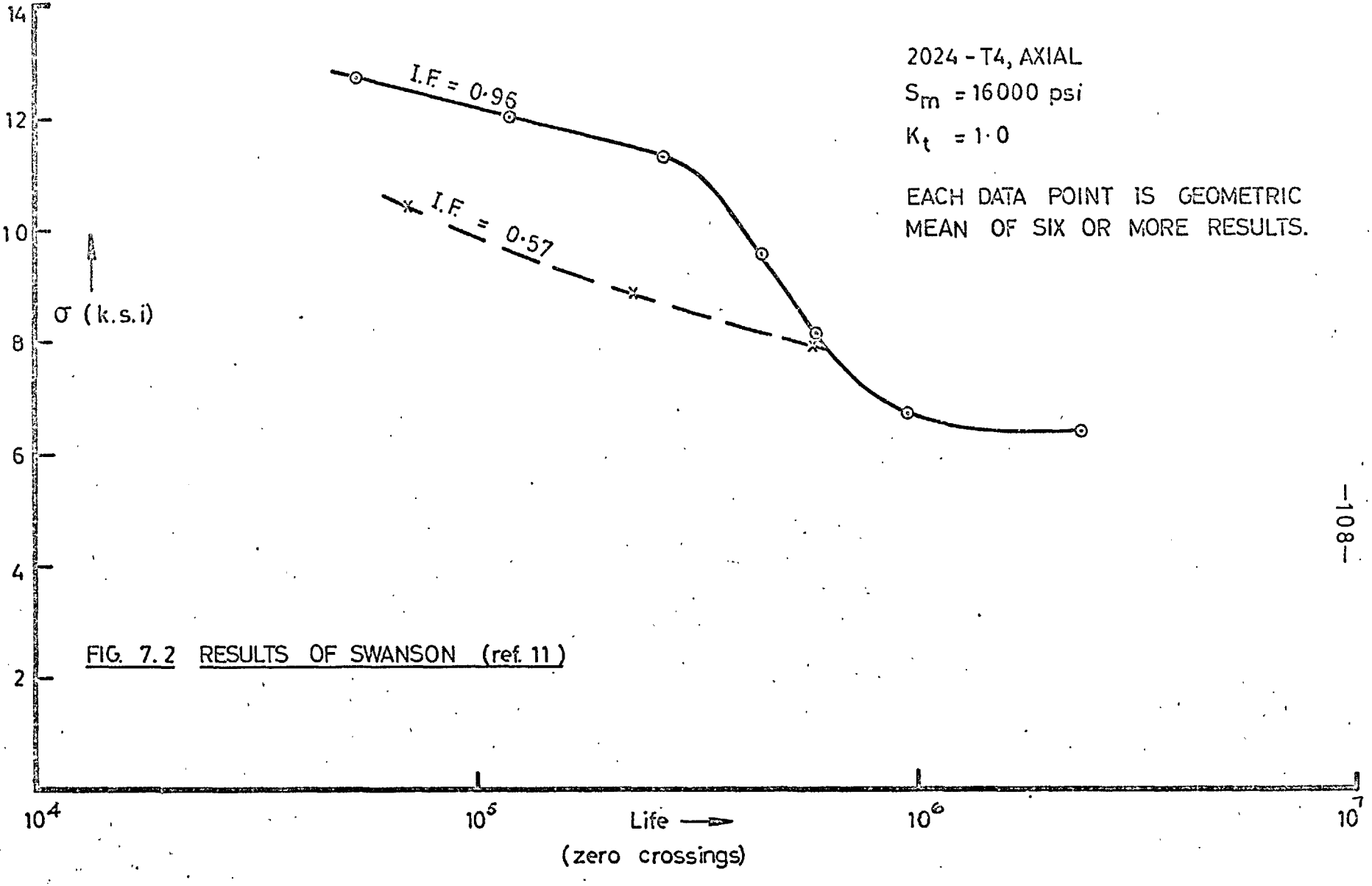

FIG. 7.2 RESULTS OF SWANSON (ref. 11)

8. CONCLUSIONS

A digital recording system has been designed and manufactured enabling the recording and analysis of continuous random signals. The system incorporates design features which have led to its comparatively low cost - and yet it has been found to be adequate for the purposes for which it was designed. One limiting feature in its design philosophy, namely the accumulative error characteristic, has been found to be acceptable.

This type of design could be used for much faster systems, recording over long periods. The use of higher packing densities on magnetic-tape, or higher tape speeds, or buffering the information to magnetic tape into larger blocks, would mean that much faster following rates could be achieved. The limitation of accumulative errors through drop-outs could be overcome by periodic (although relatively infrequent) resetting of the counter to zero and subsequent recycling. This could be an automatic feature of a faster system, and need not require an extra information channel for the recorder. An unused bit pattern (for example a pulse on both polarity channels simultaneously) could be used for the recycling.

The recording system has been used only to find various histograms. However power spectral density distributions are also obtainable. Instead of punching paper tape for maxima and minima, the digital value of the recorded signal can be punched at a constant rate through automatic triggering of the sampling facility which is available on the system console. The power spectrum is then obtained by Fourier transform of the auto-correlation function using any

of the normal digital methods. With the present configuration of the system, power spectra of signals with frequency contents up to 100c/s or more are obtainable in this way.

Most of the salient features of the results of the recordings have been discussed in Chapter 5, where comparisons of the counting methods are made on the basis of probability density distributions. It is the practice of some authors to compare counting methods using cumulative plots of the data. Probability density distributions show the proportion of events at each stress level, so that comparisons can be made using any chosen criteria in selecting the important ranges of stress for the comparison. Cumulative plots on a log scale are useful only in high-lighting events at higher stress levels.

The linear cumulative damage estimates have indicated the potentially large differences in estimated lives that can be obtained from different counting methods, particularly with wider bandwidth loading.

The establishing of the range distributions has brought to light several interesting points. The criterion for adequate representation of the ranges should be the agreement of the peak distribution with the theoretical distribution. For the cases considered here this apparently requires an overall average at at least $7\frac{1}{2}$ data points per cycle. This figure will, of course, be directly related to the minimum amount of digital data required to compute power spectral densities; an amount corresponding to a sampling rate of three times the maximum frequency content. Sampling at a rate lower than this leads to the effect known as aliasing, where power at frequencies greater than the

Nyquist frequency (half the sampling rate) is folded back into lower frequency regions of the spectrum.

This figure has an important bearing on random fatigue testing using digital techniques. There is now an increasing tendency towards digital representation of random loading. The continuous signal is not really fully represented unless the individual ranges are adequately described by the digital information. Thus the criterion for power spectrum calculations (of 3 data points per maximum frequency) is a necessary condition for the representation of the signal (otherwise the spectrum itself, is not properly prescribed, and therefore the distribution of ranges is not properly prescribed.)

The range distributions themselves may be of use in the development of crack propagation theories which up to now have assumed a Rayleigh distribution of ranges. The distributions are clearly not Rayleigh, even for the smallest bandwidth case considered (Irregularity Factor = 0.89) It is interesting to note that the range distributions become more like Rayleigh shape distributions when the size of the smallest detected range increases.

The review of random fatigue-test results has established that the commonly held view of the irregularity factor having no effect is not really substantiated. Some of the works which have led to this view have certain shortcomings which place limitations on the conclusions which can be drawn from them. The values of irregularity factor quoted by Fuller are not reliable, Naumann's data for his cases A and D does not lead to the expected peak distributions. Another work (Clevenson and Steiner) contained a trend which has been either overlooked or considered insignificant. This

trend does however agree with that formed by Swanson. A further conclusion may be drawn from Clevenson and Steiner's work. On the basis of their results the lives under random loading are similar for any spectrum shape, provided that the irregularity factor is approximately constant.

9 APPENDICES

9.1 Digital Recording System Units

9.1.1 The Logic Unit

(a) Circuit Design

The requirements of the logic unit are fan-in and fan-out of ten, switching times of 5 μs or less (for operation at 20 kc) and low cost. These are achieved with the circuit of Fig. 9.1 which incorporates two diode feedback circuits.

The diode circuits have the following properties:

1) They prevent both saturation and cutting-off of the transistor (improving switching times).

2) They limit and stabilize the output voltage by providing feedback circuits for each state of the logic unit, thus providing good fan-in and fan-out characteristics.

(b) Circuit Details

In the circuit of Fig. 9.1 the logic unit is in the state '1' when its output potential is nominally -2.75v, and at '0' when -.3v. With the unit at '0' diode D1 conducts forming the feedback circuit and in the '1' state D2 conducts.

When switching from either state to the other the conducting diode in the first state must not close early. Premature closure of the diode would reverse the effect of the input voltage causing the switch.

9.1.2 The Binary Unit

The bistable unit of Fig. 9.2 can be switched by a positive-going pulse applied through a capacitive network to the base of the transistor which is at '0'. The capacitive network includes directing circuits controlled by the bistable itself which direct the pulse to that transistor. The binary unit thus formed switches with each input pulse. A similar gating circuit is directed by the polarity control and selects the output from one or other of the transistors depending on the polarity state. This output circuit produces a positive-going pulse for the switch '1' to '0' of the selected transistor.

The reversible binary counter is formed by connecting two or more binaries through their respective input and output circuits. In the diagram of Fig. 9.3 the state of the counter is defined by the right-hand collectors. When adding the outputs are derived from the right-hand collectors and when subtracting the left-hand ones are used. The counting sequences (with decimal equivalents) is shown in the diagram.

9.1.3 Input Amplifiers

The main amplifier (operating from the virtual earth potential) is d.c. differential. Germanium p-n-p and silicon n-p-n transistors are used in sequence. The circuit (Fig. 9.4) incorporates both a balance control and balance monitoring meter on the system console.

The main amplifier drives two single stage d.c. differential amplifiers in parallel which control the pulse gate and polarity circuits. The gains of the amplifiers (see Fig. 9.5) are pre-set to operate the pulse gate at $\pm$2.5mV

and the polarity control at ±1.5mV.

9.1.4 Gate Triggering Circuit

The gate triggering circuit consists of a conventional Schmidt trigger set at -2.2v followed by a driving stage for the monostable (Fig. 9.6)

9.1.5 Current Switches

The current switches incorporate a silicon n-p-n transistor and wirewound resistors. The transistors have very low leakage current when switched off and low slope resistance and stable collector-to-emitter voltage when saturated. In the circuit of Fig. 9.7 the stability of the output current is determined by the -4v supply to the emitter and the transistor V_{ce}.

Fig. 9.7 shows the characteristics of the circuit, where the total possible variation in base current is shown in relation to the minimum base current to ensure saturation. In this configuration the variation of V_{ce} due to temperature is 1% per ^{o}C (in the worst possible case). However as V_{ce} is 1/25 of V_r the effect of temperature on the current from the switch is 0.04% per ^{o}C. The leakage current is small (0.3 μA per switch), but in any case has no effect (at constant temperature) as the main amplifiers are balanced at the start of a recording, thus accommodating any static out-of-balance at the virtual earth. The variation of leakage current with temperature (approximately ±0.2 μA for ±10^{o}C) is also negligible.

The -4v supply is derived from the recording system main d.c. supply and is extremely stable.

9.1.6 -4v Supply

The design of this unit is based on similar units made in the department, Fig. 9.8. To obtain a lower variation of V_o with I_o a higher gain first stage is used, which is also made differential to reduce the variation of V_o with temperature. To virtually eliminate the variation of V_o with the main d.c. supply the first and second stages are run off a Zener diode.

The final circuit (Fig. 9.9) has an extremely stable output voltage (less than $\pm$.02% drift overall).

9.1.7 Operating Facilities

To operate the system several facilities are incorporated on the console.

1. Record/Replay: a switch which selects the mode of operation.
2. D.C./A.C. Input: the input signal may be d.c. or a.c. coupled. In the latter case a d.c. bias of half full-scale is added.
3. Reset: a push-button which resets all counters to zero (used prior to a recording or replaying).
4. Hold/Record: a switch which places or removes an inhibit on the gate. This switch is used to lock the recording system prior to a recording whilst the system is reset.
5. Bias/Signal: a switch which selects for recording either a built-in constant bias of half full scale, or the input signal. Recording of the bias before and after a

recording provides a means of detecting any drift in the system.

6. Manual Sample: during replay the contents of the counter can be punched onto paper tape by manual triggering of the data output channel. This may be done prior and subsequent to a replay to check the signal bias, thus detecting and drift in the system.

7. Balance potentiometer and meter: this provides the means of balancing the main input amplifier prior to a recording.

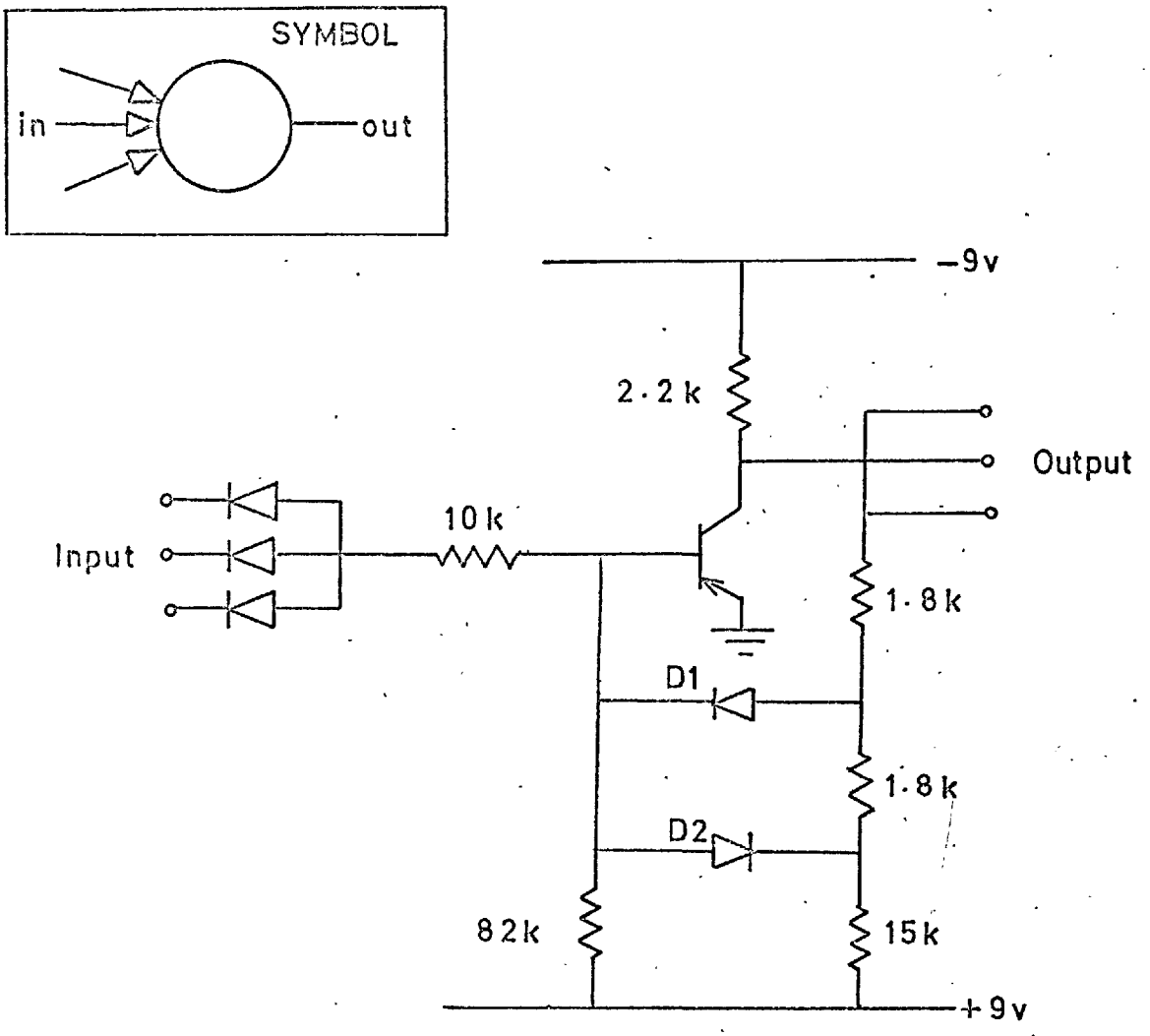

FIG. 9.1 CIRCUIT OF LOGIC UNIT

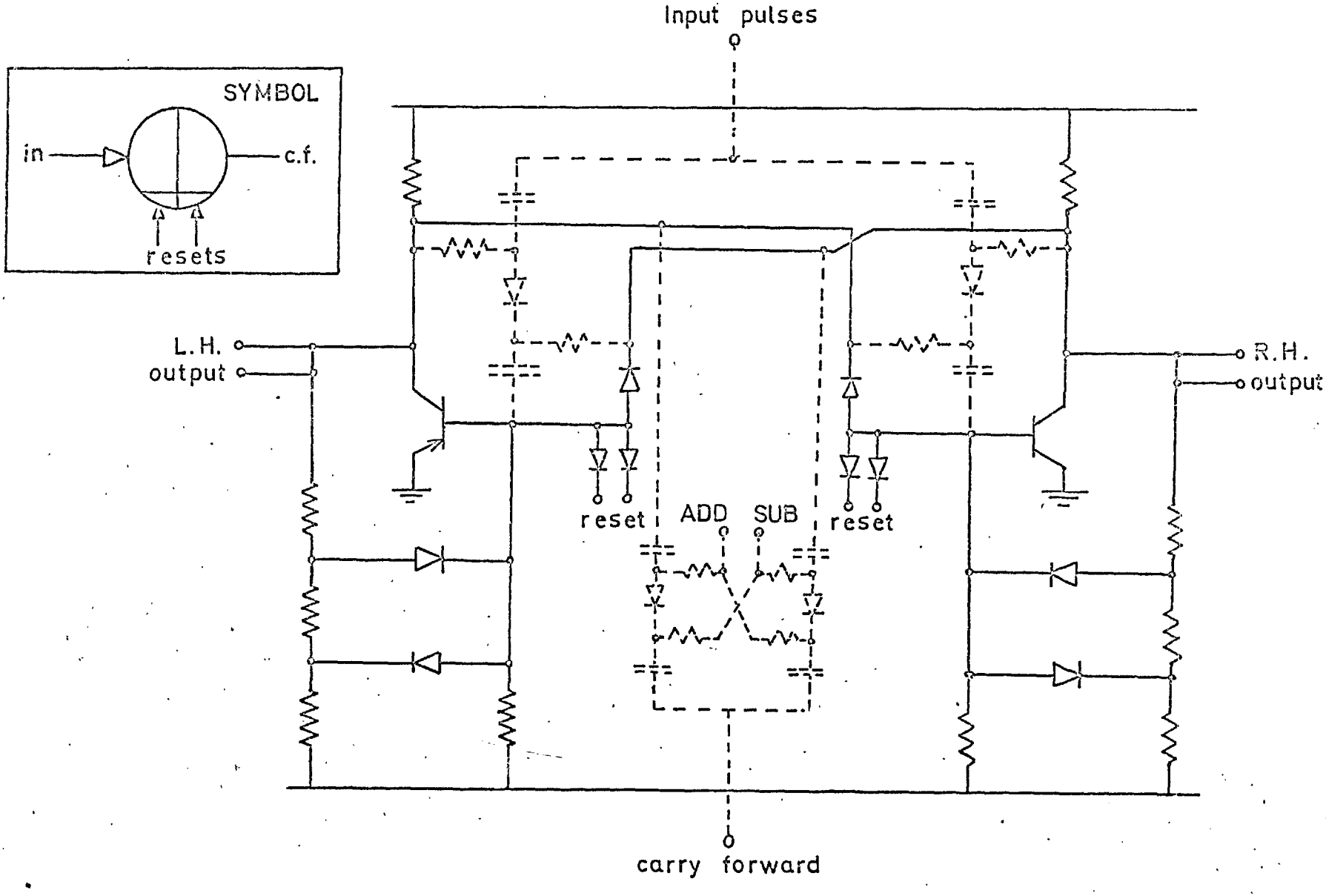

FIG. 9.2 CIRCUIT OF BINARY UNIT

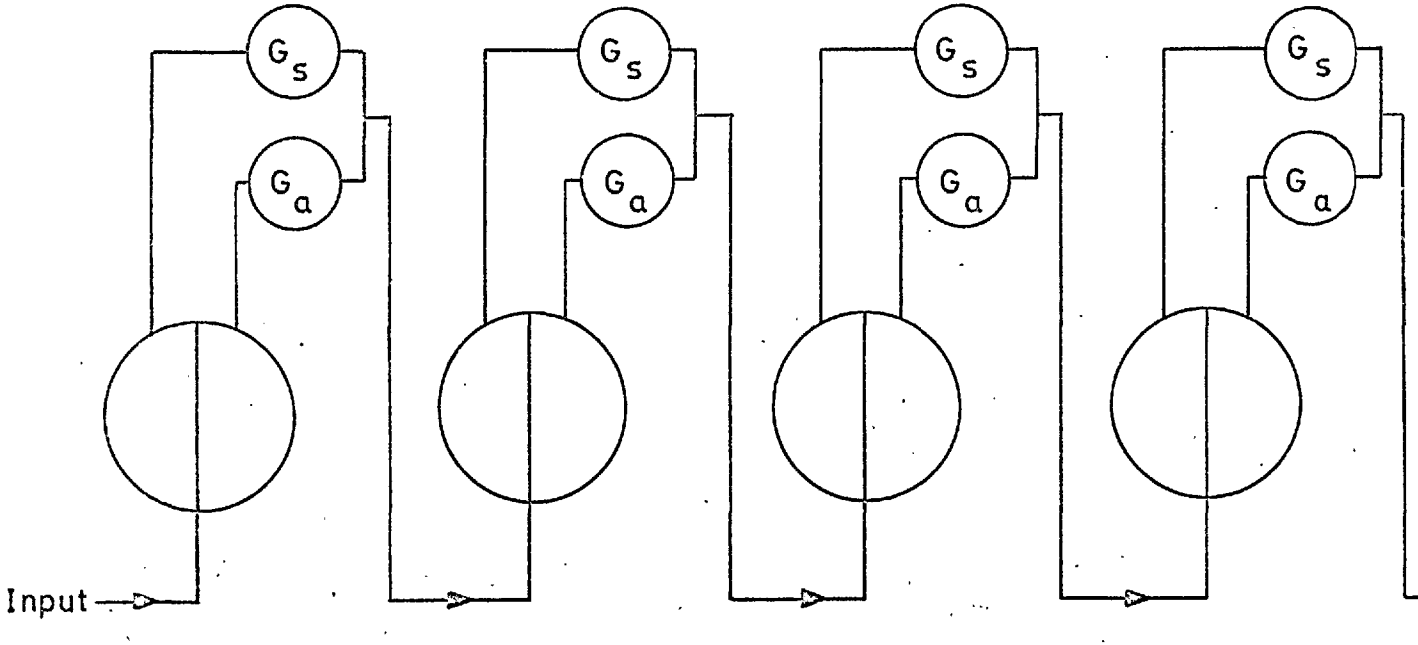

counting sequence		
	add	sub
0	0000	0000
1	1000	1000
2	0100	0100
3	1100	1100
4	0010	0010
5	1010	1010
6	0110	0110
7	1110	1110
	(0001)	(1011)
8	0111	0111
9	1111	1111

FIG. 9.3 REVERSIBLE BINARY COUNTER

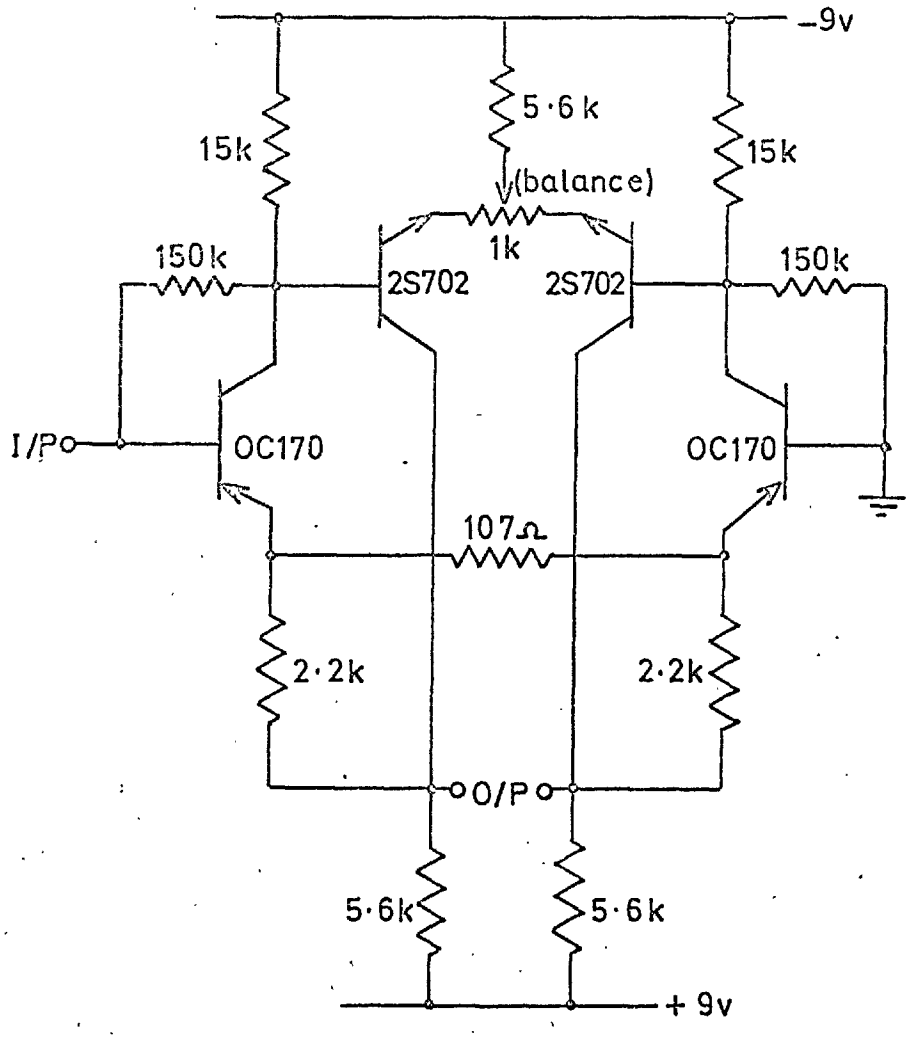

FIG. 9.4 MAIN I/P AMPLIFIER

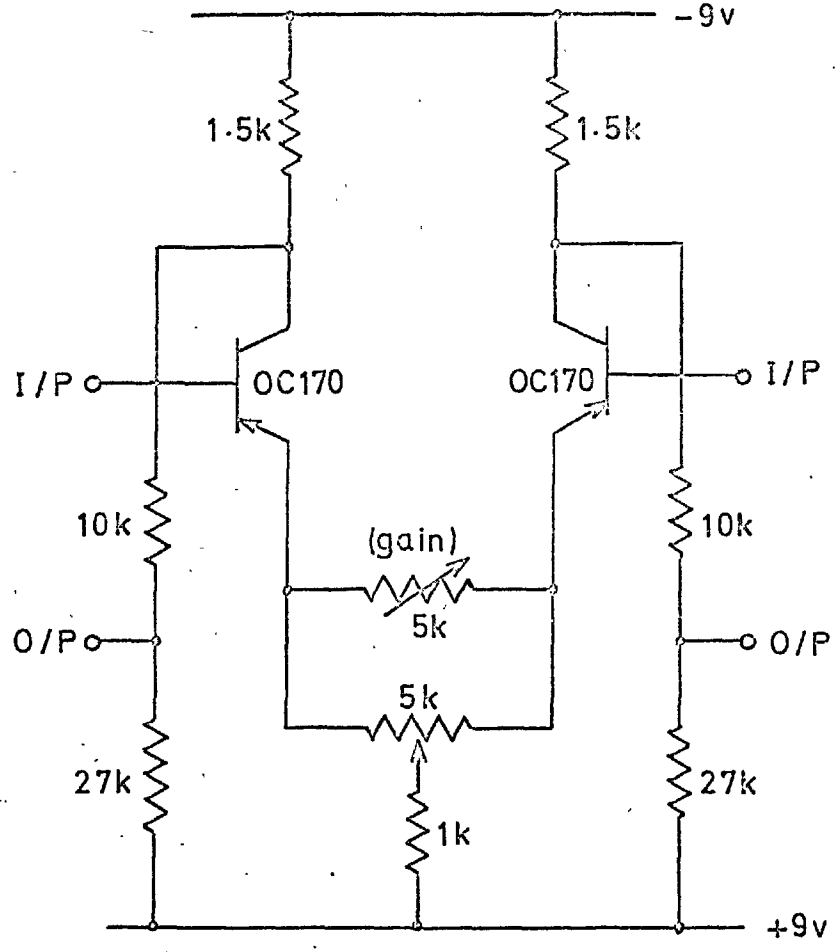

FIG. 9.5 2nd STAGE AMPLIFIER

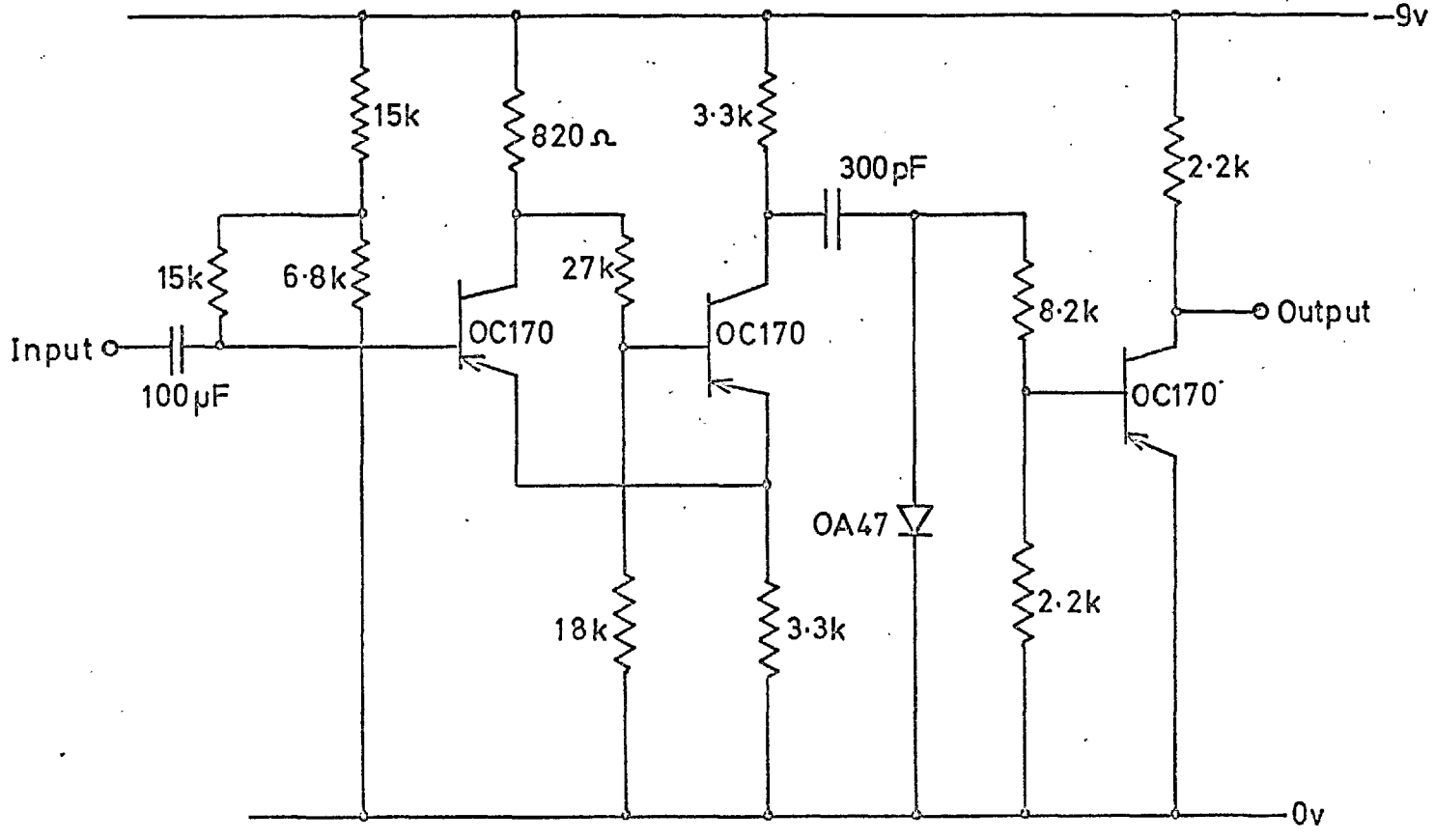

FIG. 9.6 GATE TRIGGERING CIRCUIT

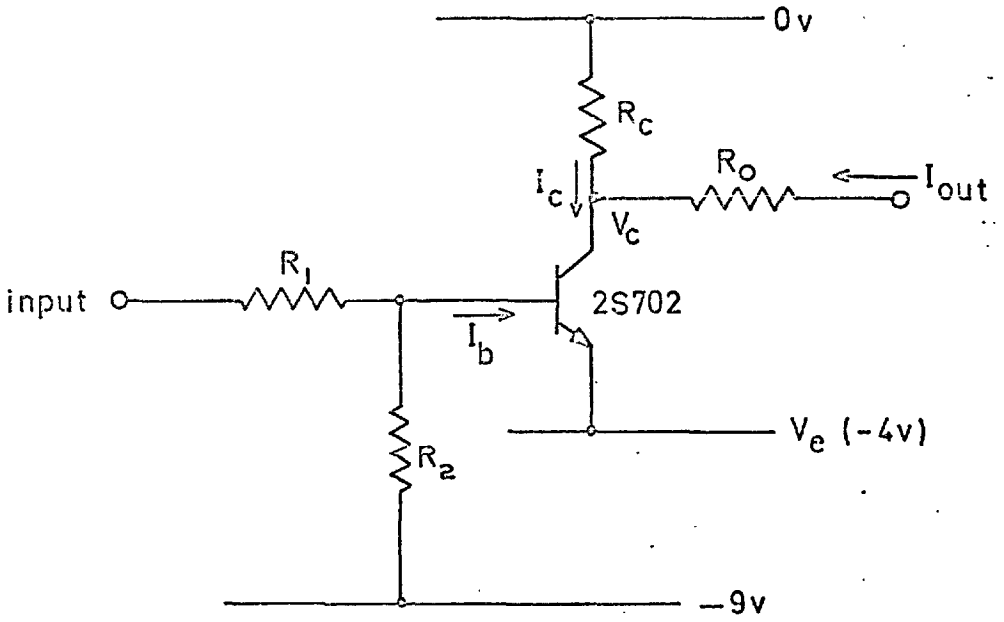

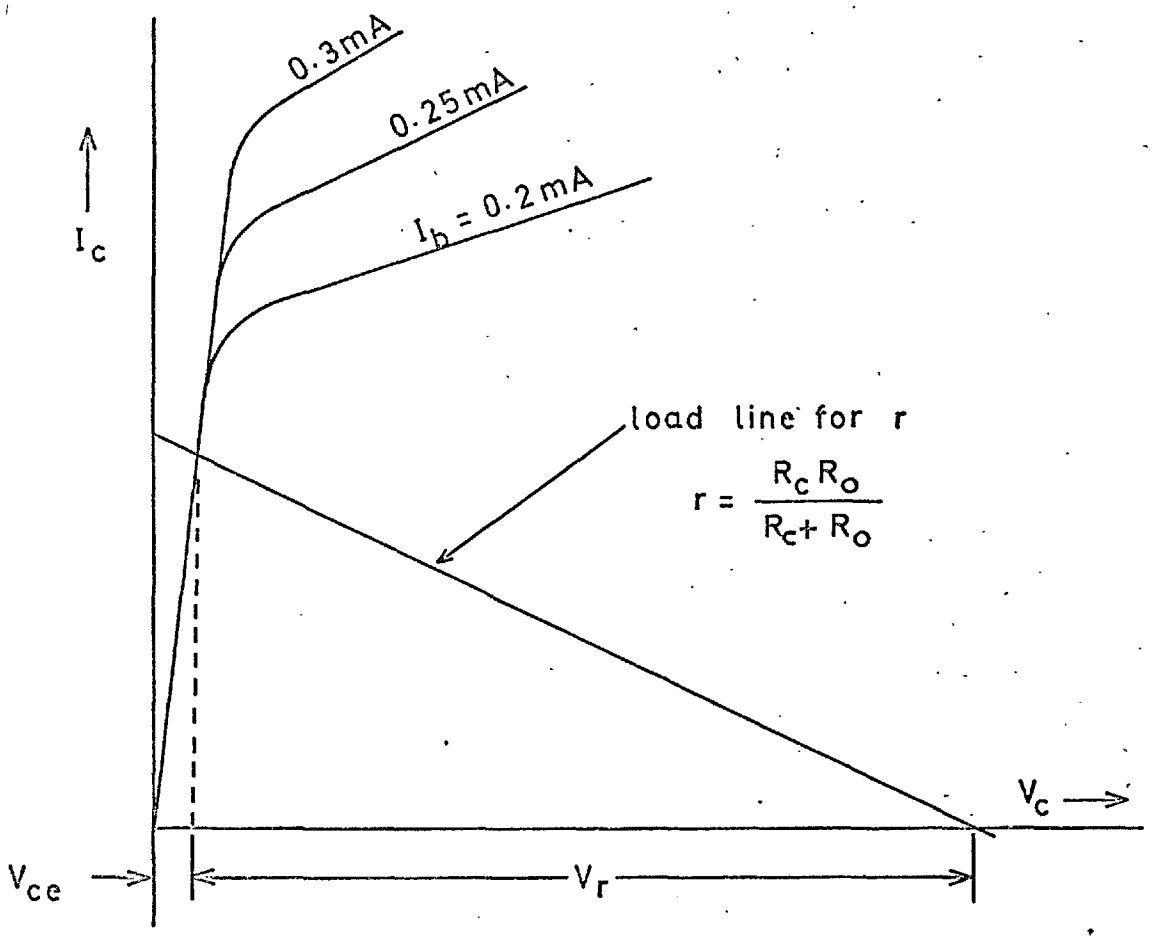

FIG. 9.7 CIRCUIT & CHARACTERISTICS OF CURRENT SWITCHES

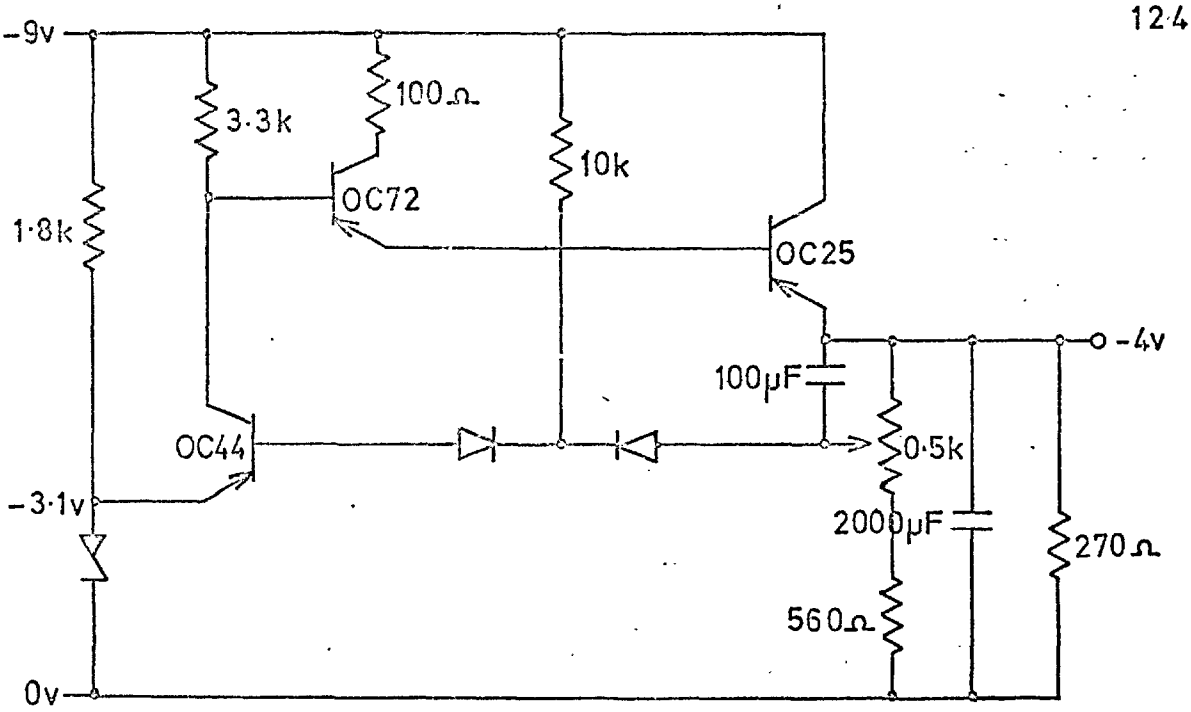

FIG. 9.8 ORIGINAL -4v SUPPLY UNIT

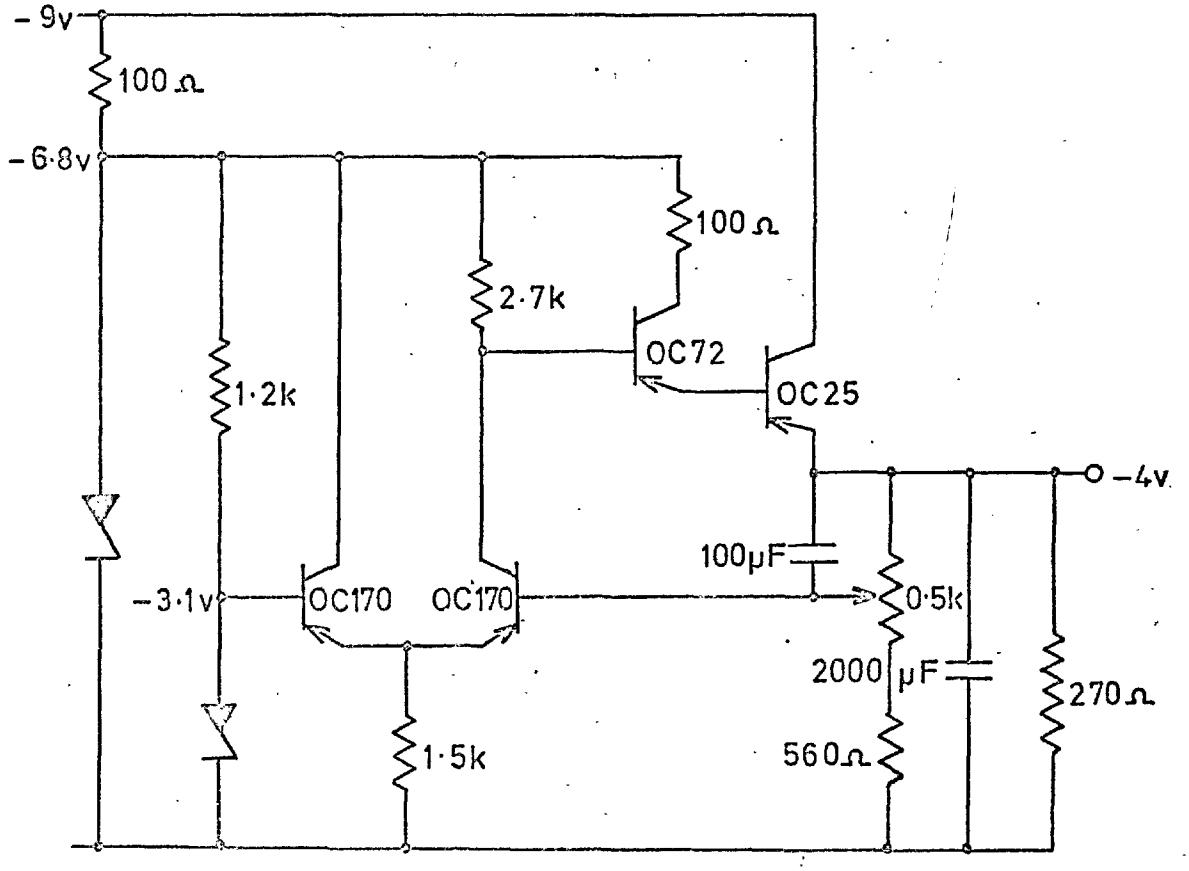

FIG. 9.9 FINAL -4v SUPPLY UNIT

9. APPENDICES (continued)

9.2 Data Processing

9.2.1 Introduction

Three types of counting methods are employed; Range-Mean for ranges greater than 0, 2.5, 5, 7.5 and 10% full scale, Peak and Mean-Crossing Peak. An eighth count, the Range, is obtained from the Range-Mean data.

The following data parameters are computed;

- Number of data points
- Mean value of data
- Number of maxima and minima (N_i)
- Number of zero crossings (N_o)
- Irregularity Factor N_o/N_i
- R.M.S. value of peaks
- R.M.S. value of continuous function
- Number of data points rejected

The programmes are run a second time factoring the data so that the r.m.s. of the continuous function is 10% full scale (to relate the conditional Range-Mean counts to the function) and adjusting the mean value (by typically .15%) to exactly 50% full scale.

To illustrate the counting methods the flow diagrams show the logic relevant only to the descriptions of the methods. The programmes themselves are given in Appendix 3.

9.2.2 Counting Methods

1. Conditional Range - Mean Count.

All ranges less than P (see diagram) are ignored. In the diagram only the range J - M is counted. Points of inflexion are ignored.

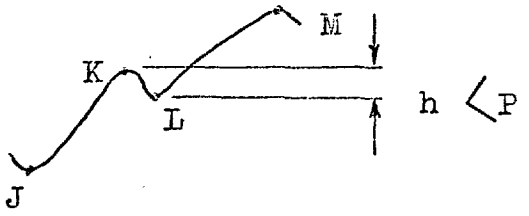

Fig. 9.10 gives the flow diagram of the analyses with P taking the values 0, 25, 50, 75, 100.

2. Peak Count

All maxima above and minima below the mean are counted (In the diagram below the points J, K, L, M, N, O.).

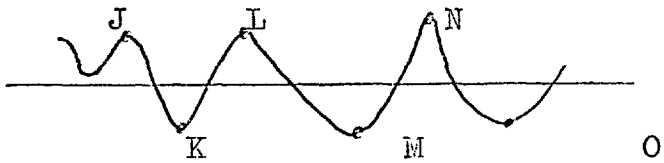

The flow diagram for this analysis is in Fig. 9.11.

3. Mean-Crossing Peak Count.

Between each crossing of the mean value the highest maxima above and the lowest minima below the mean are counted (in the diagram below the points J, K, L, M.)

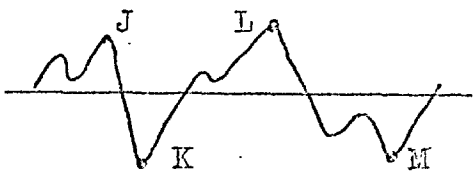

(Flow diagram Fig. 9.12).

9.2.3 The Control Programme.

The data tape is divided naturally by the original discrete magnetic tape files into blocks of up to 3000 records. A read-compute-read cycle is employed with blocks of records to obtain efficient usage of the computer.

The main programme performs the data-handling; reading an input block, checking for incorrect records and entering the block into an array. It then transfers control to the processing subroutines and repeats the cycle for each input block. After the last file is processed control is transferred to subroutines which calculate the data parameters and print out the results.

The incorrect records encountered either contained spurious characters or were two or four digit numbers. These were ignored (except for the record made of them) and were typically one in five thousand.

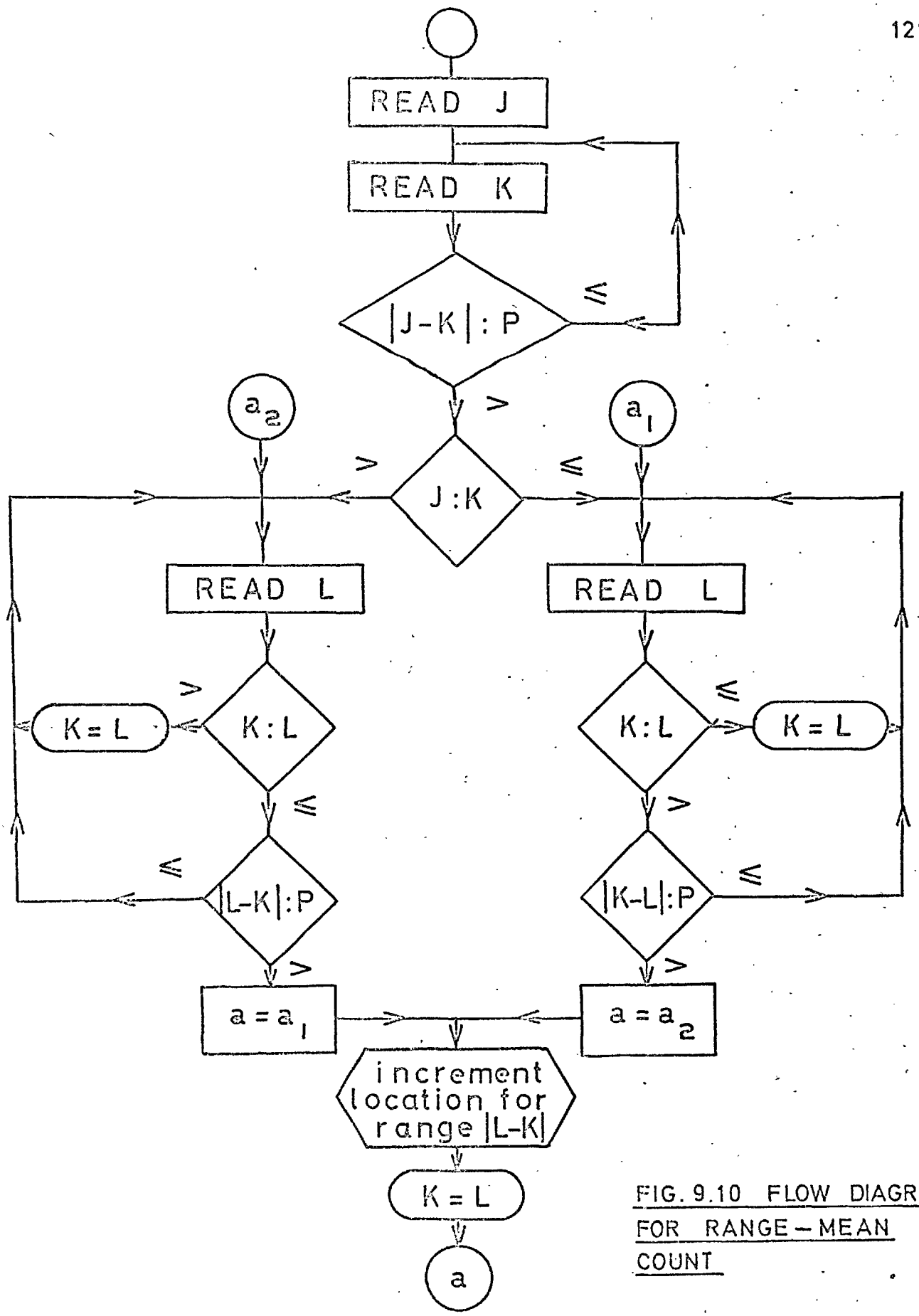

FIG. 9.10 FLOW DIAGRAM FOR RANGE – MEAN COUNT

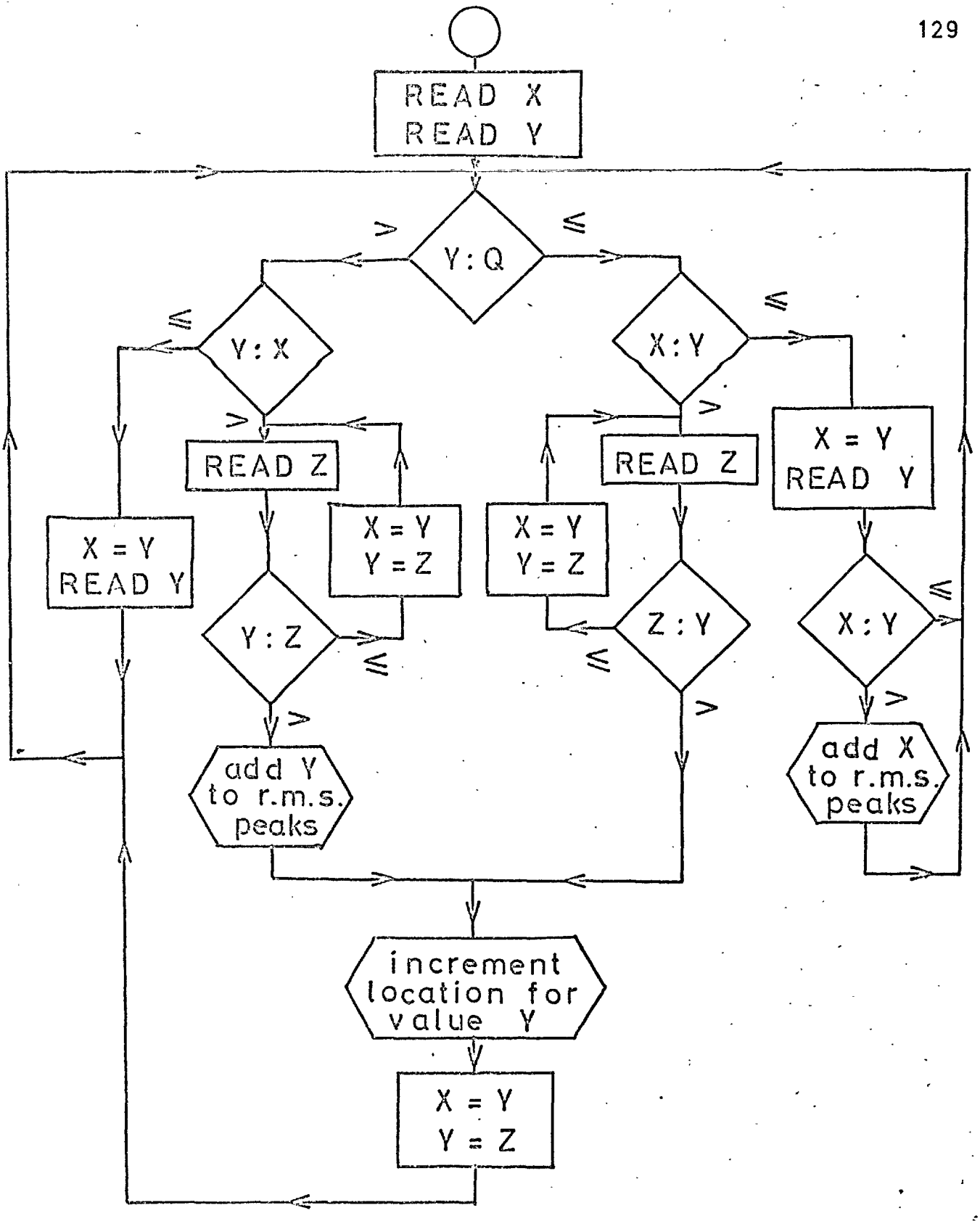

FIG. 9.11 FLOW DIAGRAM FOR PEAK COUNT

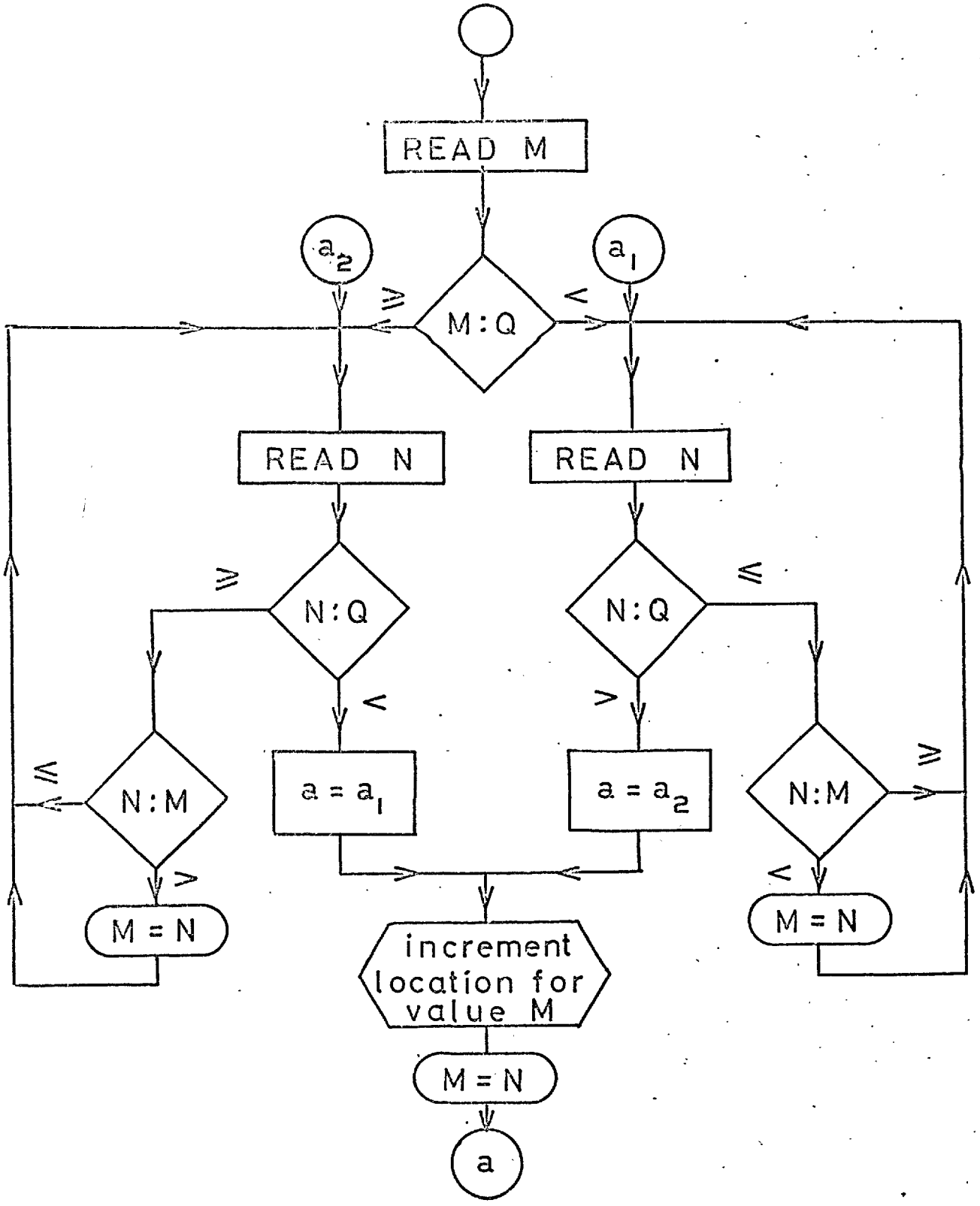

FIG. 9.12 FLOW DIAGRAM FOR M.C.P. COUNT

9. APPENDICES (continued)

9.3 Computer Programmes

The programmes are written for the Atlas computer in Extended Mercury Autocode (EMA).

```
main>9000
auxiliary(0,0)
dumps 0

title
fatigue data processing

routine 1

70)n=1(10)11
l=50n-25
m=l+450
o=n+9
newline
newline
space

i=l(50)m
print(i)5,0
space
space
repeat
newline

i=0(20*)380
newline
space
j=n(1)o
k=i+j+r
print(bk)5,0
space
space
repeat
repeat

repeat

return
**
```

```
routine 2

75)n=1(10)11
l=50n-25
m=l+450
o=n+9
newline
newline
space

i=l(50)m
print(i)5,0
space
space
repeat
newline
newline
space

i=n(1)o
k=i+n
print(bk)5,0
space
space
repeat

repeat

return
**
```

```
routine 3

75)n=1(10)31
l=25n-25
m=l+225
o=n+9
newline
newline
space
i=&l(25)n
print(i)5,o
space
space
repeat
newline
newline
space

i=n(1)o
k=i+r
print(bk)5,o
space
space
repeat

repeat

return
**.
```

```
routine 4

>>range mean analysis, ranges >p

17)pn=o(1)4
p=25pn
j=c(2pn)
k=c(2pn+1)
t=o
jump 45,sn≠1
j=2o

32)t=t+1
in=j-2t
in=$mod(in)

22)jump 36,p>in
k=2t
jump 33,j>k

>>loop for k>j

36)r)=37)
jump 45
37)jump 38,l>k
in=k-l
in=$mod(in)
jump 36,p>in

>>set table for j>k loop
r)=33)

>>calculate location

58)in=j&-k
in=$mod(in)
kn=j+k

ln=1(1)2o
mn=5oln
jump 59,mn>in
repeat

59)nn=1(1)2o
mn=1oonn
jump 6o,mn>kn
repeat

6o)in=2onn+lm+16p-2o
bin=bin+1

>>ranges analysis, ranges > p
in=2o4o+2opn+ln
bin=bin+1

j=k
k&=l

>>go to opposite loop
jump(r)

38)k=l
jump 36

>>loop for j>k

33)r)=34)
jump 45

34)jump 35,k>l
in=k-l
in=$mod(in)
jump 33,p>in
```

```
>>set lable for j>k loop

r)=36)
jump 58

35)k=l
jump 33

45)jump 50,t=0
t=t+1
l=at
jump(r)

50)c(2pn)=j
c(2pn+1)=k
.

repeat
return


24)p=0(25)100%
newline
newline
newline
caption
range% mean analysis, ranges >
print(p)3,0
r=16p
jumpdown(r1)

repeat



pn=0(1)4
p=25pn
newline
newline
newline
caption
range analysis, ranges >
print(p)3,0
r=2040+20%pn
jumpdown(r2)

repeat

return
**
```

```
routine 5
>>mean crossing peak analysis


17)t=0
jump 50,sn≠1
m=a0
jump 45,m>qn

>>loop for qn>m


42)s)=70)
jump 50
70)jump 43,qn>n
jump 47

43)jump42,n>m
m=n
jump 42


>>loop for m>qn

45)s%)=60)
jump 50
60)jump 46,n>qn
jump 48

46)jump 45,m>n
m=n
jump 45



50)jump 51,t=0
t=t+1
n=at
jump(s)

47)in=1
jn=20
s)=45)
jump 49

48)in=21
jn=40
s)=42)

49)kn=in(1)jn
l=%25kn
jump 80,l>m
repeat

80)kn=kn+2000
bkn=bkn+1
```

```
m=n
jump(s)


24)newline
newline
newline
caption
mean crossing peak analysis
r=2000
jumpdown(r3)

51)return
**


routine 6

>>peak counting analysis
t=0
jump 10,sn≠1
x=a0
y=a1
w=qn


t=1
10)jump 50,y>w
jump 21,y>x
12)jump 93,t=0
t=t+1
z=at
jump 22,y>z

in=1
jn=20
jump 90

21)jump 93,t=0
t=t+1
x=y
y=at
jump 10,y>x
c=x-500
c10=c10+c*c
b=b+1
jump 10

20)jump 93,t=0
t=t+1
x=y
y=at
jump 10


22)x=y
y=z
jump 12


50)jump 20,x>y
52)jump 93,t=0
t=t+1
z=at
jump 62,z>y


in=21
jn=40

c=y-500
c10=c10+c*c
b=b+1


90)kn=in(1)jn
ln=25kn
jump 91,ln>y
repeat

91)jn=kn+2140
bjn=bjn+1

x=y
y=z
jump 10


62)x=y
y=z
jump 52


93)return



24)newline
newline
newline
caption
peak analysis
r=2140
jumpdown (rxx3)

return
**
```

```
routine 7

>>compute cumulative results


1)k=o(20)380
i=19(-1)1
j=i+k+r
bj=bj+b(j+1)
repeat
repeat


return
**
```

```
routine 8

>>compute cumulative results


1)i=19(-1)1
j=i+r
bj=bj+b(j+1)
repeat

return
**
```

```
routine 9

>>cumulative range analysis
1)p=o(25)100
r=16p
newline
newline
newline
caption
cumulative range mean results, ranges >
print(p)3,0
jumpdown(r7)
jumpdown(r1)
repeat

loop,m=0@inc(5)20
newline
newline
newline
caption
cumulative range results, ranges >
p=5m
print(p)3,0
r=2040+4m
jumpdown(r8)
jumpdown(r2)
repeat
return
```

```
routine 10

>>compute cumulative results


*1)j=2(1)20
i=r+j
bi=bi+b(i-1)
repeat


j=39(-1)21
i=r+j
bi=bi+b(i+1)
repeat

return
**
```

```
routine 11

>>cumulative m-c-p analysis


1)newline
newline
newline
caption
cumulative m-c-p results
r=2000
jumpdown(r*10)
jumpdown(r3)
return
**
```

```
routine 12

>>cumulative peak analysis

1)newline
newline
newline
caption
cumulative peak results
r=2140
jumpdown(r10)
jumpdown(r3)
return
**
```

```
routine 13

>> print out data parameters

20)newline                          newline
caption                             caption
no. of data tapes =                 r. m. s.  value of peaks =
print(n)3,0                         jump 22,b=0
                                    c10=c10/b
newline                             c10=$sqrt(c10)
caption                             print(c10)0,6
no. of data points =
print(on)6,0
                                    newline
newline                             caption
caption                             r. m. s.  value of function =
mean value of data =                c10=c10/$sqrt(1+do*do)
do=do/on                            print(c10)0,6
print(do)0,6

                                    return
newline
caption                             22)newline
no. of maxima and minima =          caption
j=0                                 r.m.s. vlue not evaluated , b=0
i=1(1)400
j=j+bi                              return
repeat                              **
print(j)6,0

newline
caption                             routine 14
no. of zero crossings =
k=0                                 >> scale to 100 r.m.s. function
i=2001(1)2040
k=k+bi                              1)i=1(1)0
repeat                              ai=ai-e
print(k)6,0                         ai=ai*3
                                    ai=ai+300
newline                             do=do+ai
caption                             repeat
no/n1 =                             return
do=k/j                              **
print(do)0,4

newline
caption
no. of data points rejected =
print(a)3,0
```

```
chapter o

a≥6ooo
b≥2200
c≥1o
d≥1o

1)i=o(1)6ooo

ai=o
repeat

i=o(1)2200
bi=o
repeat

i=o(1)1o
ci=o
repeat

i=o(1)1o
di=o
re*peat


>>read no. of tapes and mean value
read(rn)
read(qn)
read(e)
read(f)
read(ao)



g=1oo/f
ao=ao-e
ao=ao*g
ao=ao+5oo



do=ao
sn=1
a=-rn
b=o
```

```
on=1
3)o=o
2)o=o+1
6)read(ao)
jump 6,ao>1ooo
jump 6,1>ao
jump2


o)a=a+1
o=o-1

jn=o
1o)readch(in)
jump 15,in≠$code(*)
12)jn=jn+1
jump 1o,jn≠3
jump 17

15)jump 2,in=$code(n)
readch(in)
jump 12,in=$code(*)
jump 15


17)on=on+o
jumpdown(r14)
jumpdown(r4)
jumpdown(r5)
jumpdown(r6)

4)sn=sn+1
jump 2o,sn=rn+1
jump 3

2o)jumpdown(r13)
jumpdown(r4/24)
jumpdown(r5/24)
jumpdown(r6/24)
jumpdown(r9)
jumpdown(r11)
jumpdown(r12)


end
close

***t
```

9 APPENDICES (continued)

9.4 S-N Curves

The S-N curves are derived from ref. 7. and are of the form $S = aN^b$. In order to refer the numerical data of the histograms to a stress scale, the maximum possible peak value ($\frac{1}{2}$ full-scale excursion from the mean) plus the mean value is made equal to the ultimate stress divided by a safety factor (1.5). This latter stress will be referred to as the proof stress. The mean stress is the proof stress divided by 3.5. This means that the probability of exceeding the proof load is of the order of 10^{-6} for a Rayleigh distribution of peaks and is, of course, lower for irregularity factors less than unity.

The stress scale is arbitrary (ultimate = 700, therefore Proof = 466.7, Mean = 133.3) and the numerical scale of the histograms factored by 0.667.

i.e. Mean + 500 x 0.667 = Proof

The basic SN curves are then defined by the first co-ordinate (500, 10^4) and the second co-ordinate (250, at three successive values of N, 10^7, 10^6, 10^5). These three curves correspond to the following Al.alloy cases (ref. 7);

(i) High Slope - lugs with interference (E.05.04)
(ii) Medium Slope - lugs without interference (E.05.03)
(iii) Low Slope - alloy in bending (E.07.01)

Although in the data sheets these curves have fatigue limits, the contributions to the estimated lives from the regions of the curves where discrepancies occur are insignificant. The 'damage intensity' is negligibly small in these regions.

The above curves are defined for the zero mean stress cases. The curves corresponding to non-zero mean stress are derived from the R-M diagram of data sheet A.00.01 (ref. 7), using a value of unity for the parameter defining the effect of the mean stress. Thus the relationship between the stress amplitudes (Sa) at mean values (Sm) and the equivalent stress amplitude (Sa_o) giving the same fatigue life at zero mean stress is

$$Sa = Sa_o / (1 - Sm/S_{ult})$$

where S_{ult} is the ultimate stress.

The ratio Mean/Proof has no effect on the comparative lives (eg. peak to range) for these S-N curves, except for comparisons involving mean values (i.e. range-mean method). The comparison between estimates from differing counting methods depends largely only on the slope of the S-N curve.

9 APPENDICES (continued)

9.5 Tables of Data

On the following pages are tabulated the probability density distributions relating to the data from Leybold (ref. 10) and Naumann (ref. 9) followed by the distributions relating to the recordings of filtered random noise and car suspension loads.

Finally the output tabulations are given from the data analysis programmes for the recordings of filtered random noise and car suspension loads.

TABLES OF DATA FROM LEYBOLD AND NAUMANN

Naumann uses the same data as Leybold except for case D, for which Naumann introduces a different case D. Therefore the following letter code for these joint results is used:

SOURCE	Nau/Ley A	Nau/Ley B	Nau/Ley C	Leybold D	Naumann D
LETTER CODE	A	B	C	D	E

PEAK DISTRIBUTIONS

$\frac{x}{\sigma}$	A	B	C	D	E
0.1	.327	.359	.249	.234	.370
0.3	.394	.403	.351	.339	.440
0.5	.448	.438	.446	.458	.483
0.7	.491	.447	.519	.526	.510
0.9	.491	.420	.548	.575	.501
1.1	.461	.385	.541	.563	.449
1.3	.424	.350	.482	.503	.392
1.5	.363	.289	.417	.429	.316
1.7	.297	.219	.351	.332	.243
1.9	.212	.184	.263	.265	.179
2.1	.158	.123	.197	.193	.124
2.3	.115	.096	.132	.136	.082
2.5	.073	.061	.095	.092	.052
2.7	.048	.044	.058	.054	.030
2.9				.038	

TABLES OF DATA FROM LEYBOLD AND NAUMANN (CONTD)

RANGE DISTRIBUTIONS (ALL RANGES)

$\frac{x}{\sigma}$	A	B	C	D	E
0.1	.469	1.060	.449	.421	.416
0.3	.526	.811	.367	.353	.634
0.5	.625	.724	.457	.426	.798
0.7	.687	.633	.555	.535	.889
0.9	.689	.525	.597	.607	.742
1.1	.605	.399	.594	.589	.575
1.3	.487	.309	.535	.525	.389
1.5	.359	.212	.443	.446	.234
1.7	.244	.143	.325	.345	.126
1.9	.149	.093	.240	.244	.061
2.1	.085	.049	.173	.184	.028
2.3	.045	.022	.106	.125	.013
2.5	.018	.013	.071	.079	
2.7			.042	.050	
2.9			.024	.030	

TABLES OF DATA FROM LEYBOLD AND NAUMANN (CONTD)

DISTRIBUTIONS OF MEAN VALUES

	B		C		D	
$\frac{x}{\sigma_f}$	$\frac{x}{\sigma_m}$	$p(\frac{x}{\sigma_m})$	$\frac{x}{\sigma_m}$	$p(\frac{x}{\sigma_m})$	$\frac{x}{\sigma_m}$	$p(\frac{x}{\sigma_m})$
0.0	0.0	.393	0.0	.402	0.0	.409
0.2	0.27	.390	0.572	.341	0.763	.297
0.4	0.54	.348	1.144	.204	1.527	.120
0.6	0.81	.291	1.716	.092	2.291	.028
0.8	1.08	.216	2.288	.029	3.054	.004
1.0	1.35	.157	2.86	.007		
1.2	1.62	.109				
1.4	1.89	.063				
1.6	2.16	.038				
1.8	2.43	.022				
2.0	2.70	.012				

RANDOM NOISE 2-9 c/s : PROBABILITY DENSITY DISTRIBUTIONS

$\frac{x}{\sigma}$	PEAK	RANGE	MCP	$\frac{x}{\sigma_m}$	MEAN
0.125	.286	.566	.247	0.507	.356
0.375	.402	.510	.273	1.523	.118
0.625	.460	.536	.348	2.538	.016
0.875	.542	.544	.463	3.553	.0014
1.125	.483	.548	.451		
1.375	.414	.447	.392		
1.625	.339	.324	.325		
1.875	.236	.231	.246		
2.125	.169	.136	.169		
2.375	.105	.079	.104		
2.625	.062	.038	.062		
2.875	.033	.023	.033		
3.125	.024	.010	.024		

RANDOM NOISE 2-25 c/s : PROBABILITY DENSITY DISTRIBUTIONS

$\frac{x}{\sigma}$	PEAK	RANGE	MCP	$\frac{x}{\sigma_m}$	MEAN
0.125	.329	.634	.281	0.424	.373
0.375	.423	.572	.288	1.272	.168
0.625	.430	.576	.343	2.12	.042
0.875	.489	.571	.360	2.97	.006
1.125	.455	.508	.380		
1.375	.405	.422	.368		
1.625	.314	.307	.288		
1.875	.218	.191	.226		
2.125	.165	.115	.152		
2.375	.093	.054	.108		
2.625	.062	.027	.058		
2.875	.037		.037		
3.125	.019		.020		

CAR SUSPENSION LOADS : PROBABILITY DENSITY DISTRIBUTIONS

$\frac{x}{\sigma}$	PEAK	RANGE	MCP	$\frac{x}{\sigma_m}$	MEAN
0.125	.354	1.344	.312	0.311	.389
0.375	.439	.864	.242	0.933	.253
0.625	.413	.599	.214	1.555	.114
0.875	.423	.442	.197	2.177	.038
1.125	.356	.280	.202	2.799	.008
1.375	.304	.199	.196		
1.625	.226	.126	.150		
1.875	.154	.070	.113		
2.125	.112	.039	.082		
2.375	.060	.023	.052		
2.625	.043	.010	.035		
2.875	.023		.021		

OUTPUT FROM DATA ANALYSIS PROGRAMME

The results are tabulated on the following pages as follows:

Range Mean:

Each column heading is the medium value of ranges in the group

	1st column	2nd column
eg.	25 (Ranges, 0 → 50)	75 (Ranges, 50 → 100) etc.

The heading for each row should be taken as the same for the corresponding column, except that each row relates to the grouping of mean values.

eg.	1st row	(25)	(Means 0 → 50)
	2nd row	(75)	(Means 50 → 100)

Peak and M.C.P:

The numbers in the odd numbered rows correspond to the peak value for each group. The numbers in the even rows (and below each peak value) are the number of peak counts in the corresponding group of peaks. Each peak value quoted is the lower limit of the peak values in the group.

eg. 0 (Minima between 0 and 25) 25 (Minima between 25 and 50)

.....

500 (Maxima between 500 and 525) 525 (Maxima between 525 and 550)

Filtered Random Noise 2-25 c/s

Number of maxima and minima	23383
Number of mean crossings	17114
Irregularity Factor	0.732
Mean Value	500.00
R.M.S. value of signal	100.26
R.M.S. value of maxima	124.24

25	75	125	175	225	275	325	375	425	475
0	0	0	0	0	0	0	0	0	0
0	0	0	0	0	0	0	0	0	0
0	0	0	0	0	0	0	0	0	0
0	0	0	0	0	0	0	0	0	0
0	0	0	0	0	0	0	0	0	0
2	5	1	0	1	0	1	0	1	0
35	20	15	14	4	6	8	2	2	2
188	131	91	91	78	74	55	39	20	10
557	483	479	485	437	298	252	173	101	41
1115	1076	1110	1032	953	841	599	347	208	102
1063	987	1050	1134	993	778	558	363	218	105
527	480	487	460	389	374	262	148	91	46
179	137	113	113	103	86	55	40	25	9
38	23	23	11	12	8	3	5	4	3
4	1	1	2	0	0	2	0	1	0
1	1	0	0	0	0	0	1	0	0
0	0	0	0	0	0	0	0	0	0
0	0	0	0	0	0	0	0	0	0
0	0	0	0	0	0	0	0	0	0
0	0	0	0	0	0	0	0	0	0

525	575	625	675	725	775	825	875	925	975
0	0	0	0	0	0	0	0	0	0
0	0	0	0	0	0	0	0	0	0
0	0	0	0	0	0	0	0	0	0
0	0	0	0	0	0	0	0	0	0
0	0	0	0	0	0	0	0	0	0
0	0	0	0	0	0	0	0	0	0
1	0	0	0	0	0	0	0	0	0
6	2	0	0	0	0	0	0	0	0
21	12	5	2	1	0	0	0	0	0
51	19	10	3	2	0	0	0	0	0
51	25	7	4	0	0	0	0	0	0
25	12	4	5	0	1	0	0	0	0
5	4	2	0	2	0	0	0	0	0
1	0	0	0	0	0	0	0	0	0
0	0	0	0	0	0	0	0	0	0
0	0	0	0	0	0	0	0	0	0
0	0	0	0	0	0	0	0	0	0

RANGE MEAN ANALYSIS, RANGES >

25	75	125	175	225	275	325	375	425	475
0	0	0	0	0	0	0	0	0	0
0	0	0	0	0	0	0	0	0	0
0	0	0	0	0	0	0	0	0	0
0	0	0	0	0	0	0	0	0	0
0	0	0	0	0	0	0	0	0	0
0	2	1	0	0	0	1	0	1	0
10	11	7	8	3	4	5	2	2	2
57	76	55	65	64	64	52	34	20	11
170	356	375	415	414	289	255	175	111	42
419	936	1044	1033	1021	901	649	373	220	113
413	845	976	1149	1044	857	608	399	243	115
148	353	400	401	364	378	270	151	95	51
34	79	80	80	81	65	48	34	25	9
8	12	10	7	6	6	2	5	1	4
0	0	1	0	0	0	2	0	1	0
0	0	0	0	0	0	0	0	0	0
0	0	0	0	0	0	0	0	0	0
0	0	0	0	0	0	0	0	0	0
0	0	0	0	0	0	0	0	0	0
0	0	0	0	0	0	0	0	0	0

525	575	625	675	725	775	825	875	925	975
0	0	0	0	0	0	0	0	0	0
0	0	0	0	0	0	0	0	0	0
0	0	0	0	0	0	0	0	0	0
0	0	0	0	0	0	0	0	0	0
0	0	0	0	0	0	0	0	0	0
0	0	0	0	0	0	0	0	0	0
0	0	0	0	0	0	0	0	0	0
5	2	0	0	0	0	0	0	0	0
22	14	5	2	2	0	0	0	0	0
53	21	10	3	2	0	0	0	0	0
55	29	7	4	0	0	0	0	0	0
28	14	4	6	0	1	0	0	0	0
3	4	3	0	2	0	0	0	0	0
1	0	0	0	0	0	0	0	0	0
0	0	0	0	0	0	0	0	0	0
0	0	0	0	0	0	0	0	0	0
0	0	0	0	0	0	0	0	0	0

25	75	125	175	225	275	325	375	425	475
0	0	0	0	0	0	0	0	0	0
0	0	0	0	0	0	0	0	0	0
0	0	0	0	0	0	0	0	0	0
0	0	0	0	0	0	0	0	0	0
0	0	0	0	0	0	0	0	0	0
0	2	0	0	0	0	1	0	1	0
0	4	4	3	1	3	5	2	1	2
0	45	38	43	46	41	48	31	20	10
1	271	290	353	379	275	268	179	116	47
0	783	973	1021	1051	955	690	402	231	125
0	697	894	1138	1080	906	639	424	257	125
0	274	308	344	331	362	280	160	102	56
0	47	59	62	57	55	40	32	22	10
0	7	3	3	3	3	1	3	1	3
0	0	1	0	0	0	0	0	1	0
0	0	0	0	0	0	0	0	0	0
0	0	0	0	0	0	0	0	0	0
0	0	0	0	0	0	0	0	0	0
0	0	0	0	0	0	0	0	0	0
0	0	0	0	0	0	0	0	0	0

525	575	625	675	725	775	825	875	925	975
0	0	0	0	0	0	0	0	0	0
0	0	0	0	0	0	0	0	0	0
0	0	0	0	0	0	0	0	0	0
0	0	0	0	0	0	0	0	0	0
0	0	0	0	0	0	0	0	0	0
0	0	0	0	0	0	0	0	0	0
0	0	0	0	0	0	0	0	0	0
7	2	0	0	0	0	0	0	0	0
23	15	5	2	2	0	0	0	0	0
57	23	10	3	2	0	0	0	0	0
60	29	8	4	0	0	0	0	0	0
30	14	4	6	0	1	0	0	0	0
4	5	3	0	2	0	0	0	0	0
1	0	0	0	0	0	0	0	0	0
0	0	0	0	0	0	0	0	0	0
0	0	0	0	0	0	0	0	0	0
0	0	0	0	0	0	0	0	0	0

25	75	125	175	225	275	325	375	425	475
0	0	0	0	0	0	0	0	0	0
0	0	0	0	0	0	0	0	0	0
0	0	0	0	0	0	0	0	0	0
0	0	0	0	0	0	0	0	0	0
1	0	0	0	0	0	0	0	0	0
0	0	0	0	0	0	0	0	1	0
0	0	4	0	1	1	5	2	1	2
0	10	19	25	29	33	42	32	18	10
1	95	215	286	335	256	266	183	117	48
0	358	872	1009	1062	1015	733	427	242	133
0	331	792	1106	1095	948	679	454	268	131
0	97	232	291	290	334	277	168	105	59
0	18	46	46	39	49	32	34	21	11
0	2	1	1	2	2	1	2	0	1
0	0	0	0	0	0	0	0	1	0
0	0	0	0	0	0	0	0	0	0
0	0	0	0	0	0	0	0	0	0
0	0	0	0	0	0	0	0	0	0
0	0	0	0	0	0	0	0	0	0
0	0	0	0	0	0	0	0	0	0

525	575	625	675	725	775	825	875	925	975
0	0	0	0	0	0	0	0	0	0
0	0	0	0	0	0	0	0	0	0
0	0	0	0	0	0	0	0	0	0
0	0	0	0	0	0	0	0	0	0
0	0	0	0	0	0	0	0	0	0
0	0	0	0	0	0	0	0	0	0
0	0	0	0	0	0	0	0	0	0
7	3	0	0	0	0	0	0	0	0
24	15	5	2	2	0	0	0	0	0
59	24	10	3	2	0	0	0	0	0
65	32	8	5	0	0	0	0	0	0
30	14	4	6	0	1	0	0	0	0
5	6	3	0	2	0	[illegible]	[illegible]	[illegible]	0
1	0	0	0	0	0	RANGE MEAN ANALYSIS, RANGES > 75			0
0	0	0	0	0	0	[illegible]	[illegible]	[illegible]	0
0	0	0	0	0	0	0	0	0	0
0	0	0	0	0	0	0	0	0	0

25	75	125	175	225	275	325	375	425	475
0	0	0	0	0	0	0	0	0	0
0	0	0	0	0	0	0	0	0	0
0	0	0	0	0	0	0	0	0	0
0	0	0	0	0	0	0	0	0	0
1	0	0	0	0	0	0	0	0	0
0	0	0	0	0	0	0	0	0	0
0	0	2	0	0	1	3	1	1	1
0	0	10	13	21	24	37	29	17	10
0	0	145	220	269	232	261	189	117	51
0	0	735	954	1068	1063	783	454	253	140
0	1	663	1043	1092	988	718	484	286	137
0	0	181	224	243	294	279	170	110	61
0	0	31	28	24	41	24	32	20	11
0	0	0	0	1	1	0	1	0	1
0	0	0	0	0	0	0	0	1	0
0	0	0	0	0	0	0	0	0	0
0	0	0	0	0	0	0	0	0	0
0	0	0	0	0	0	0	0	0	0
0	0	0	0	0	0	0	0	0	0
0	0	0	0	0	0	0	0	0	0

525	575	625	675	725	775	825	875	925	975
0	0	0	0	0	0	0	0	0	0
0	0	0	0	0	0	0	0	0	0
0	0	0	0	0	0	0	0	0	0
0	0	0	0	0	0	0	0	0	0
0	0	0	0	0	0	0	0	0	0
0	0	0	0	0	0	0	0	0	0
0	1	0	0	0	0	0	0	0	0
7	3	0	0	0	0	0	0	0	0
26	16	5	2	2	0	0	0	0	0
61	25	11	3	2	1	0	0	0	0
66	33	8	5	0	0	0	0	0	0
32	14	4	6	0	1	0	0	0	0
5	6	3	0	2	0	0	0	0	0
1	0	0	0	0	0	0	0	0	0
0	0	0	0	0	0	0	0	0	0
0	0	0	0	0	0	0	0	0	0
0	0	0	0	0	0	0	0	0	0

MEAN CROSSING PEAK ANALYSIS

0	25	50	75	100	125	150	175	200	225
0	0	2	0	10	16	25	55	110	163
250	275	300	325	350	375	400	425	450	475
308	425	666	852	1111	1044	1077	1038	825	830
500	525	550	575	600	625	650	675	700	725
815	857	969	1027	1176	1040	834	656	465	322
750	775	800	825	850	875	900	925	950	975
178	104	61	24	14	6	6	2	0	1

PEAK ANALYSIS

0	25	50	75	100	125	150	175	200	225
0	0	2	0	10	16	25	55	110	183
250	275	300	325	350	375	400	425	450	475
289	466	648	889	1231	1260	1526	1271	1186	984
500	525	550	575	600	625	650	675	700	725
941	1284	1240	1330	1401	1136	948	624	501	294
750	775	800	825	850	875	900	925	950	975
178	105	61	26	12	6	6	2	0	1

Filtered Random Noise 2-9 c/s

Number of maxima and minima	12947
Number of mean crossings	10254
Irregularity Factor	0.792
Mean Value	500.03
R.M.S. value of signal	99.964
R.M.S. value of maxima	127.52

25	75	125	175	225	275	325	375	425	475
0	0	0	0	0	0	0	0	0	0
0	0	0	0	0	0	0	0	0	0
0	0	0	0	0	0	0	0	0	0
0	0	0	0	0	0	0	0	0	0
0	0	0	0	0	0	0	0	0	0
0	0	0	2	0	0	0	1	0	0
10	1	1	3	3	2	2	0	1	0
66	35	21	22	23	12	7	12	6	9
273	186	214	192	171	154	128	89	53	32
597	600	589	642	674	563	384	257	163	92
566	578	654	687	705	536	381	294	153	81
251	214	219	202	184	168	136	84	57	39
66	36	34	10	12	10	10	8	6	1
7	0	4	0	1	1	0	0	0	0
2	0	0	0	0	0	0	1	0	0
0	0	0	0	0	0	0	0	0	0
0	0	0	0	0	0	0	0	0	0
0	0	0	0	0	0	0	0	0	0
0	0	0	0	0	0	0	0	0	0
0	0	0	0	0	0	0	0	0	0

525	575	625	675	725	775	825	875	925	975
0	0	0	0	0	0	0	0	0	0
0	0	0	0	0	0	0	0	0	0
0	0	0	0	0	0	0	0	0	0
0	0	0	0	0	0	0	0	0	0
0	0	0	0	0	0	0	0	0	0
0	0	0	0	0	0	0	0	0	0
0	0	0	0	0	0	0	0	0	0
5	3	2	0	0	0	0	0	0	0
17	8	5	2	0	0	0	0	0	0
40	25	11	6	4	2	1	0	0	0
37	22	7	8	6	5	0	0	0	0
17	13	7	0	1	0	0	0	0	0
5	3	0	0	0	0				0
1	0	0	0	0	0				0
0	0	0	0	0	0	0	0	0	0
0	0	0	0	0	0	0	0	0	0
0	0	0	0	0	0	0	0	0	0

RANGE MEAN ANALYSIS, RANGES >

25	75	125	175	225	275	325	375	425	475
0	0	0	0	0	0	0	0	0	0
0	0	0	0	0	0	0	0	0	0
0	0	0	0	0	0	0	0	0	0
0	0	0	0	0	0	0	0	0	0
0	0	0	0	0	0	0	0	0	0
0	0	0	2	0	0	0	1	0	0
3	0	0	3	2	0	2	0	0	0
10	28	12	17	15	8	6	11	6	9
59	110	150	151	151	152	129	93	53	32
222	521	576	671	705	605	402	266	167	96
239	505	602	709	736	583	405	309	156	82
74	145	171	159	174	160	136	86	61	39
10	15	20	5	8	7	7	7	6	1
2	0	3	0	1	1	0	0	0	0
0	0	0	0	0	0	0	1	0	0
0	0	0	0	0	0	0	0	0	0
0	0	0	0	0	0	0	0	0	0
0	0	0	0	0	0	0	0	0	0
0	0	0	0	0	0	0	0	0	0
0	0	0	0	0	0	0	0	0	0

525	575	625	675	725	775	825	875	925	975
0	0	0	0	0	0	0	0	0	0
0	0	0	0	0	0	0	0	0	0
0	0	0	0	0	0	0	0	0	0
0	0	0	0	0	0	0	0	0	0
0	0	0	0	0	0	0	0	0	0
0	0	0	0	0	0	0	0	0	0
0	0	0	0	0	0	0	0	0	0
6	3	2	0	0	0	0	0	0	0
18	8	5	2	0	0	0	0	0	0
41	26	11	6	4	2	1	0	0	0
38	22	7	8	6	5	0	0	0	0
17	13	7	0	1	0	0	0	0	0
5	3	0	0	0	0	0	0	0	0
1	0	0	0	0	0	0	0	0	0
0	0	0	0	0	0	0	0	0	0
0	0	0	0	0	0	0	0	0	0
0	0	0	0	0	0	0	0	0	0

25	75	125	175	225	275	325	375	425	475
0	0	0	0	0	0	0	0	0	0
0	0	0	0	0	0	0	0	0	0
0	0	0	0	0	0	0	0	0	0
0	0	0	0	0	0	0	0	0	0
0	0	0	0	0	0	0	0	0	0
0	0	0	1	0	0	0	1	0	0
0	0	0	1	1	0	2	0	0	0
0	12	4	10	8	2	6	11	5	9
1	66	104	104	127	143	125	94	55	33
0	436	547	658	740	643	416	289	176	99
0	414	570	717	767	614	417	326	160	82
1	95	113	123	146	152	137	83	63	39
0	4	7	3	4	4	7	7	6	1
0	0	2	0	1	1	0	0	0	0
0	0	0	0	0	0	0	1	0	0
0	0	0	0	0	0	0	0	0	0
0	0	0	0	0	0	0	0	0	0
0	0	0	0	0	0	0	0	0	0
0	0	0	0	0	0	0	0	0	0
0	0	0	0	0	0	0	0	0	0

525	575	625	675	725	775	825	875	925	975
0	0	0	0	0	0	0	0	0	0
0	0	0	0	0	0	0	0	0	0
0	0	0	0	0	0	0	0	0	0
0	0	0	0	0	0	0	0	0	0
0	0	0	0	0	0	0	0	0	0
0	0	0	0	0	0	0	0	0	0
0	0	0	0	0	0	0	0	0	0
6	3	2	0	0	0	0	0	0	0
18	9	5	2	0	0	0	0	0	0
42	26	11	6	4	2	1	0	0	0
40	22	7	8	6	5	0	0	0	0
17	13	7	0	1	0	0	0	0	0
5	3	0	0	0	0	0	0	0	0
1	0	0	0	0	0	0	0	0	0
0	0	0	0	0	0	0	0	0	0
0	0	0	0	0	0	0	0	0	0
0	0	0	0	0	0	0	0	0	0

25	75	125	175	225	275	325	375	425	475
0	0	0	0	0	0	0	0	0	0
0	0	0	0	0	0	0	0	0	0
0	0	0	0	0	0	0	0	0	0
0	0	0	0	0	0	0	0	0	0
0	0	0	0	0	0	0	0	0	0
0	0	0	0	0	0	0	1	0	0
0	0	0	0	1	0	1	0	0	0
0	5	4	2	3	1	4	7	3	8
1	22	67	78	103	135	128	95	57	34
0	199	471	632	767	662	431	295	182	101
0	166	512	713	806	646	435	334	165	85
0	33	64	78	118	145	134	85	63	39
0	2	5	1	2	2	4	7	5	1
0	0	2	0	0	0	0	0	0	1
0	0	0	0	0	0	0	0	0	0
0	0	0	0	0	0	0	0	0	0
0	0	0	0	0	0	0	0	0	0
0	0	0	0	0	0	0	0	0	0
0	0	0	0	0	0	0	0	0	0
0	0	0	0	0	0	0	0	0	0

525	575	625	675	725	775	825	875	925	975
0	0	0	0	0	0	0	0	0	0
0	0	0	0	0	0	0	0	0	0
0	0	0	0	0	0	0	0	0	0
0	0	0	0	0	0	0	0	0	0
0	0	0	0	0	0	0	0	0	0
0	0	0	0	0	0	0	0	0	0
0	0	0	0	0	0	0	0	0	0
7	3	2	0	0	0	0	0	0	0
20	9	5	2	0	0	0	0	0	0
43	27	11	7	4	2	1	0	0	0
41	23	8	9	6	5	0	0	0	0
16	13	7	0	1	0	0	0	0	0
2	3	0	0	0	0	0	0	0	0
1	0	0	0	0	0	0	0	0	0
0	0	0	0	0	0	0	0	0	0
0	0	0	0	0	0	0	0	0	0
0	0	0	0	0	0	0	0	0	0

25	75	125	175	225	275	325	375	425	475
0	0	0	0	0	0	0	0	0	0
0	0	0	0	0	0	0	0	0	0
0	0	0	0	0	0	0	0	0	0
0	0	0	0	0	0	0	0	0	0
0	0	0	0	0	0	0	0	0	0
0	0	0	0	0	0	0	1	0	0
0	0	0	0	1	0	1	0	0	0
1	1	1	1	1	0	4	7	3	8
0	0	44	42	83	124	130	93	60	34
0	0	377	601	785	686	442	303	186	102
0	0	435	674	817	680	448	345	166	85
0	0	32	51	96	133	134	90	64	39
0	0	1	1	1	2	3	5	5	0
0	0	2	0	0	0	0	0	0	1
0	0	0	0	0	0	0	0	0	0
0	0	0	0	0	0	0	0	0	0
0	0	0	0	0	0	0	0	0	0
0	0	0	0	0	0	0	0	0	0
0	0	0	0	0	0	0	0	0	0
0	0	0	0	0	0	0	0	0	0

525	575	625	675	725	775	825	875	925	975
0	0	0	0	0	0	0	0	0	0
0	0	0	0	0	0	0	0	0	0
0	0	0	0	0	0	0	0	0	0
0	0	0	0	0	0	0	0	0	0
0	0	0	0	0	0	0	0	0	0
0	0	0	0	0	0	0	0	0	0
0	0	0	0	0	0	0	0	0	0
7	3	2	0	0	0	0	0	0	0
20	9	5	2	0	0	0	0	0	0
43	27	11	7	4	2	1	0	0	0
41	23	8	9.	6	5	0	0	0	0
16	13	7	0	1	0	0	0	0	0
6	3	0	0	0	0	0	0	0	0
1	0	0	0	0	0				0
0	0	0	0	0	0	0	0	0	0
0	0	0	0	0	0	0	0	0	0
0	0	0	0	0	0	0	0	0	0

RANGE MEAN ANALYSIS, RANGES > 100

MEAN CROSSING PEAK ANALYSIS

0	25	50	75	100	125	150	175	200	225
0	0	0	6	7	14	18	36	53	104
250	275	300	325	350	375	400	425	450	475
178	264	365	554	642	689	769	578	450	400
500	525	550	575	600	625	650	675	700	725
399	434	547	727	770	647	496	431	283	160
750	775	800	825	850	875	900	925	950	975
97	54	39	17	14	10	1	1	0	0

PEAK ANALYSIS

0	25	50	75	100	125	150	175	200	225
0	0	0	6	7	14	18	42	48	104
250	275	300	325	350	375	400	425	450	475
194	248	368	564	664	795	839	756	676	455
500	525	550	575	600	625	650	675	700	725
472	626	733	916	769	676	534	397	299	147
750	775	800	825	850	875	900	925	950	975
97	59	34	17	14	10	1	1	0	0

Car Suspension Loads

Number of maxima and minima	15143
Number of mean crossings	6964
Irregularity Factor	0.460
Mean Value	500.02
R.M.S. value of signal	100.06
R.M.S. value of maxima	110.13

25	75	125	175	225	275	325	375	425	475
0	0	0	0	0	0	0	0	0	0
0	0	0	0	0	0	0	0	0	0
0	0	0	0	0	0	0	0	0	0
2	0	0	0	1	0	1	0	0	0
7	3	2	1	1	2	2	0	1	0
46	26	17	6	5	3	1	1	1	1
165	98	58	30	19	11	1	3	2	4
423	234	173	102	68	38	27	15	4	2
698	477	340	244	145	107	72	35	20	16
1075	745	562	446	271	206	133	83	48	21
1107	803	542	454	291	199	127	72	37	23
894	586	380	265	178	136	76	39	24	12
457	216	142	100	65	39	32	14	8	5
131	76	44	20	17	11	5	4	1	1
31	5	7	4	2	2	1	0	0	1
9	1	1	0	0	1	0	0	0	0
2	1	0	0	0	0	0	0	0	0
0	0	0	0	0	0	0	0	0	0
0	0	0	0	0	0	0	0	0	0
0	0	0	0	0	0	0	0	0	0

525	575	625	675	725	775	825	875	925	975
0	0	0	0	0	0	0	0	0	0
0	0	0	0	0	0	0	0	0	0
0	0	0	0	0	0	0	0	0	0
0	0	0	0	0	0	0	0	0	0
0	0	0	0	0	0	0	0	0	0
0	1	0	0	0	0	0	0	0	0
2	4	1	0	0	0	0	0	0	0
4	2	0	0	0	0	0	0	0	0
6	1	1	0	0	0	0	0	0	0
4	4	1	0	0	0	0	0	0	0
5	2	1	0	0	0	0	0	0	0
3	2	0	1	0	0	0	0	0	0
4	1	1	0	0	0	0	0	0	0
3	1	0	0	0	0	0	0	0	0
0	0	0	0	0	0	0	0	0	0
0	0	0	0	0	0	0	0	0	0
0	0	0	0	0	0	0	0	0	0

25	75	125	175	225	275	325	375	425	475
0	0	0	0	0	0	0	0	0	0
0	0	0	0	0	0	0	0	0	0
0	0	0	0	0	0	0	0	0	0
0	0	0	0	1	0	0	0	0	0
0	0	1	1	1	1	0	0	0	0
11	10	11	4	4	2	1	1	0	1
54	66	43	23	15	11	5	3	5	4
142	159	131	77	62	47	38	14	6	1
208	337	263	227	164	126	82	43	25	18
349	571	501	419	331	251	108	98	54	21
420	617	475	460	331	242	148	84	45	26
228	421	342	277	190	164	88	44	28	12
93	123	119	83	68	55	52	13	9	4
29	39	29	12	19	10	4	3	1	2
7	3	3	1	3	2	1	0	0	1
3	0	0	0	0	1	0	0	0	0
0	1	0	0	0	0	0	0	0	0
0	0	0	0	0	0	0	0	0	0
0	0	0	0	0	0	0	0	0	0
0	0	0	0	0	0	0	0	0	0

525	575	625	675	725	775	825	875	925	975
0	0	0	0	0	0	0	0	0	0
0	0	0	0	0	0	0	0	0	0
0	0	0	0	0	0	0	0	0	0
0	0	0	0	0	0	0	0	0	0
0	0	0	0	0	0	0	0	0	0
2	1	0	0	0	0	0	0	0	0
2	2	1	0	0	0	0	0	0	0
5	3	0	0	0	0	0	0	0	0
7	0	1	1	0	0	0	0	0	0
6	4	1	0	0	0	0	0	0	0
6	2	1	0	0	0	0	0	0	0
4	2	0	1	0	0	0	0	0	0
5	0	1	0	0	0	0	0	0	0
2	2	0	0	0	0	0	0	0	0
0	0	0	0	0	0	0	0	0	0
0	0	0	0	0	0	0	0	0	0
0	0	0	0	0	0	0	0	0	0

25	75	125	175	225	275	325	375	425	475
0	0	0	0	0	0	0	0	0	0
0	0	0	0	0	0	0	0	0	0
0	0	0	0	0	0	0	0	0	0
0	0	0	0	0	0	0	0	0	0
0	0	1	0	0	1	0	0	0	0
0	8	9	2	2	2	1	1	0	1
0	39	29	14	10	12	5	4	2	4
0	103	91	70	57	42	37	14	6	3
0	242	225	203	172	141	97	51	27	20
0	416	416	402	349	287	184	109	59	25
0	441	415	462	367	274	175	93	46	28
0	274	276	250	195	168	99	46	30	12
0	73	89	76	60	32	35	14	9	4
0	26	19	8	15	11	4	3	1	2
0	1	2	1	3	3	1	0	0	1
0	0	0	0	0	1	0	0	0	0
0	0	0	0	0	0	0	0	0	0
0	0	0	0	0	0	0	0	0	0
0	0	0	0	0	0	0	0	0	0
0	0	0	0	0	0	0	0	0	0

525	575	625	675	725	775	825	875	925	975
0	0	0	0	0	0	0	0	0	0
0	0	0	0	0	0	0	0	0	0
0	0	0	0	0	0	0	0	0	0
0	0	0	0	0	0	0	0	0	0
0	0	0	0	0	0	0	0	0	0
2	1	0	0	0	0	0	0	0	0
2	5	1	0	0	0	0	0	0	0
5	3	0	0	0	0	0	0	0	0
8	0	1	2	0	0	0	0	0	0
7	5	1	0	0	0	0	0	0	0
6	2	1	0	0	0	0	0	0	0
5	2	0	1	0	0	0	0	0	0
5	0	1	0	0	RANGE MEAN ANALYSIS, RANGES > 50				0
2	2	0	0	0	0	0	0	0	0
0	0	0	0	0	0	0	0	0	0
0	0	0	0	0	0	0	0	0	0
0	0	0	0	0	0	0	0	0	0

25	75	125	175	225	275	325	375	425	475
0	0	0	0	0	0	0	0	0	0
0	0	0	0	0	0	0	0	0	0
0	0	0	0	0	0	0	0	0	0
0	0	0	0	0	0	0	0	0	0
0	0	0	0	0	1	0	0	0	0
0	0	1	3	1	0	2	1	0	1
0	10	16	10	14	9	4	4	2	4
0	20	70	53	56	38	33	14	6	4
0	93	161	186	170	151	102	59	31	21
0	150	349	386	346	309	201	117	65	26
0	137	337	463	377	294	184	105	48	29
0	97	203	229	198	168	103	52	32	13
0	16	55	69	58	51	36	11	11	4
0	5	14	8	15	8	5	2	1	1
0	0	0	0	2	3	1	2	0	1
0	0	0	0	0	0	0	0	0	0
0	0	0	0	0	0	0	0	0	0
0	0	0	0	0	0	0	0	0	0
0	0	0	0	0	0	0	0	0	0
0	0	0	0	0	0	0	0	0	0

525	575	625	675	725	775	825	875	925	975
0	0	0	0	0	0	0	0	0	0
0	0	0	0	0	0	0	0	0	0
0	0	0	0	0	0	0	0	0	0
0	0	0	0	0	0	0	0	0	0
0	0	0	0	0	0	0	0	0	0
2	1	0	0	0	0	0	0	0	0
2	5	1	0	0	0	0	0	0	0
5	3	0	0	0	0	0	0	0	0
8	2	1	2	0	0	0	0	0	0
7	5	1	0	0	0	0	0	0	0
6	2	1	0	0	0	0	0	0	0
5	2	0	1	0	0	0	0	0	0
5	0	1	0	0	0	0	0	0	0
2	2	0	0	0	0	0	0	0	0
0	0	0	0	0	0	0	0	0	0
0	0	0	0	0	0	0	0	0	0
0	0	0	0	0	0	0	0	0	0

25	75	125	175	225	275	325	375	425	475
0	0	0	0	0	0	0	0	0	0
0	0	0	0	0	0	0	0	0	0
0	0	0	0	0	0	0	0	0	0
0	0	0	0	0	0	0	0	0	0
0	0	0	0	0	0	0	0	0	0
0	0	7	3	1	0	0	0	0	1
0	0	12	6	10	9	3	4	3	5
0	0	52	41	50	55	34	14	7	5
0	0	121	155	163	150	106	66	32	21
0	0	297	368	341	318	211	129	67	28
0	0	272	424	383	309	191	119	49	29
0	0	152	207	195	173	106	54	33	14
0	0	38	54	49	30	35	11	11	4
0	0	9	6	14	8	3	2	1	1
0	0	0	0	1	3	1	2	0	1
0	0	0	0	0	0	0	0	0	0
0	0	0	0	0	0	0	0	0	0
0	0	0	0	0	0	0	0	0	0
0	0	0	0	0	0	0	0	0	0
0	0	0	0	0	0	0	0	0	0

525	575	625	675	725	775	825	875	925	975
0	0	0	0	0	0	0	0	0	0
0	0	0	0	0	0	0	0	0	0
0	0	0	0	0	0	0	0	0	0
0	0	0	0	0	0	0	0	0	0
0	0	0	0	0	0	0	0	0	0
2	1	0	0	0	0	0	0	0	0
2	5	0	0	0	0	0	0	0	0
5	3	0	1	0	0	0	0	0	0
6	2	2	3	0	0	0	0	0	0
8	5	1	0	0	0	0	0	0	0
7	5	1	0	0	0	0	0	0	0
5	2	0	1	0	0	[illegible]	[illegible]	[illegible]	0
5	0	1	0	0	0	0	0	0	0
2	2	0	0	0	0	0	0	0	0
0	1	0	0	0	0	0	0	0	0
0	0	0	0	0	0	0	0	0	0
0	0	0	0	0	0	0	0	0	0

MEAN CROSSING PEAK ANALYSIS

0	25	50	75	100	125	150	175	200	225
4	1	1	5	5	4	7	23	44	71
250	275	300	325	350	375	400	425	450	475
107	140	224	253	300	350	378	450	427	628
500	525	550	575	600	625	650	675	700	725
523	488	362	367	413	381	315	203	172	91
750	775	800	825	850	875	900	925	950	975
60	35	16	12	5	4	3	2	0	0

PEAK ANALYSIS

0	25	50	75	100	125	150	175	200	225
4	1	3	3	5	4	8	23	47	93
250	275	300	325	350	375	400	425	450	475
120	211	302	407	575	630	786	766	818	675
500	525	550	575	600	625	650	675	700	725
666	842	799	814	690	577	450	280	212	106
750	775	800	825	850	875	900	925	950	975
69	40	19	12	5	4	3	2	0	0

REFERENCES

1. RICE, S.O., 'Mathematical Analysis of Random Noise' Bell Syst. Tech. J., Vol 23, p 282; Vol 24, p 46 (1944-5)

2. CARTWRIGHT, D.E. and LONGUET-HIGGINS, M.S., 'The Statistical Distribution of the Maxima of a Random Function', Proc. Roy. Soc. A, vol. 237, p 212 (1956)

3. SWANSON, S.R., 'Random Load Fatigue Testing: A State of the Art Survey', Materials Research and Standards, MTRSA, Vol. 8, No. 4, p 10. (1968)

4. KOWALEWSKI, J., 'On the Relation Between Fatigue Lives Under Random Loading and Under Corresponding Programme Loading' contained in 'Full Scale Fatigue Testing of Aircraft Structures' Ed. by F.J. Plantema and J. Schijve, Pergammon Press 1961

5. LOEVE, M., 'Probability Theory', Van Nostrand

6. SCHIJVE, J., 'The Analysis of Random Load-Time Histories with Relation to Fatigue Tests and Life Calculations' contained in 'Fatigue of Aircraft Structures' Ed. by W. Barrois and E.L. Ripley, Pergammon Press 1963.

7. Engineering Sciences Data (Aeronautical Series), Fatigue Data Sheets. (previously R.Ae.Soc. Data Sheets, Fatigue)

8. GRACE, G.R., 'Measurement of Input Loads into a Vehicle Structure', Advanced School of Automobile Engineering Cranfield, Thesis (1963) -

9. NAUMANN, E.C., 'Fatigue Under Random and Programmed Loads', NASA TN D-2629, Feb. 1965

10. LEYBOLD, H.A., 'Techniques for Examining the Statistical and Power Spectral Properties of Random Time Histories', Virginia Polytechnic Inst., MS Thesis 1963

11. SWANSON, S.R., 'An Investigation of the Fatigue of Aluminium Alloy Due to Random Loading', UTIA Rep. 84 Feb. 1963

12. McCULLOCH, A.J., MELCON, M.A., et al, 'Investigation of the Representation of Aircraft Service Loadings in Fatigue Tests', ASD-TR-61-435, Jan 1962.

13. CLEVENSON, S.A., and STEINER, R., 'Fatigue Life Under Random Loading for Several Power Spectral Shapes', NASA TR R-266, Sept. 1967

14. FORSYTH, P.J.E., 'A Two-Stage Process of Fatigue Crack Growth', Symposium on Crack Propagation, Cranfield, 1961.

15. OROWAN, E., 'Fatigue in Aircraft Structures', Columbia University Conference 1956, (Discussion on C.E. Phillips paper, p 121), Academic Press.

16. JACOBY, G., 'Review of Fractographic Analysis Methods for Fatigue Fracture Surfaces'. Col. Univ., Dept. of Civ. Eng. and Eng. Mech., Tech Rep. 37, July 1966

17. SCHIJVE, J., 'Fatigue Life and Crack Propagation Under Random and Programmed Load Sequences', contained in 'Current Aeronautical Fatigue Problems', Ed by J.

Schijve, J.R., Heath-Smith and E.R. Welbourne, Pergammon Press, 1965

18. JACOBY, G., 'Application of Microfractography to the Study of Crack Propagation Under Fatigue Stresses', AGARD Rep. 541, 1966.

19. FULLER, J.R., 'Research on Techniques of Establishing Random Type Fatigue Curves for Broad Band Sonic Loading', ASD-TDR-62-501, Oct. 1962. (Also SAE Paper 671c, April 1963).

20. SCHIJVE, J., 'Fatigue Crack Propagation in Light Alloy Sheet Material and Structures', contained in 'Advances in Aeronautical Sciences', Vol 3, Ed by Th. von Karman Pergammon Press, 1961.

21. SCHIJVE, J., 'Analysis of the Fatigue Phenomenon in Aluminium Alloys', NLR Tech. Rep. M2122, also in NLR Rep. and Trans. Vol. XXIX, 1964.